Experimental Investigations of Flow Behavior in Pulsed Plate Columns Using Radioactive Particle Tracking

A thesis Submitted in partial fulfilment of the requirements for the degree of

DOCTOR OF PHILOSOPHY

by

Pillajetti Premsagar

Roll No. : 166107023

Department of Chemical Engineering

Indian Institute of Technology Guwahati

August 2023

Declaration

I hereby affirm that the research presented in this thesis titled **"Experimental investigation of flow behaviour in a pulsed column using radioactive particle tracking"** is original and was undertaken by me at the Department of Chemical Engineering, Indian Institute of Technology Guwahati, Guwahati, India, under the guidance of Associate Professor Raghvendra Gupta and Professor Rajesh Upadhyay. This work has not been submitted to any other institution for any academic degree or diploma. I have adhered to the guidelines provided by the Institute while composing this thesis, and I have abided by the standards and regulations outlined in the Ethical Code of Conduct of the Institute. Whenever I have utilized external materials (such as data, theoretical analyses, figures, and text), I have appropriately acknowledged them by referencing them within the thesis text and detailing their sources in the references section. Additionally, I have sought permission from the copyright holders of these sources whenever necessary.

Pillajetti Premsagar
(Research Scholar)
Roll No: 166107023
Department of Chemical Engineering
IIT Guwahati, Guwahati – 781039
Assam, India

Date: 27th March 2023
Place: IIT Guwahati

CERTIFICATE

It is certified that the research encompassed within the thesis titled **"Experimental Investigations of Flow Behavior in Pulsed Columns Using Radioactive Particle Tracking",** submitted by **Pillajetti Premsagar**, bearing a roll number **166107023**, a scholar in the Department of Chemical Engineering at the Indian Institute of Technology Guwahati, Guwahati, India, as part of his pursuit of a Doctor of Philosophy, was conducted under my guidance. I further assert that this work has not been submitted to any other institution in pursuit of a similar degree.

Dr. Raghvendra Gupta
Associate Professor
Department of Chemical Engineering
Indian Institute of Technology Guwahati
(IITG)Guwahati- 781039
Assam, India

Dr. Rajesh Kumar Upadhyay
Professor
Department of Chemical Engineering
Indian Institute of Technology Varanasi
(IITBHU), Guwahati- 221005
Uttar Pradesh, India

ACKNOLEDGEMENT

As I reflect on the journey that has brought me to this point and stroll down memory lane, a flood of memories tied to the IITG campus rushes into my mind. As I embark on the task of composing my PhD thesis, I am filled with gratitude toward the numerous individuals who have offered both direct and indirect support, enabling me to navigate the highs and lows of my seven-year-long expedition.

First and foremost, I humbly extend my profound gratitude to my Lord Jesus Christ for His unfailing plans and purposes, His love and mercy in my life, and for granting me the doctoral opportunity at IITG. I am thankful for being chosen for the industrial collaborative PhD project and for the supportive supervisors. Gratitude goes to my father, Pillajetti Gnananandam, for his continuous mental support, and to my mother, Sowjanya, for her unwavering faith in me.

A special place of gratitude is reserved for my supervisor, Prof. Rajesh Upadhyay, whose guidance and mentorship have nurtured a culture of optimism, faith, and continual learning in my work. I owe a debt of gratitude to Rajesh sir for exposing me to the industrial realm through the BRNS-collaborated project and for assisting me in honing my skills in Computational Fluid Dynamics (CFD) tools, Densitometry techniques employing radioactive source Cs137, and delving into the domain of high-speed image processing techniques.

I extend my thanks to my supervisor, Dr. Raghvendra Gupta, for enhancing my scientific writing and for the encouragement and motivation he provided during the peak of my PhD journey. A heartfelt thank you to Dr. K. K. Singh for fostering a pleasant work environment and aiding in scientific writing. The access to laboratory facilities and the support they provided are deeply appreciated. I am indebted to Dr. H.J. Pant and his students for their timely supply of radioactive sources. My thanks also go to Shri K.T. Shenoy, Head of ChED,

for facilitating access to laboratory facilities at BARC. The nurturing environment, positive encouragement, persistent motivation, and future-oriented optimism that have been instilled, alongside invaluable guidance, by Dr. Nirvik Sen and Dr. Sunil Goswamy, are deeply appreciated. Dr. Nirvik Sen's experienced vision for planning experimental conditions and the assistance provided in the design of the column are truly valued.

The encouraging and constructive support provided by my doctoral committee members, Prof. S. K. Majumdar, Prof. Anugrah Singh, and Prof. Amaresh Dalal, has been indispensable in guiding me through the learning process and facilitating the completion of my research.

A heartfelt thank you to my colleague Dr. Trilok Tribedi for his unwavering support, open sharing, and forward-thinking mindset. His presence and friendship during intense periods have been invaluable, particularly in the realm of RPT learning. His generosity in sharing his experimental experience as part of our team has been remarkable. I extend my gratitude to fellow colleagues Roushni Kumari, Dr. Lipika Kalo, and Keshav for their positivity and spirited contributions. Lastly, my deep appreciation to my sisters Budi, Bhanu, and my well-wisher Latha aunty, as well as my supporter Sachiv sir from IITBHU, my brother Kalasagar, my friends Rajeev, Pavan, Nikitha, Mukesh, and Mohita, my pastors Daniel and Vijay, my best friend Varaprasad, brother Charakho, Arban, Bongli and sisters Christina, Adeline, Pheni, Iban, and Pampi from the Fellowship. Your companionship and unwavering encouragement have made you a part of my extended family, and I am deeply grateful for your presence and positivity.

Pillajetti Premsagar **IIT Guwahati**

Abstract

This thesis investigates the hydrodynamic behavior within Pulsed Sieved Plate Columns (PSPC), which play a crucial role in liquid-liquid extraction processes across diverse industries, including mineral processing, pharmaceuticals, and the nuclear fuel cycle. Despite their wide application, there is a lack of experimental insights into the local hydrodynamics within PSPCs. Efficient separation requires effective contact between phases, facilitated by increased interfacial contact area. Pulsation in these columns promotes continuous delivery of new drops, enhancing separation opportunities. Our research focuses on quantifying mixing through the measurement of the local velocity of liquid streamlines. A key advantage of pulsed columns is their mechanical simplicity, resulting in reduced maintenance needs and corrosion concerns, which is particularly advantageous in nuclear fuel processing. The absence of corrosion-resistant components in these columns allows for easy maintenance and remote control, which is vital for handling radioactive materials. Our study introduces a novel approach using radioactive particle tracking to capture local field information within pulsed columns.

The main objective of this research is to understand the flow behavior and local velocity distribution resulting from pulsation intensities and two-phase flow effects in pulsed columns. Experimental investigations are carried out in laboratory-scale (76mm diameter) and pilot-scale (210mm diameter) pulsed sieve plate columns. Various plate configurations, pulsation intensities, and flow conditions are explored using non-intrusive radioactive particle tracking. Experiments are conducted in three stages: no-flow conditions to study the impact of pulsation alone, single-phase conditions to investigate the effects of continuous aqueous flow and varying pulsation intensities, and multiphase conditions to examine the influence of dispersed phase flow rates. Results reveal significant fluctuating velocity components due to pulsation, with axial fluctuations dominating and radial fluctuations also being notable. Fluctuations in

axial direction decrease during single-phase flow compared to no-flow conditions, resulting in lower axial RMS velocity and turbulent kinetic energy. The slotted plate structure displays higher radial RMS values, while the sieve plate structure shows elevated axial RMS values. Furthermore, multiphase scenarios intensify axial and radial fluctuations. Column diameter variations result in slightly decreased local velocities with larger diameters. Increased diameter reduces the axial dispersion and local velocity. Annular zones exhibit increased fluctuations compared to central and peripheral zones in both column diameters, indicating elevated mixing and enhanced mass transfer.

This work provides a comprehensive exploration of the velocity field within pulsed sieve plate extraction columns, utilizing the radioactive particle tracking technique. The study spans various operational modes, plate configurations, and column diameters, providing insights into the intricate hydrodynamics and effects of pulsation and flow conditions in PSPCs. The findings offer valuable insights for designing and optimizing efficient liquid-liquid extraction processes. Ultimately, this thesis culminates in a comprehensive analysis of local hydrodynamics within a 3-inch laboratory-scale column, driving the design of a pilot-scale column with a 9-inch diameter. Local hydrodynamic effects, particularly in relation to pulsation and flow conditions, are thoroughly explored, with implications drawn from both experimental and scale-up studies.

As we peer into the future, opportunities abound for advancing research within the domain of pulsed column processes. Novel plate designs hold promise for innovation, while multiphase studies encompassing critical parameters present avenues for comprehensive insights. The interplay between drop size distribution, velocity fluctuations, and mass transfer outcomes offers an exciting avenue for further exploration. Leveraging existing data and incorporating advanced computational methods and artificial intelligence models offer the potential to revolutionize pulsed column processes, driving enhanced efficiency, optimized designs, and

elevated understanding. This dynamic interplay positions pulsed column processes at the forefront of liquid-liquid extraction advancements.

Keywords: Pulsed column, Sieve plate, Slotted plate, Hydrodynamic Investigation, Liquid-Liquid extraction, Radioactive particle tracking, Pilot scale, Scale-up, Turbulent kinetic energy

Graphical Abstract

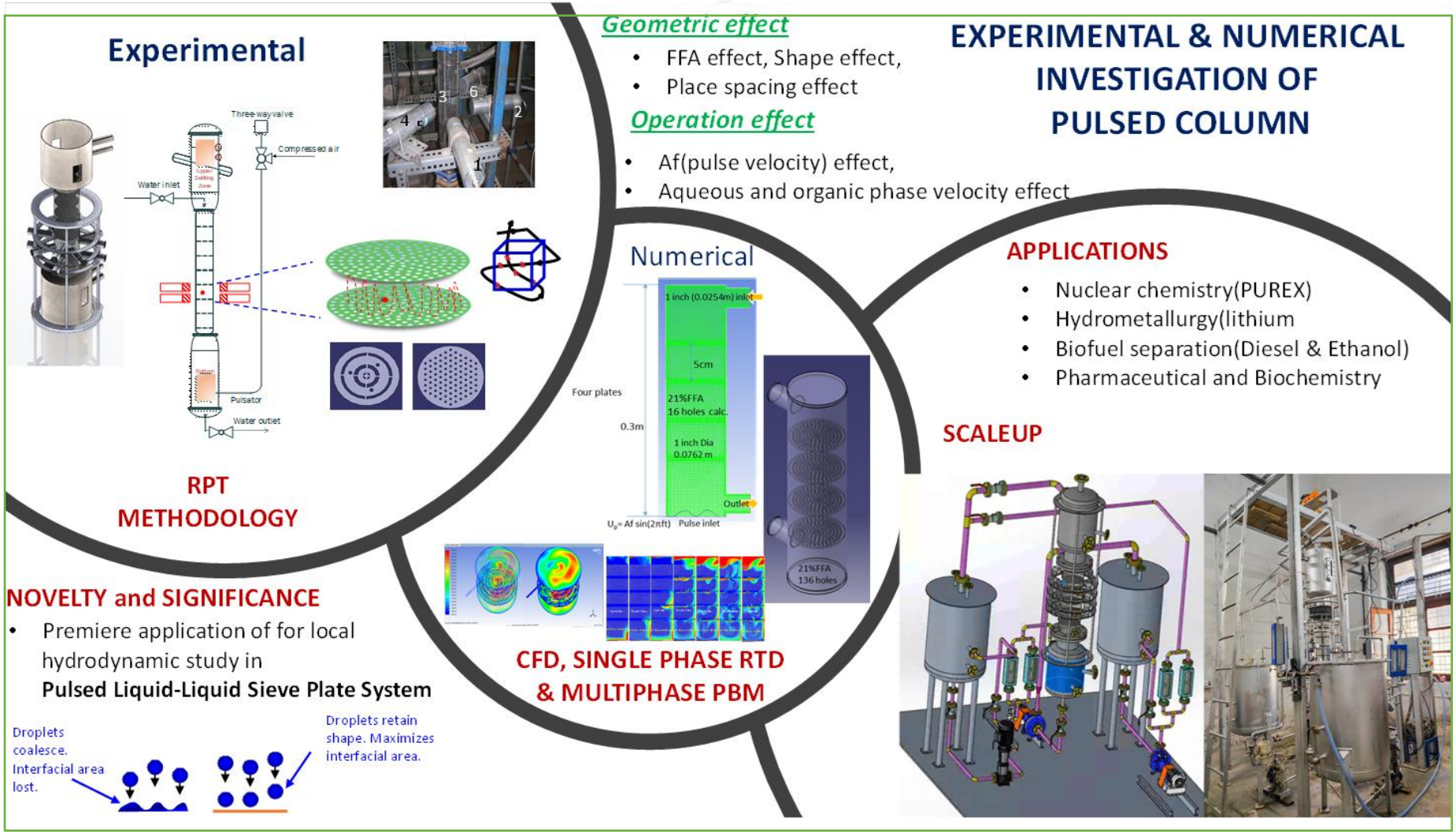

Contents

List of Figures

List of Tables

Nomenclature

D	Column Diameter	cm
d	Plate spacing	cm
Af	Pulsation Intensity	cm/s
LPH	The flow rate of the aqueous phase	litres/hour
$\emptyset$	Fractional Free area	[-]
f	Frequency	Hz
TKE	Turbulent kinetic energy	cm^2/s^2
V_c	Continuous (Aqueous) phase velocity	cm/s
V_d	Dispersed (Organic) phase velocity	cm/s

Abbreviations

$PSPC$	Pulsed Sieve Plate column
RMS	Root Mean Square
CFD	Computational Fluid Dynamics

Prefix and Suffix

q	Index for three-dimensional component
r	Radial component
θ	Azimuthal component
z	Axial component

CHAPTER-I

Introduction

भारतीय प्रौद्योगिकी संस्थान गुवाहाटी
Indian Institute of Technology Guwahati

Chapter 1 : Introduction

Graphical abstract

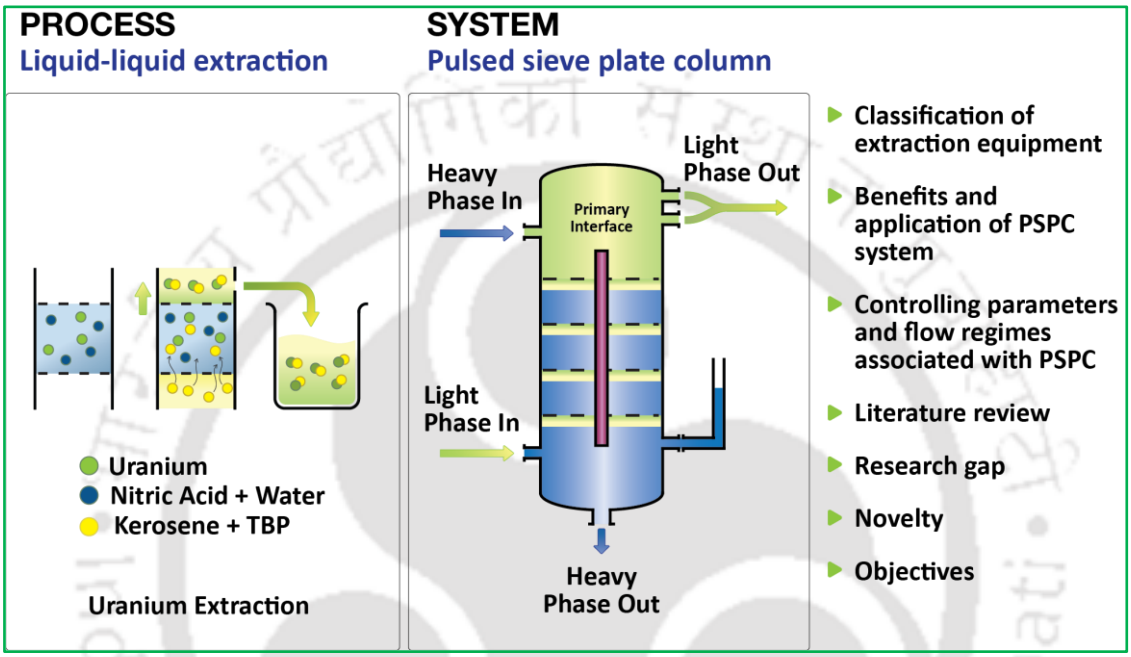

भारतीय प्रौद्योगिकी संस्थान गुवाहाटी
Indian Institute of Technology Guwahati

Abstract

In this chapter, the motivation for selecting the pulsed sieve plate extraction column and the criteria for choosing the investigating parameters are discussed. Additionally, a brief overview of the utilization of the pulsed sieve plate extraction column in the context of liquid-liquid extraction processes, specifically uranium enrichment and nuclear fuel reprocessing, is provided. The chapter also explores the applications of the liquid-liquid extraction process and highlights the significance of the pulsed sieve plate column. Various types of extraction equipment commonly used in the industry are examined, emphasizing the specific advantages offered by the pulsed column. Moreover, the chapter explains the design parameters, geometric considerations, and operational variables that influence the efficiency of extraction and the flow regimes within the pulsed sieve plate extraction column (PSPC). Furthermore, the chapter details the motivation behind the research presented in the thesis literature review, highlights the novelty of the study, and outlines the objectives of the investigation conducted in the reported work.

भारतीय प्रौद्योगिकी संस्थान गुवाहाटी
Indian Institute of Technology Guwahati

1.1 Liquid-liquid extraction (LLE)

Liquid-liquid extraction, also known as solvent extraction, is a separation technique used to separate and purify compounds from a mixture. It involves the transfer of one or more components of a liquid mixture into another immiscible liquid phase, based on the differences in their solubilities or partition coefficients.

The process of liquid-liquid extraction typically involves the following steps:

1. Selection of Solvents: Two immiscible solvents are chosen, one being the original liquid mixture (feed or source phase) and the other serving as the extracting solvent (extract or solvent phase). The choice of solvents depends on the specific compounds being separated and their solubilities in each solvent.
2. Mixing: The two liquid phases are mixed together, allowing for mass transfer between them. The compounds of interest in the feed phase distribute themselves between the two phases based on their relative affinities for each solvent.
3. Separation: After sufficient mixing, the two liquid phases are allowed to separate into distinct layers due to their immiscibility. This results in the formation of an organic phase (containing the extracted compounds) and an aqueous phase (containing the remaining components).
4. Recovery: The organic phase, which contains the desired compounds, is separated from the aqueous phase. Various techniques such as decantation, separation funnels, centrifugation, or specialized equipment like liquid-liquid extractors can be employed for efficient separation.

Liquid-liquid extraction offers a versatile and efficient means of separation, allowing for the extraction, purification, and isolation of compounds from liquid mixtures. The need for liquid-liquid extraction arises in various scenarios (Godfrey et al., 1995; Jahya et al., 2005), including:

1. Separation of Components: Liquid-liquid extraction allows for the separation of different components from a mixture based on their solubilities or partition coefficients in different solvents. It enables the isolation of specific compounds or the removal of impurities.
2. Purification: Liquid-liquid extraction helps in purifying compounds by selectively transferring them into a different solvent phase. It can remove impurities, unwanted byproducts, or contaminants present in the original mixture.
3. Concentration: Liquid-liquid extraction can be used to concentrate a specific compound in a solution. By repeatedly extracting the target compound into a small volume of the extracting solvent, its concentration can be increased.
4. Isolation of Products: In chemical synthesis, liquid-liquid extraction is often employed to separate and isolate products from reaction mixtures. It aids in the purification and recovery of valuable compounds.
5. Sample Preparation: Liquid-liquid extraction is utilized as a sample preparation technique in analytical chemistry. It helps extract analytes of interest from complex matrices, making them amenable to analysis by various instruments or methods.

1.1.1 Modes of LLE

Liquid- liquid extraction process can be operated in a single stage or in a multistage. In the context of liquid-liquid extraction (LLE), a stage refers to a discrete step or unit within the extraction process. It represents a point where the two liquid phases, the feed phase and the solvent phase, come into contact and undergo mixing and separation. The purpose of a stage is

to facilitate the transfer of the desired solute(s) from the feed phase to the solvent phase. Single-stage liquid-liquid extraction (LLE) refers to a simple extraction process where only one stage is involved. In this process, the feed phase and the solvent phase are mixed together, allowing for mass transfer of the solute(s). The resulting mixture is then separated into two distinct phases, with the solute(s) being transferred from the feed phase to the solvent phase. Single-stage LLE is typically used for basic separations or when a relatively low level of purity or concentration is required. On the other hand, multistage liquid-liquid extraction involves multiple stages arranged in series. Each stage consists of mixing the feed phase with the solvent phase, followed by phase separation. The solvent phase from one stage becomes the feed phase for the next stage, and the process continues iteratively. The purpose of multistage LLE is to enhance the separation efficiency and achieve higher levels of solute concentration in the solvent phase. It is commonly used for complex separations or when a higher degree of purification or enrichment is desired. Multi stage extraction can be operated in three modes namely co-current, counter-current, and cross-current extraction. Each mode represents a distinct flow configuration of the liquid phases, which significantly affects the efficiency and performance of the extraction process. Different contacting ways for the extraction process are shown in Figure 1.1.

1. Co-Current Extraction: In co-current extraction, both the feed phase and the extracting solvent flow in the same direction. This mode offers a high initial extraction rate due to the significant concentration gradient at the entrance. However, as the two phases move together, the concentration difference diminishes, potentially leading to a decrease in extraction efficiency.
2. Counter-Current Extraction: Counter-current extraction involves the feed phase and the extracting solvent flowing in opposite directions. This configuration ensures efficient

mass transfer and high extraction efficiencies throughout the length of the extraction equipment. The concentration gradient is maintained, allowing for continuous extraction and optimal solvent utilization.

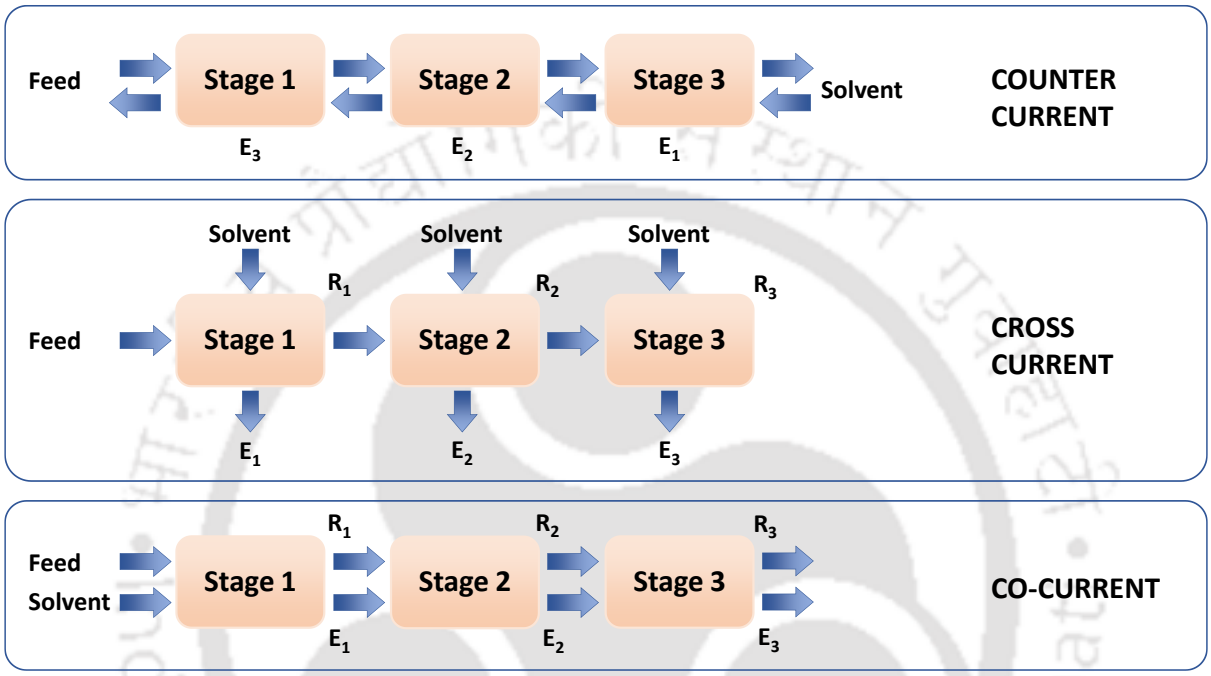

Figure 1.1: Modes of contact of Liquid-liquid extraction

3. Cross-Current Extraction: Cross-current extraction, a hybrid mode, combines elements of co-current and counter-current extraction. In this mode, the feed phase and the extracting solvent flow at an angle to each other. Cross-current extraction offers moderate extraction efficiencies, striking a balance between the high initial extraction rate of co-current extraction and the continuous extraction of counter-current extraction.

1.1.2 Application of LLE

Here are some detailed applications of liquid-liquid extraction:

1. Pharmaceutical Industry: Liquid-liquid extraction plays a crucial role in pharmaceutical manufacturing processes, including drug discovery, purification, and formulation. It is used for the separation and purification of active pharmaceutical ingredients (APIs) from reaction mixtures, removal of impurities, isolation of natural products from plant extracts, and concentration of drug compounds.
2. Chemical Industry: Liquid-liquid extraction is extensively used in the chemical industry for separation, purification, and recovery of valuable compounds. It aids in the removal of impurities, separation of byproducts, and concentration of desired chemicals. It is also employed in the production of specialty chemicals, flavors, fragrances, and dyes.
3. Environmental Analysis: Liquid-liquid extraction is employed in environmental analysis to extract and concentrate analytes from complex matrices. It is used for sample preparation in water and soil analysis, air monitoring, and detection of pollutants and contaminants. It enables the extraction and preconcentration of trace amounts of substances for subsequent analysis using various instrumental techniques.
4. Nuclear Industry: Liquid-liquid extraction is used in the nuclear industry for the extraction and separation of radioactive elements and isotopes. It plays a vital role in the production of nuclear fuel, separation of isotopes for medical and industrial applications, and the treatment of radioactive waste.
5. Food and Beverage Industry: Liquid-liquid extraction is utilized in the food and beverage industry for the extraction and purification of flavors, aromas, and bioactive compounds. It enables the separation and concentration of desirable

components from raw materials, such as fruit juices, essential oils, and natural extracts.

6. Petroleum Industry: Liquid-liquid extraction is employed in the petroleum industry for the separation and purification of hydrocarbons and other components from crude oil and petroleum products. It aids in the removal of impurities, such as sulfur compounds, aromatics, and heavy metals, to meet product quality specifications.
7. Biotechnology and Biochemical Processes: Liquid-liquid extraction is used in biotechnology and biochemical processes for the extraction and purification of biomolecules, enzymes, proteins, and bioactive compounds. It helps in downstream processing, separation of target molecules, and concentration of valuable products from fermentation broths and cell cultures.
8. Metal Extraction and Mining: Liquid-liquid extraction is utilized in the extraction and separation of metals from ores, mining solutions, and industrial waste streams. It enables the recovery and purification of metals such as copper, nickel, uranium, and rare earth elements.
9. Analytical Chemistry: Liquid-liquid extraction serves as an important sample preparation technique in analytical chemistry. It allows the extraction and concentration of analytes from complex matrices, facilitating their detection and quantification using various analytical techniques.

These applications highlight the versatility and importance of liquid-liquid extraction in various industries and scientific disciplines, enabling the separation, purification, concentration, and recovery of valuable compounds from complex mixtures (Benedict et al., 1981; Tsouris et al., 1994; Yung et al., 2012; Mehrkesh et al., 2013; Ghadiri et al., 2020).

Among the mentioned applications, the recovery of lithium metal and uranium mineral, is of particular importance due to the increasing demand in next-generation energy sources. Lithium metal is essential for advanced energy storage solutions, particularly in lithium-ion batteries used in EVs, portable electronics, and renewable energy storage. The extraction and production of lithium metal are of utmost importance for the development of advanced and sustainable energy storage solutions. At the same time, alternate energy resource is nuclear power which uses uranium mineral. Nuclear power provides low-carbon electricity without greenhouse gas emissions. Uranium is the primary fuel for nuclear reactors, undergoing fission to release substantial energy. Nuclear power plants can reliably generate large amounts of electricity, offering a scalable solution for countries aiming to reduce carbon footprint. However, uranium mining and nuclear power entail environmental and safety considerations, such as proper waste management and reactor safety protocols. Uranium extraction from pure nuclear fuel involves a process called reprocessing, which typically includes the melting of uranium rods in a nuclear reactor during the consumption by nuclear fission process. The example of uranium extraction which is our current focus of interest is detailed in Figure 1.2. The method for extracting uranium from the melted rods involves the use of organic solvents such as dodecane/kersone and tributyl phosphate (TBP). In this process, the melted uranium rods from the acidic medium of 3N nitric acid are dissolved in dodecane/kerosine, which acts as the organic solvent.

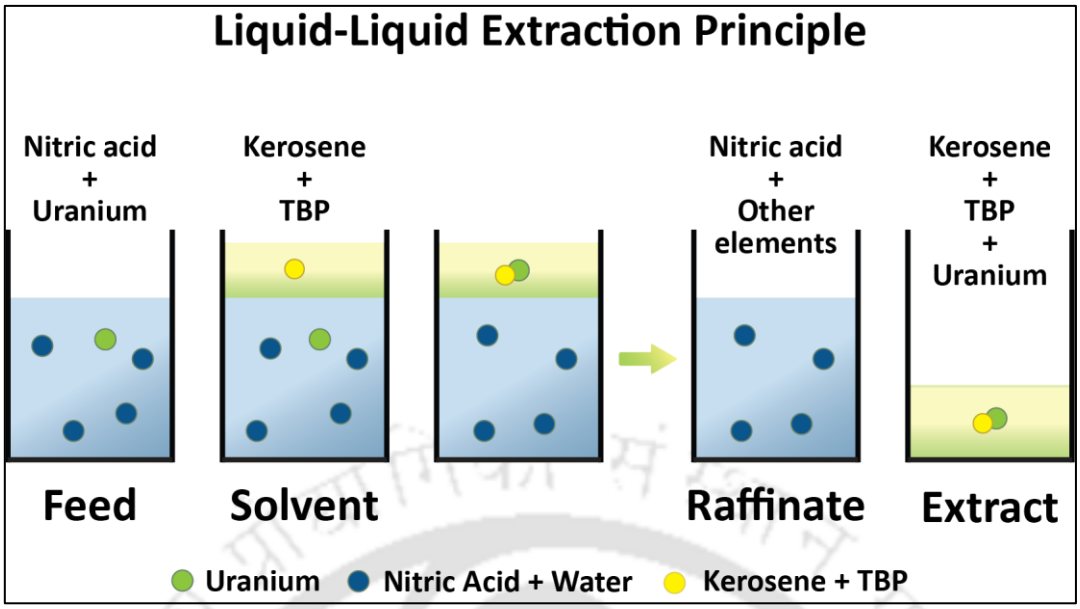

Figure 1.2: Liquid-Liquid extraction principle

Dodecane helps in separating the uranium from other components present in the rods. TBP, which is mixed with dodecane/kerosine, serves as a complexing agent to selectively extract uranium ions. The uranium containing dodecane/kerosine solution is then subjected to a series of chemical processes to separate and purify the uranium. This typically involves using different solvents and techniques to separate uranium from impurities and other radioactive elements. This process is called back extraction and is shown in Figure 1.3.

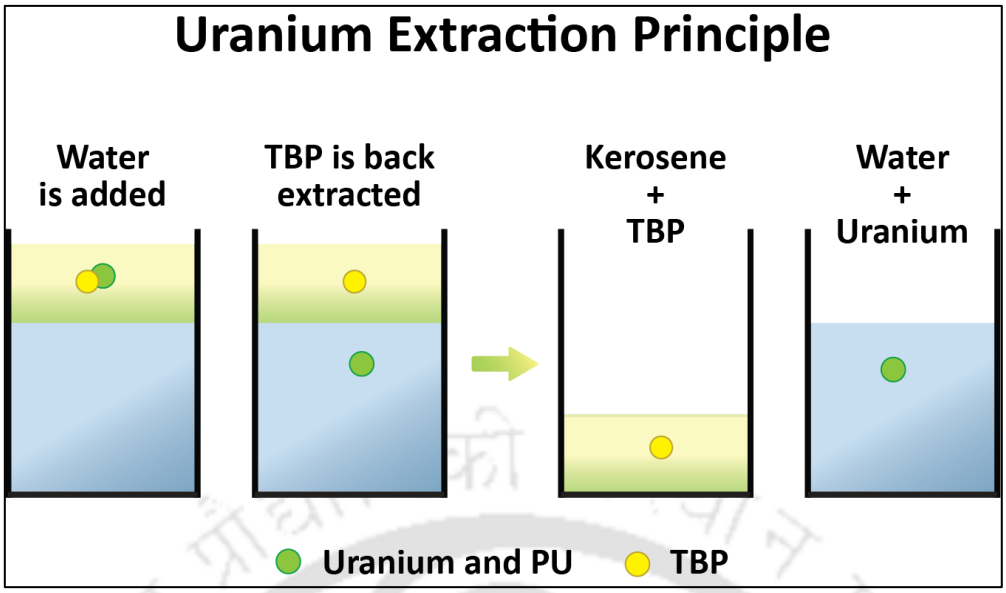

Figure 1.3: Uranium back extraction process

1.1.3 Classification of extraction equipment

The literature suggests various methods of agitation for extraction, and there are numerous notable phenomena that can impact the effectiveness of liquid-liquid extraction columns. Two common types of extraction equipment are mixer settlers and column contactors, which can be further classified based on their operation mode as static or agitated, Figure 1.4 provides a classification of extraction equipment based on size and agitation mode, which can help in selecting the appropriate extractor.

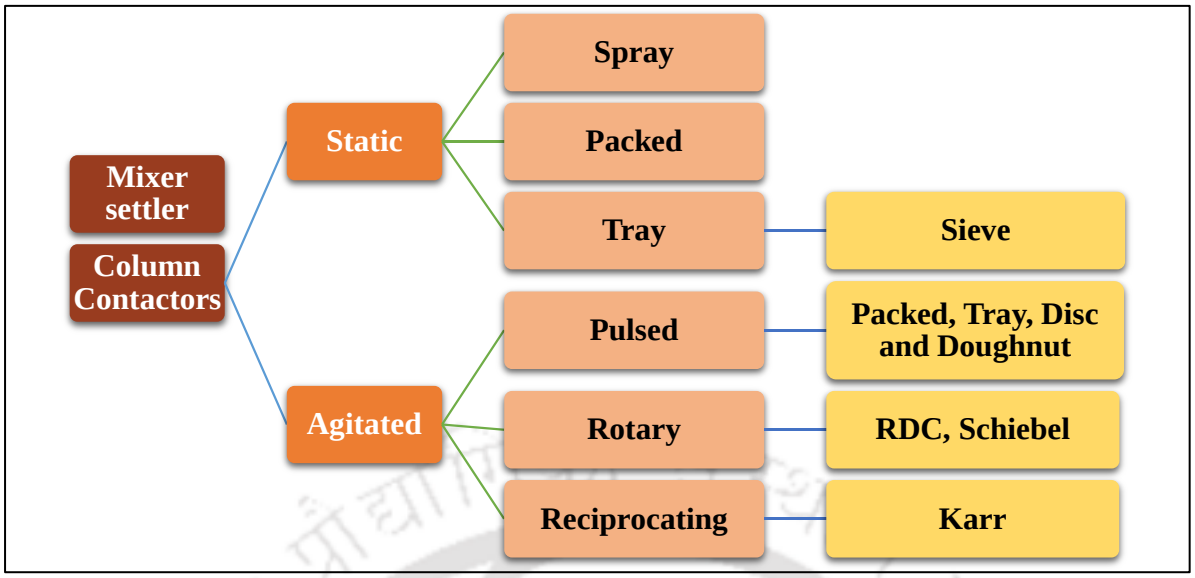

Figure 1.4: Classification of extraction equipment

1. Mixer Settlers: Mixer settlers are widely used in liquid-liquid extraction processes and consist of two main sections: a mixing section and a settling section. The mixing section promotes intimate contact between the two liquid phases, allowing for efficient mass transfer. The settling section allows the separated phases to separate based on density differences. Mixer settlers can be classified as follows:

   a. Static Mixer Settlers: Static mixer settlers operate without any mechanical agitation. They rely on gravity and residence time for phase separation. Static mixer settlers are simple in design, require less maintenance, and are suitable for processes where gentle mixing and separation are sufficient.

   b. Agitated Mixer Settlers: Agitated mixer settlers incorporate mechanical agitation to enhance mass transfer and improve phase separation. The agitation promotes greater interfacial area and facilitates the transfer of solutes between the two liquid phases. Agitated mixer settlers are suitable for applications requiring faster kinetics and higher efficiency.

2. Column Contactors: Column contactors, also known as extraction columns or extraction towers, are vertical vessels where liquid-liquid extraction takes place in a continuous countercurrent flow arrangement. These columns consist of multiple stages or trays to maximize contact between the liquid phases. Column contactors can be classified based on their operation mode:

    a. Static Column Contactors:

    Static column contactors operate without any mechanical agitation. They rely on gravity and the interaction between the liquid phases as they flow through the trays or packing. Static column contactors are often used in processes where separation requirements can be achieved without agitation.

    b. Agitated Column Contactors:

    Agitated column contactors incorporate mechanical agitation, such as the use of stirrers or impellers, to enhance mixing and mass transfer. The agitation helps to create a greater interfacial area and promotes efficient transfer of solutes between the liquid phases. Agitated column contactors are commonly used when higher extraction efficiency and faster kinetics are desired.

Specialized Designs: Within the classification of extraction equipment, there are various specialized designs that cater to specific extraction requirements. Some notable examples include:

a. Pulsed Extraction Equipment: Pulsed extraction equipment utilizes periodic variations in flow rates, pressure, or other operational parameters to enhance mass transfer and improve extraction efficiency.

b. Rotary Disc Contactor (RDC): The RDC design involves a rotating disc or a series of discs, providing increased interfacial area and promoting efficient mass transfer between the liquid phases. The rotation of the discs aids in mixing and separating the phases.

c. Scheibel Column: Scheibel columns are designed with a specific packing arrangement, such as structured packing or random packing, to enhance the contact between the liquid phases and promote efficient extraction.

d. Karr Column: Karr columns, also known as Karr extraction columns, are column contactors designed with special internals, such as sieve trays or bubble cap trays, to optimize mass transfer efficiency and separation performance.

1.2 Pulsed sieve plate column

A pulsed sieve plate extraction column is a type of separation column used in chemical engineering and industrial processes for the separation of liquid-liquid or gas-liquid mixtures. In order to fully understand a pulsed sieve plate extraction column (Van Dijck et al., 1935), a three-way solenoid valve is utilized in the pneumatic leg, and the operation is described in greater detail below.

1. Column Setup:
    - The pulsed sieve plate extraction column consists of multiple vertically arranged sieve plates or trays, designed to promote mass transfer between liquid phases
    - The plates are stacked on top of each other, creating a vertical flow path for the liquids in between the stages

- A three-way solenoid valve is integrated into the column as part of the pneumatic leg system for time rated control of compressed air

2. Pneumatic Leg:
    - The pneumatic leg is a key component that controls the flow of gas or air into the column.
    - It assists in generating the pulsation or oscillation required for efficient mass transfer.
    - The three-way solenoid valve is responsible for directing the flow of gas or air into the column.

The schematic of pulse sieve plate column (PSPC) with its components of active section, disengagement section and pulse leg is shown in the Figure 1.5

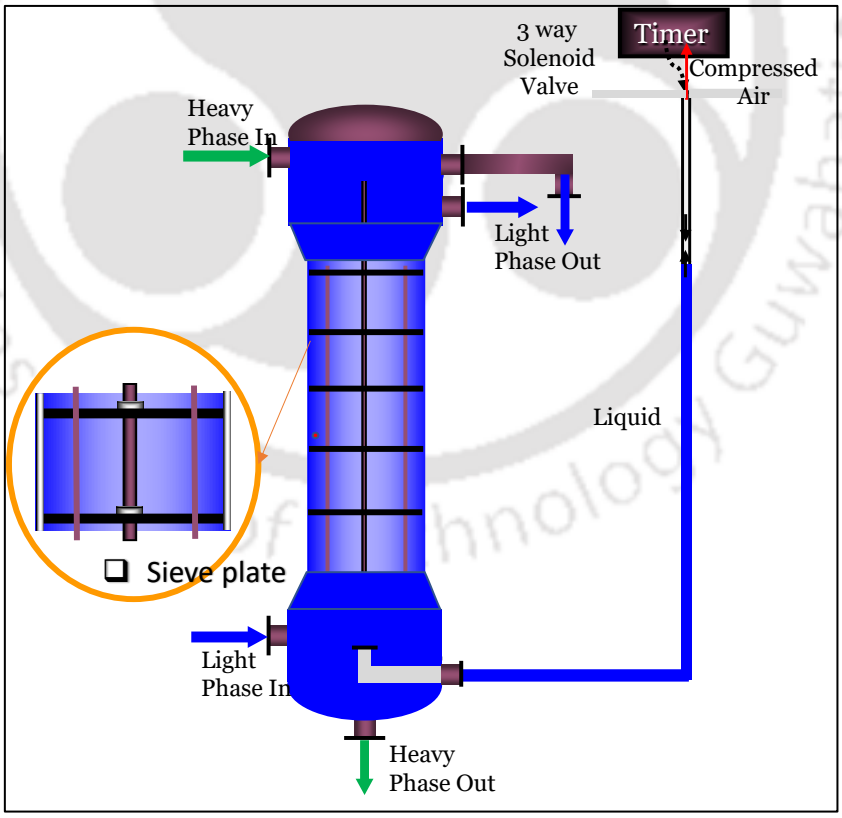

Figure 1.5: Schematic of pulse sieve plate column (PSPC)

3. Operation:
    - The pulsed sieve plate extraction column operates in cycles, typically consisting of two strokes: upstroke and downstroke.
    - This mechanism introduces intermittent pressure or flow variations within the column, causing pulsating movements of the liquid phases
    - The three-way solenoid valve plays a crucial role in regulating the flow of gas or air during these strokes.
    - As the feed mixture and solvent flow through the column, the solute molecules transfer from the feed phase to the solvent phase, based on their affinity and distribution coefficients. The pulse action within the column helps increase the contact time between the two phases, resulting in improved extraction efficiency
4. Upstroke:
    - During the upstroke, the three-way solenoid valve is set to allow the flow of gas or air from an external source into the pneumatic leg.
    - This leads to the pressurization of the pneumatic leg, exerting pressure on the liquid in the column.
5. Pulsation Generation:
    - As the pneumatic leg gets pressurized, the gas or air pushes the liquid phase in the column upwards.
    - The increased pressure induces the formation of dispersed liquid droplets promoting interfacial contact between the liquid phases.

- This pulsation generated by the pneumatic leg enhances the mass transfer rates and improves the separation efficiency of the column.

6. Downstroke:
    - After the upstroke, the three-way solenoid valve switches its position to redirect the flow of gas or air out of the pneumatic leg.
    - This depressurizes the pneumatic leg, causing the liquid phase to move downwards due to gravity.
7. Shifting Dispersed Phases:
    - During the downstroke, the liquid phase that was dispersed during the upstroke now shifts its position within the column.
    - The downward movement of the liquid phase allows for the exchange of dispersed phases, further aiding in separation.
8. Repeating the Cycle:
    - The cycle comprising the upstroke and downstroke is repeated continuously to maintain the pulsation and promote effective mass transfer.
    - The three-way solenoid valve switches between allowing the flow of gas or air into the pneumatic leg during the upstroke and redirecting the flow out of the pneumatic leg during the downstroke.

By utilizing a three-way solenoid valve in the line of the pneumatic leg of pulsed sieve plate extraction column, the pulsation required for enhanced mass transfer and separation is achieved. The valve's ability to control the flow of gas or air allows for the cyclic operation of the column, facilitating the movement of liquid phases and promoting efficient extraction process.

1.2.1 Specific benefits and applications of PSPC

Pulsed columns are particularly useful in nuclear industries because they lack mechanical parts and can be remotely agitated. Pulsed sieve-plate columns require less maintenance and can be operated remotely with ease. Pulsing the fluid in the light phase will create shear stresses on the fluid across the sieve plates, resulting in the systematic production of droplets. The strong turbulence created by columns of pulsating air permits greater dispersion and a larger contact area between phases. Pulsed sieve plate extraction columns offer several benefits and find applications in various industries. Here are the specific benefits and applications of these columns:

Benefits of Pulsed Sieve Plate Columns:

1. Enhanced Mass Transfer: Pulsed operation in these columns improves mass transfer rates by promoting better interfacial contact between the liquid and vapor phases. The pulsation helps in breaking up stagnant liquid films, creating oscillating drops or bubbles that enhance the transfer of solutes or components (Amani et al., 2017; Bart et al., 2008)
2. Improved Separation Efficiency: The pulsation generated in these columns increases the driving force for mass transfer, leading to improved separation efficiency. The oscillating drops or bubbles facilitate better mixing and distribution of components, allowing for more effective extraction or distillation.
3. Reduced Equipment Size: Pulsed sieve plate extraction columns can achieve the same separation efficiency as traditional columns but with smaller equipment size. The enhanced mass transfer rates and improved separation efficiency enable the design of more compact columns, resulting in cost savings and reduced footprint.

4. Flexibility in Operation: Pulsed sieve plate extraction columns offer flexibility in operation. The pulsation can be adjusted to optimize the extraction or distillation process for specific applications. By varying the frequency, amplitude, and duration of the pulsation, the column's performance can be tailored to meet desired separation goals.

1.2.2 Applications of pulsed sieve plate columns

Solvent Extraction: Pulsed sieve plate extraction columns are widely used in solvent extraction processes, particularly in the purification and separation of metals or valuable compounds from ores, concentrates, or waste streams. They are employed in industries such as mining, metallurgy, and recycling.

1. Liquid-Liquid Extraction: These columns are utilized for liquid-liquid extraction processes, where two immiscible liquid phases are contacted to selectively transfer components from one phase to another. Pulsed sieve plate extraction columns enable efficient separation of components based on their solubility or partitioning properties.
2. Distillation: Pulsed sieve plate extraction columns find application in distillation processes, where they help separate components based on their different boiling points. The enhanced mass transfer rates provided by the pulsation facilitate efficient vapor-liquid contact, allowing for improved separation of volatile components.
3. Chemical and Petrochemical Industries: Pulsed sieve plate extraction columns are utilized in various chemical and petrochemical industries for separation, purification, and recovery processes. They are employed in the production of specialty chemicals, pharmaceuticals, polymers, and fuels, among others.
4. Environmental Remediation: These columns play a role in environmental remediation processes, such as the removal of pollutants or contaminants from wastewater or

industrial effluents. Pulsed sieve plate extraction columns aid in the separation and recovery of valuable resources while mitigating environmental impact.

5. Research and Development: Pulsed sieve plate extraction columns are also used in research and development activities, where scientists and engineers explore new separation techniques or optimize existing processes. They provide a versatile platform for studying and improving mass transfer phenomena in liquid-liquid or gas-liquid systems.

Overall, pulsed sieve plate extraction columns offer benefits such as enhanced mass transfer, improved separation efficiency, reduced equipment size, and operational flexibility. They find applications in solvent extraction, liquid-liquid extraction, distillation, chemical and petrochemical industries, environmental remediation, and research and development, contributing to efficient separation processes in various fields.

1.2.3 Parameters of PSPC

Pulsed column operation depends on the specific conditions related to its shape and how it is operated. The performance of the column is influenced by various factors, such as flooding limits, regime transitions, droplet size, hold-up, and mass transfer. These factors are affected by both the geometric and operational parameters of the pulsed column. Geometric parameters can be divided into two categories: plate spacing and fractional-free area. The behaviour of the fluid in the pulsed columns is influenced by geometric factors such as the area of the plate openings, the diameter and spacing between plates, the thickness of the plates, and the structure of the plate openings. Operational parameters, such as the flow rates of the phases, the amplitude and frequency of the pulsation, also play a role in determining the behaviour of the fluid. Different types of plates are used for extraction applications, and the efficiency of dispersion is affected by the fractional free area of the plates and the pitch of the openings. It

is recommended to have a fractional free area of 21 to 23 percent for extraction applications. The size of the dispersed phase is crucial for efficient mass transfer. Apart from geometric design characteristics, the operating parameters also impact the performance of the column. These parameters include the pulsation velocity, which is determined by the amplitude and frequency of the pulsation, and the flow rates or superficial velocities of the phases. The pulsation velocity is the product of the pulsating frequency and amplitude, representing the displacement per unit time and having the units of velocity. The pulsating amplitude refers to the extent of liquid displacement in the active column. The pulsation frequency is defined by the rate at which the three-way solenoid valve opens and closes. The typical range for pulse velocity in pulsed columns is between 10 mm/s and 50 mm/s. In the Pulsed sieve plate column (PSPC), it is important to maintain similar residence times for both phases by keeping the flow rates of both phases low. The flow rate of the organic phase should be slightly higher than that of the aqueous phase. The bottom distributor is used to introduce kerosene/dodecane into the column

1.2.4 Flow regimes of PSPC

A flow regime map, also known as a flow regime diagram, is a graphical representation that classifies the different flow regimes that occur in a multiphase system, typically involving gas-liquid or liquid-liquid flows. It is also defined as the description of flow structure or distribution of one fluid to the other. It provides a visual depiction of the dominant flow patterns or regimes as a function of relevant operating parameters, such as flow rates, fluid properties, and vessel geometry. Flow regime maps play a crucial role in reactor design and development. They help in understanding flow behavior, selecting and sizing reactors, evaluating performance, ensuring process safety, and guiding reactor optimization efforts. By leveraging the information provided by flow regime maps, engineers can design reactors that operate within

the desired flow regimes, leading to efficient and reliable processes. Flow regimes in pulsed-sieve plate columns depend on the operating and geometric parameters of the column, as well as the liquid-liquid system's characteristics. Patwardhan et al. discovered three stable regimes (mixer-settler, dispersion, and emulsion) and one unstable regime, with transitions happening between these regimes based on pulsation circumstances. At both low and high pulsation intensities, flooding is possible, and its presence can lead to unstable regimes defined by local phase inversions. Hold-up, drop size, and drop fragmentation are crucial metrics for describing the various flow regimes. Understanding the various flow regimes in pulsed sieve plate columns is essential for maximizing their performance in liquid-liquid separations. Figure 1.6 illustrates the different flow regimes in the PSPC. The hydrodynamic characteristics of pulsed-sieve plate columns are dependent on their operating parameters and geometric parameters. Patwardhan et al. observed three stable regimes, namely mixer settler, dispersion, and emulsion, and one unstable regime for a constant liquid flow rate (Sen et al., 2015). The transition between different regimes is influenced by pulsing conditions (amplitude and frequency), flow rates of the liquid-liquid system, and column geometry. Flooding occurs at higher and lower pulsation intensities.

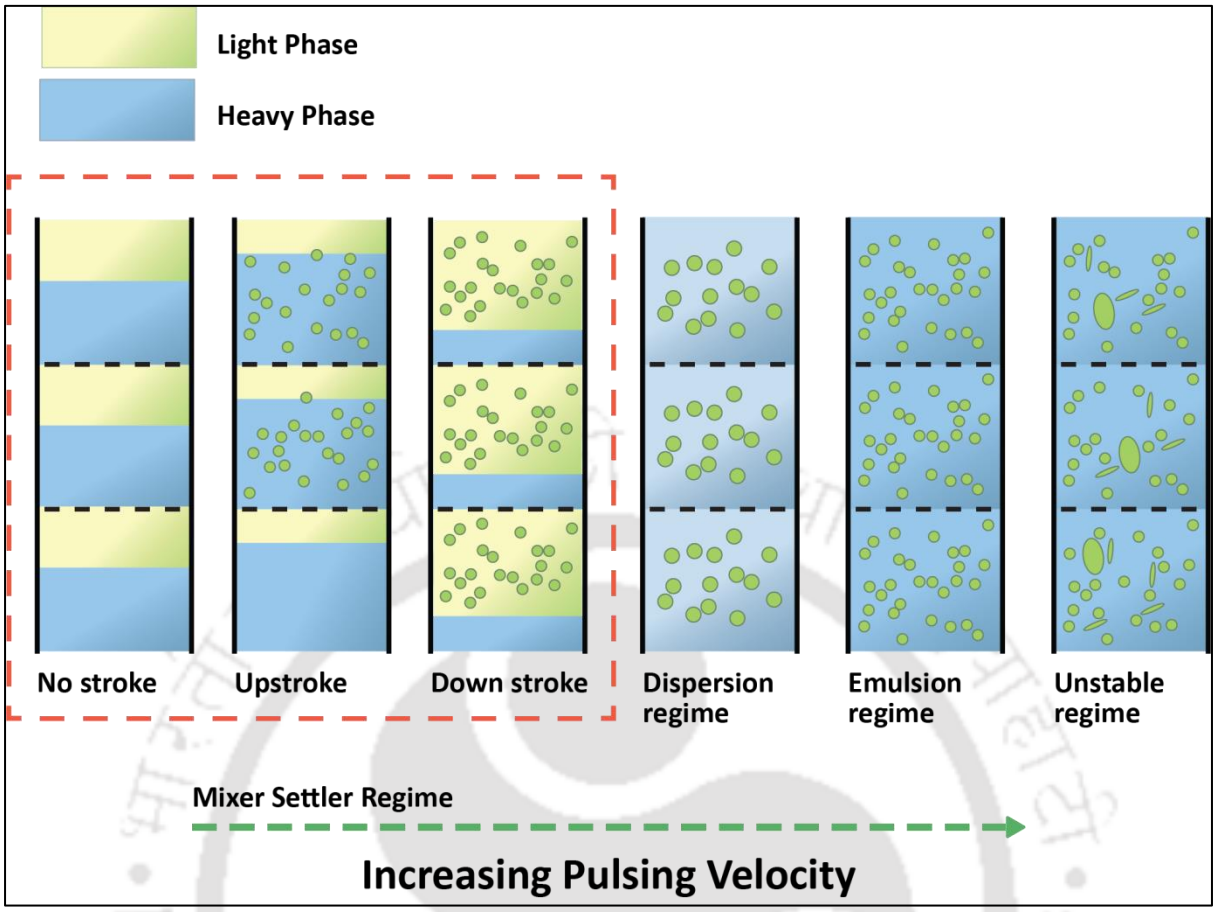

Figure 1.6: Flow regimes of pulsed sieve plate column (hold up)

In plate systems with insufficient pulsing inundation, drops are unable to travel through small-diameter holes, leading to flooding. In systems with higher interfacial tension due to density differences, no flow occurs, whereas systems with lower interfacial tension allow small drops to penetrate plate holes. The mixer-settler regime divides the light and heavy phases into discrete layers, reducing phase separation and hold-up. The drop size distribution is uneven in the dispersion phase, starting at the minimum hold-up point. The emulsion regime enhances inertial and shear forces, causing drops to break and form emulsions. The unstable regime is characterized by localized phase inversion at different points of the column, resulting in smaller drop sizes and higher hold-up. Excessive pulsing inundation occurs when shear pressures on drops increase, resulting in smaller drops with a lower terminal rise velocity compared to the

superficial velocity of the continuous phase. Drops travel through the exit of the continuous phase with higher pulse velocities, leading to flooding (Yadav et al. 2008).

The dispersion regime and emulsion regime are critical stages in the liquid-liquid extraction process within pulsed columns. These regimes are responsible for achieving a uniform distribution of the two liquid phases and ensuring optimal mixing within the column. Successfully operating the column within these regimes presents a significant challenge of interest. In our current work, we are primarily focused on addressing this challenge and exploring the operation of the dispersion regime as a key area of investigation.

1.3 Literature survey on PSPC

Table 1.1: Literature on PSPC

Author Name	Column Details	Single Phase/ Multiphase	Numerical/Experimental	Conditions of Operation	Measurement Parameter	Key Conclusions
Rao et. Al., (1977)	50.8 mm dia, 1 m length	Single Phase	Experimental	Continuous phase velocity, pulse amplitude, frequency	Residence Time Distribution (RTD), Mixing behavior	Two distinct regions for superficial velocity observed, the impact of turbulence on dispersion coefficient
Hartmut et al. (1980)	80 and 225 mm diameters	Single Phase	Experimental	Operating conditions of pulsed sieve plate columns	Axial hold-up profiles, Drop size distributions (DSD)	Validated fluid dynamics model for water-toluene system without mass transfer
Britsch et al., (1983)	300 mm column	Multiphase	Experimental	Phase distribution effect on	Residence Time Distribution (RTD),	Impact of pulse amplitudes on back mixing

				mixing efficiency	Dispersion coefficients	varied with phase ratio
Lorenz et al., (1990)	80 and 225 mm 29nalyses, 23% FFA, plate spacing is 10mm	Single Phase	Experimental	Various sieve plate designs, operating parameters	Drop size, Hold-up, Flooding throughput	System, pulsation conditions, and plate shape influenced PSPC hydrodynamics
Angelov et al., (1998)	Column dia290 mm, disk dia 254 mm, 23%FFA, 45mm plate spacing	Single Phase	Experimental	PIV, LDA techniques for velocity field distribution	Turbulent energy parameters	Energy distribution influenced by pulsed flow, impact on drop size prediction
Nabli et al., (2002)	288mm diameter	Single Phase	Numerical	Geometric and dynamic parameters	Hydrodynamics of pulsed columns	CFD used for contactor design, refining parameter values
Bhujalski et al., (2006)	1m height, 0.1m dia	Single Phase	Experimental	Disc-doughnut internals, varying pulsation intensities	2D computational grid, Low Reynolds Number k-turbulence model	Impact of internal geometry on flow hydrodynamics
Yadav. Et al., (2007)	50 mm diameter and 50cm length	Multiphase	Experimental	Pulsed sieve plate extraction column design	Drop size distribution, Mass transfer correlations	Correlation between flooding, drop size, and hold-up for column design
Din et al., (2008)	50 mm diameter and 2m length	Multiphase	Experimental	Hydrodynamic properties of	Residence Time Distribution (RTD),	Effective use of 68Ga as a radiotracer for water labeling

				continuous phase	Surface velocities	
Yadav et al., (2010)	50 mm diameter and 50cm length	Single Phase	Numerical	Eulerian-Eulerian approach, k-means turbulence model	Hydrodynamics of plate extraction columns	CFD model analyzed impact of down-comer geometry
Drumm et al., (2011)	Lab-scale 150 mm	Single Phase	Numerical	Micro- and macro-phenomena, CFD models with PBM	Multiphase turbulence models, Kernel closures	Improved liquid-liquid extraction design using CFD models
Changchun. Et al., (2011)	400 mm diameter and 1.4 cm diameter	Multiphase	Experimental	Downcomer structure modifications	Flow pattern optimization	Adjustments in downcomer structure reduced reverse flow area
Din et al. (2013)	50 mm diameter and 2m length	Multiphase	Experimental	Effect of surface velocity on axial dispersion	Axial dispersion, Slip velocity	Axial dispersion decrease with increasing surface velocity of continuous phase
Amokrane et al., (2014)	50 mm diameter	Multiphase	Numerical	Droplet transport, fragmentation, coalescence	Turbulent variables, CFD model validation	Influence of turbulent variables on dispersed phase behavior
J. Li et al., and Bardin et al. (2014)	30 mm diameter	Multiphase	Numerical	Flow behavior, phase distribution, residence time distribution	Interfacial mass transfer, CFD simulations	Insight into flow patterns, mixing efficiency in multiphase mode
J. Wang et al., (2014)	30 mm diameter	Single Phase	Numerical	Pulsation-induced flow patterns,	Velocity profiles, Turbulence	CFD simulations provided insights into

				plate geometry	characteristics	velocity field distribution
Sen at al., (2015)	76 mm diameter, 2D representation	Single Phase	Numerical	Pulsed sieve-plate extraction columns	Computational fluid dynamics (CFD) approach	2D simulations validated with experimental data, reduced computational effort
Khatir et al., (2016)	150 mm diameter, PSPC in nuclear fuel reprocessing	Single Phase	Numerical	Unsteady flow simulations, RANS model, k-epsilon turbulence model	Comparison of RANS, k-epsilon turbulence, LES models	CFD methodology for investigating complex flow systems

1.3.1 Drop Size Distribution (DSD)

1.3.1.1 Multiphase mode operation

1.3.1.1.1 Experimental Studies

Many investigators conducted experimental studies on drop size distribution in multiphase mode operation of pulsed sieve plate extraction columns. They employed techniques like image analysis, laser diffraction, and dynamic light scattering to measure the drop sizes and distribution across different plate heights, offering insights into the liquid-liquid dispersion and phase separation efficiency.

Yadav. Et al., (2007) examined pulsed sieve plate extraction column design and hydrodynamics and mass transfer correlations. These relationships were investigated against 50 years of experimental data. The pulsed sieve plate extraction column diameter was determined by the prediction ability of distinct flooding correlations. The correlation of Tribess and Brunello predicted maximum flooding curves for all approved liquid-liquid systems. All

Kumar and Hartland correlations overpredicted drop size due to a greater interfacial tension exponent (0.6) and the absence of hole diameter. Srinivasulu et al. predicted drop size well. Hold-up was overpredicted by both key empirical correlations. Generated equation was used to calculate hold-up using the slip velocity correlation of Venkatnarsaiah and Verma , which matched the experimental value. Thus, pulsed sieve plate extraction columns should be predicted using the Vslip correlation. Pilot-scale mass transfer experiments were advised due to poor correlations. The study found a correlation between flooding, drop size, and hold-up, which can be used to construct pulsed columns and reduce experimental work for their design and scale up

1.3.1.1.2 Numerical Simulations

CFD simulations coupled with population balance models have been utilized to predict drop size distributions within the column. These simulations consider the interfacial mass transfer and breakup/coalescence phenomena to provide information on the drop size distribution.

The combination of experimental and numerical investigations has allowed researchers to gain a deeper understanding of the residence time distribution, drop size distribution, and velocity field distribution in pulsed sieve plate extraction columns. These studies have contributed to the optimization of column design, operational parameters, and separation performance, facilitating advancements in liquid-liquid extraction processes for various applications.

1.4 Literature gap

While considerable research has been conducted on residence time distribution and drop distribution across column diameters ranging from 1 cm to 7 cm, the investigation of velocity distribution within this diameter range remains limited, particularly when it comes to

experimental measurement. Residence time serves as a crucial global evaluation parameter for the design of chemical engineering equipment, while drop size distribution and velocity distribution between sieve plates in pulsed sieve plate extraction columns are local field parameters. Transparent systems can be used to study drop distribution, but the majority of industrial chemical engineering plants utilize opaque systems to handle temperature and pressure. Consequently, there is a significant knowledge gap in understanding velocity distribution within larger diameter columns.

To address this gap, we have chosen a column diameter of 3 inch as the focus of our study to specifically investigate velocity distribution using the radioactive particle tracking technique. This technique provides the best means for measuring the local velocity field, and its connection with mass transfer analysis enhances its relevance. By benchmarking our findings against existing literature that primarily focuses on smaller diameter columns, we aim to gain valuable insights into the behavior of larger diameter columns (9 inch). These larger columns have not been extensively investigated due to their cost complexity and operational challenges, making our research a significant contribution to the field.

1.5 Motivation of dissertation

With the pressing need to address climate change and reduce CO2 emissions, nuclear power has emerged as a crucial solution. Its ability to save our atmosphere from harmful emissions is truly remarkable. It is estimated that current nuclear energy source reduces approximately 470 million metric tons of CO2 emission every day that would have otherwise been generated by fossil fuel usage. Nuclear energy offers a viable path towards achieving net zero CO2 emissions and effectively combating the climate crisis. In fact, according to the International Energy Agency (IEA), the utilization of nuclear power has already resulted in a global reduction of

approximately 60 gigatons of CO2 emissions over the past five decades. For achieving a sustainable closed-loop nuclear fuel cycle, advanced solvent extraction method is a potential key and also the creation of reliable separation flow sheets employing pulsed sieve-plate columns (PSPCs) has been of particular interest. The global nuclear research and development community has dedicated substantial efforts to advance and adapt solvent extraction processes, aiming to benefit future generations. However, recent studies on PSPC systems have primarily relied on empirical approaches, leading to the creation of over-specified systems with inadequate performance and reliability.

While research on global reprocessing has witnessed resurgence, studies specifically focusing on PSPC systems remain limited. Only a handful of notable investigations have utilized flow simulation software to gain insights into the hydrodynamic characteristics of PSPCs in simplified geometries. Understanding local velocity fields and other crucial parameters within the mixing and non-mixing zones of the column plays a pivotal role in establishing a reliable control system for pulsed extraction columns. Such knowledge is of utmost importance in optimizing the conditions for nuclear fuel reprocessing using pulsed sieve-plate columns for the liquid-liquid extraction process, ultimately preserving unspent uranium fuel in nuclear reactors.

To evaluate these parameters effectively, the Radioactive Particle Tracking technique (RPT) emerges as a valuable evaluating tool. By employing RPT, it becomes possible to assess local velocity fields and other relevant factors such as mean velocity, fluctuational velocity, and turbulent kinetic energy. These parameters offer valuable insights for identifying and diagnosing mixing issues, thereby enabling the optimization of nuclear fuel reprocessing conditions using pulsed sieve plate columns. By leveraging this approach, we can contribute to the ongoing efforts in advancing solvent extraction technology, a pivotal step towards meeting

the increasing demand for nuclear power and reducing CO2 emissions. The35analyzation behind our research lies in understanding and optimizing the performance of the pulsed sieve plate extraction column. By understanding the operating conditions required for optimal performance, we can enhance the efficiency and effectiveness of the pulsed sieve plate extraction column.

1.6 Objective of the thesis

The main aim of the present study is to establish the knowledge of local velocity field in pulsed columns by using state of art measurement technique. The specific objectives of the work are as follows.

- Single-phase local hydrodynamic investigation in a laboratory scale pulse column with different internals
- Multiphase local hydrodynamic investigation in a laboratory scale column with different internals
- Single-phase local hydrodynamic investigation in a pilot-scale pulse column

Outline of hypothesis to achieve these objectives: our main goal is to optimize the selection of geometric and operating parameters in a pulsed sieve plate extraction column with a diameter of 7.5 cm. To achieve this, we experiments are conducted in two stages, focusing on the analysis of velocity distribution in both single-phase and multiphase flow conditions, which will ultimately allow us to evaluate the mixing performance.

Initially, we performed a fundamental analysis of the system under single-phase conditions, which was divided into two stages. In the first stage, we examined the system under a no-flow condition. The water (aqueous phase) was kept in batch mode, and we studied the effect of varying pulsation velocities by pressurizing the column through an oscillatory flow generated

by an upstroke and downstroke motion using a three-way solenoid valve. We changed the pulsation amplitude while maintaining a constant opening frequency of one second for all operating conditions. In the second stage of the single-phase study, we investigated the pulsed sieve plate column under a constant flow of the aqueous phase. Water was pumped into the column at a consistent flow rate, and we varied the pulsation velocities to understand their impact on the performance of the column.

Our second objective focused on the multiphase investigation of local hydrodynamics within the column. This involves studying the velocity distribution of water (aqueous phase) in the presence of a secondary phase. We pumped two liquids into the column and conducted this investigation in three sequential stages. In the first stage of the multiphase investigation, we maintained a constant pulsation velocity in the pulsed leg using a three-way solenoid valve while keeping the water (aqueous phase) in batch mode with no flow. The aim was to understand the effect of different flow rates of dodecane (organic phase) on the column's performance. Next, we studied the effect of organic flow rate at a constant water flow rate while maintaining a constant pulsation velocity. This stage focused on analysing the impact of different organic flow rates on the system. Finally, we investigated the column at a constant flow rate of water (aqueous phase) and a constant flow rate of dodecane (organic phase) to study the effect of pulsation velocities. This stage provided insights into the influence of different pulsation velocities on the column's performance. All of these parameters contributed to understanding the optimization of operational conditions, ultimately enhancing the efficiency and effectiveness of the pulsed sieve plate extraction column.

In addition to the above objectives, our third objective involved the investigation of a pilot-scale plant. We designed a larger column and conducted experiments, carefully selecting the operating conditions of pulsation and flow rates to establish geometric similarity and dynamic

similarity. We addressed the challenges associated with the pilot-scale setup and ensured perfect calibration of the column with all flow measurements before conducting the experiments. To achieve position reconstruction and local velocity mapping between the plates, we utilized a well-established in-house Radioactive Particle Tracking technique, employing the Monte Carlo algorithm. By analysing all these parameters and conducting pilot-scale experiments, our aim was to optimize the operational conditions of the pulsed sieve plate extraction column, ultimately enhancing its efficiency and effectiveness.

1.7 Novelty of the current research

Despite the existence of extensive literature on the experimental investigation of local hydrodynamics using techniques such as Particle Image Velocimetry (PIV), Laser Doppler Anemometry (LDA), and optical fiber probe-in Pulse-Driven Dynamic Column (PDDC), the specific study of local hydrodynamics in pulsed sieve plate columns without downcomers remains unexplored. Furthermore, there is a notable absence of information regarding the application of radiation-based measurement techniques in liquid-liquid mixing systems, particularly in pulsed sieve columns where fluid motion is primarily driven by pulsation. The lack of knowledge concerning the local velocity field in pulsed sieve columns highlights the need for comprehensive flow investigations.

To address this research gap, the current work aims to conduct a detailed examination of the local field through the implementation of the non-intrusive radioactive particle tracking technique (RPT). By utilizing RPT, the study seeks to gather valuable information regarding the velocity field, quantify fluctuations, and determine turbulence parameters through rigorous experimental investigations. This novel approach will shed light on the intricate dynamics

within pulsed sieve columns, providing essential insights for optimizing their design and operational parameters.

1.8 Structure of the thesis

1. The **first chapter** provides a concise overview of the pulsed sieve column. In this chapter, various flow regimes of PSPC and design parameters are described, along with the rationale for the current research, a problem description, and the hypothesis for solving the problem with our objectives. The uniqueness of this work is also described.
2. In the **second chapter**, experimental methods are described in detail. Mathematical expressions are used to describe the algorithm and the sequential procedure of measurement technology. In the second chapter, investigation parameters for this technology are envisioned.
3. The **third chapter** discusses the application of RPT measurement technology on the chosen PSPC system. This chapter examines the analysis of single-phase utilizing two different internals in two different scenarios (no flow, single phase). This chapter describes the systematic operation of the column and the post-processed characteristics of the measuring technology.
4. The multiphase flow investigation for the two distinct internals is covered in the **fourth chapter**, along with a summary of the comparison results.
5. The discussion of the pilot scale is presented in the **fifth chapter**, along with an explanation of the outcomes of the single-phase exploration.
6. The outcome of the study is presented in the **sixth chapter**, along with its potential applications in the future

Reference

Amani P, Esmaieli M., 2017. “Drop behavior characteristics in different operating regimes in an L-shaped pulsed sieve-plate column”. *Can. J. Chem. Eng.* https://doi.org/10.1002/cjce.22911

Amani, P., Safdari, J., Gharib, A., Badakhshan, H., Mallah, M.H., 2017. “Mass transfer studies in a horizontal pulsed sieve-plate column for uranium extraction by tri-n-octylamine using axial dispersion model”. *Prog. Nucl. Energy* 98, 71–84. https://doi.org/10.1016/j.pnucene.2017.02.010

Angelov, G., Gourdon, C., 2009. “Turbulent flow in pulsed extraction columns with internals of discs and rings: Turbulent kinetic energy and its dissipation rate during the pulsation”. *Chem. Eng. Process. Process Intensif.* 48, 592–599. https://doi.org/10.1016/j.cep.2008.07.002

Bardin.M. N., Guiraud, P., Gourdon, C., 2003. “Lagrangian simulations contribution to the knowledge of discs and doughnuts pulsed solvent extraction columns hydrodynamics”. *Chem. Eng. Process. Process Intensif.* 42, 503–516. https://doi.org/10.1016/S0255-2701(02)00072-7

Bart, H. J., Drumm, C., & Attarakih, M. M., 2008. “Process intensification with reactive extraction columns”. *Chem. Eng. & Proc. Int.*, *47*(5), 745-754. https://doi.org/10.1016/j.cep.2007.11.005

Benedict, M., Pigford, T.H., Levi H.W., 1981. Nuclear Chemical Engineering *McGraw Hill Book Company*. https://doi.org/10.1002/aic.690280428.

Bujalski, J.M., Yang, W., Nikolov, J., Solnordal, C.B., Schwarz, M.P., 2006. "Measurement and CFD simulation of single-phase flow in solvent extraction pulsed column". *Chem. Eng. Sci.* 61, 2930-2938. https://doi.org/10.1016/j.ces.2005.10.057

Britsch, R., 1983. "Extraction Column Using Radioactive Tracer Techniques". *Aqueous Phase Investigations* 34, 1400–1402.

Chen, H., Sun, Z., Song, X., Yu, J., 2014. "Key Parameter Prediction and Validation for a Pilot-Scale Rotating- Disk Contactor by CFD–− PBM Simulation". *Ind. Eng. Chem. Res*. 2014, 53, 20013−20023. https://doi.org/10.1021/ie503115w

Duan, C., Wang, B., Liu, C., Yuan, X., 2013. "Flow Pattern Optimization of a Sieve Plate Extraction Column Using Computational Fluid Dynamics Simulations and Particle Image Velocimetry Measurements". https://doi.org/10.1021/ie301446e

Din, G.U., Chughtai, I.R., Inayat, M.H., Khan, I.H., 2008. "Axial dispersion, holdup and slip velocity of dispersed phase in a pulsed sieve plate extraction column by radiotracer residence time distribution analysis". *Appl. Radiat. Isot.* 66, 1818–1824. https://doi.org/10.1016/j.apradiso.2008.07.002

Din, G.U., Chughtai, I.R., Inayat, M.H., Khan, I.H., Qazi, N.K., 2010. "Modeling of a two-phase countercurrent pulsed sieve plate extraction column–- A hybrid CFD and radiotracer RTD analysis approach". *Sep. Purif. Technol*. 73, 302–309. https://doi.org/10.1016/j.seppur.2010.04.017

Din, G.U., Khan, I.H., Chughtai, I.R., Inayat, M.H., Jin, J.H., 2013. "Radiotracer investigations to study the hydrodynamic characteristics of continuous phase in a pulsed sieve plate

extraction column". *EPJ Web Conf.* 50, 01004. https://doi.org/10.1051/epjconf/20135001004

Farakte, R.A., Hendre, N. V., Patwardhan, A.W., 2018. "CFD Simulations of Two-Phase Flow in Asymmetric Rotary Agitated Columns". *Ind. Eng. Chem. Res.* 57, 17192–17208. https://doi.org/10.1021/acs.iecr.8b02720

Ghadiri, M., Ashrafizadeh, S. N., & Taghizadeh, M., 2014 "Study of molybdenum extraction by trioctylamine and tributylphosphate and stripping by ammonium solutions". *Hydrometallurgy*, *144–145*, 151–155. https://doi.org/10.1016/j.hydromet.2014.02.009

Godfrey, J.C., Slater, M.J., 1995. "Liquid-Liquid Extraction Equipment", Wiley, New York, p.20

Haverland, H., Vogelpohl, A., Gourdon, C., Casamatta, G., 1987. Simulation of fluid dynamics in a pulsed sieve plate column. Chem. Eng. Technol. 10, 151–157. https://doi.org/10.1002/ceat.270100119

He, C., Gao, Y., Yang, S., Edwards, D.W., 2004. "Optimization of the process for recovering caprolactam from wastewater in a pulsed-sieve-plate column using green design methodologies" 17, 195–204. https://doi.org/10.1016/j.jlp.2003.12.001

Jahya, A. B., Pratt, H. R. C., & Stevens, G. W., 2005. "Comparison of the performance of a pulsed disc and doughnut column with a pulsed sieve plate liquid extraction column". *Sol. Extract. & Ion. Exc. 23*(3), 307–317. https://doi.org/10.1081/SEI-200045257

Jaradat, M., Attarakih, M., 2011. "Population Balance Modeling of Pulsed (Packed and Sieve-Plate) Extraction Columns: Coupled Hydrodynamic and Mass Transfer". *Ind. Eng. Chem. Res.* 50, 14121–14135. https://doi.org/10.1021/ie201041q

Kagan, S.Z., Aerov, M.E., Lonik, V. and Volkova, T.S., 1965. “Some Hydrodynamic and Mass Transfer Problems in Pulsed Sieve-plate Extractors”, *Intern. Chem. Eng*., 5(4), p. 656.

Kolhe, N.S., Mirage, Y.H., Patwardhan, A. V., Rathod, V.K., Pandey, N.K., Mudali, U.K., Natarajan, R., 2011. “CFD and experimental studies of single-phase axial dispersion coefficient in pulsed sieve plate column”. *Chem. Eng. Res. Des*. 89, 1909–1918. https://doi.org/10.1016/j.cherd.2011.01.020

Khooshechin, S., Ali, M., Safdari, J., Hassan, M., Badakhshan, H., 2022. “Experimental investigation on drop size distribution and mean drop size in an L-shape pulsed packed extraction column”. *Chem. Eng. Res. Des*. 179, 462–472. https://doi.org/10.1016/j.cherd.2022.01.038

Kumar A, Hartland S., 1994. “Empirical prediction of operating variables”. Hanson C (eds) Handbook of solvent extraction. Wiley, New York, p. 625–735

Lade, V.G., Pakhare, A.D., Rathod, V.K., 2014. “Mass transfer studies in pulsed sieve plate extraction column for the removal of tributyl phosphate from aqueous nitric acid”. *Ind. Eng. Chem. Res.* 53, 4812–4820. https://doi.org/10.1021/ie401384j

Laddha, G. S., Degaleesan, T. E., 1976. “Transport phenomena in liquid extraction” https://doi.org/10.1016_0009-2509(78)85219-1

Mohanty, S., 1997. “A simplified hydrodynamic model for a pulsed sieve-plate extraction column”. *Chem. Eng. & Proc*. 36, 385-395

Panahinia F, Safdari J, Ghannadi M, Amani P, Mallah M.H., 2017. "Modeling and simulation of a horizontal pulsed sieve-plate extraction column using axial dispersion model". *Sep. Sci. Technol.* 52, 1537–1552

Pratt, H.R.C., Stevens, G.W.,1992. "Science and Practice in Liquid-Liquid Extraction", Oxford University Press, Oxford, p. 491-502

Pant, H.J., Goswami, S., Samantray, J.S., Sharma, V.K., Maheshwari, N.K., 2015. "Residence time distribution measurements in a pilot-scale poison tank using radiotracer technique". *Appl. Radiat. Isot.* 103, 54–60. https://doi.org/10.1016/j.apradiso.2015.05.016

Schügerl, K., (1994). "Extraction Equipment". *Sol. Extract. In. Biotech*. Springer, Berlin, Heidelberg. https://doi.org/10.1007/978-3-662-03064-6

Sen, N., Singh, K.K., Patwardhan, A.W., Mukhopadhyay, S., Shenoy, K.T., 2015. "CFD Simulations of Pulsed Sieve Plate Column : Axial Dispersion in Single-Phase Flow CFD Simulations of Pulsed Sieve Plate Column". *Sep. Sci. Technol*. 50, 2485–2495. https://doi.org/10.1080/01496395.2015.1064136

Sheoran, M., Goswami, S., Pant, H.J., Biswal, J., Sharma, V.K., Chandra, A., Bhunia, H., Bajpai, P.K., Rao, S.M., Dash, A., 2016. "Measurement of residence time distribution of liquid phase in an industrial-scale continuous pulp digester using radiotracer technique"

Sheoran, M., Goswami, S., Pant, H. J., Biswal, J., Sharma, V. K., Chandra, A., Bhunia, H., Bajpai, P. K., Rao, S. M., & Dash, A., 2016. "Measurement of residence time distribution of liquid phase in an industrial-scale continuous pulp digester using radiotracer

technique". *Appl. Rad. & Isotopes.* 111, 10–17. https://doi.org/10.1016/j.apradiso.2016.01.025

Somkuwar, N., Kolhe, N., Rathod, V., 2014. "Hydrodynamics of a Pulsed Sieve Plate Extraction Column". *Indian Chem. Eng.* 56, 235–257. https://doi.org/10.1080/00194506.2014.910707

Schweitzer, P.A., Hanson., 1997. "Mixer-Settler Handbook of Separation Techniques for Chemical Engineering", McGraw-Hill, New York, p. 23

Tsouris, C.; Kirou, V.; Tavlarides, C. Wang Drop size distribution and holdup profiles in a multistage extraction column, *AIChE J.* **1994**,40, 407-418. https://doi.org/10.1002/aic.690400304.

Treybal, R., 1959. "Liquid Extraction". *Ind. Eng. Chem*., 51(3), 378–388. https://doi.org/10.1021/ie51395a010

Tan, B., Zhang, Y., Wang, Y., Qi, T., 2021. "Study on Dispersed-Phase Axial Dispersion in an Agitated Pulsed Solvent Extraction Column with a Step Tracer Injection Technique". https://doi.org/10.1021/acs.iecr.1c00506

Van Dijck, W. J. D., 1935. US Patent 2,011,186.

Xiaojin, T., Guangsheng, L., Jiading, W., 2005. "An improved dynamic combined model for evaluating the mass transfer performances in extraction columns" 60, 4409–4421. https://doi.org/10.1016/j.ces.2005.02.065

Yi, H., Wang, Y., Smith, K.H., Fei, W., Stevens, G.W., 2017. “Axial Dispersion and Mass Transfer of a Pulsed Solvent Extraction Column with Novel Ceramic Internals”. *Ind. Eng. Chem. Res.* 56, 3049–3058. https://doi.org/10.1021/acs.iecr.6b04601

Yadav RL, Patwardhan AW., 2008. “Design aspects of pulsed sieve plate columns”. *Chem Eng. J.* 138, 389-415. https://doi.org/10.1016/j.cej.2007.06.015

Yung, K. K. L., Smith, C. D., Bowser, T., Perera, J. M., & Stevens, G. W., 2012, “The use of an ionic liquid in a Karr reciprocating plate extraction column”. *Chem. Eng. Res. & Des. 90*(11), 2034–2040. https://doi.org/10.1016/j.cherd.2012.03.006

CHAPTER-2

Radioactive Particle Tracking

Chapter 2 : Radioactive Particle Tracking

Graphical abstract

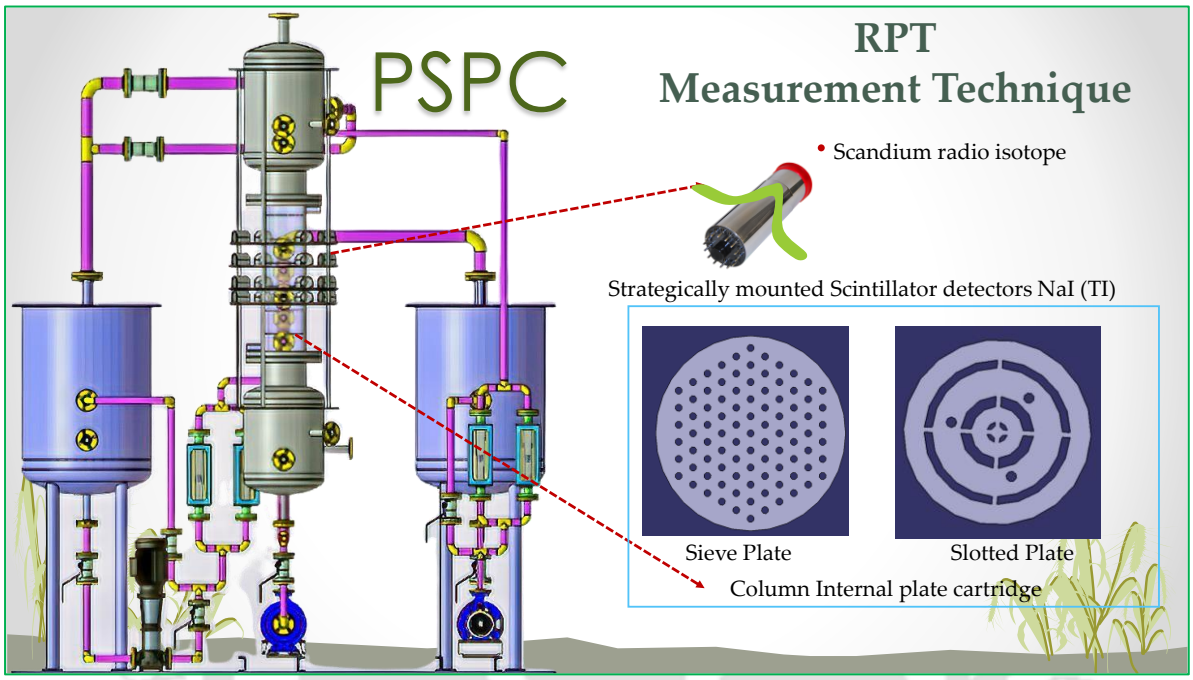

Abstract

This chapter provides a comprehensive explanation of flow measurement techniques in multiphase flows, highlighting their significance. It also focuses on the development and implementation of Radioactive Particle Tracking (RPT) methodology in diverse systems, particularly in liquid-liquid systems where benchmarking hydrodynamics is challenging. It covers various aspects of RPT implementation, starting with the selection of tracers and radiation sensing equipment. It discusses the significance of photon measuring equipment and the methodology for photon counting. The hardware requirements for RPT are also addressed, along with an analysis of performance parameters such as resolution and sensitivity. The chapter further discusses the staging of a reference system using detector positions and precise alignments of the column. It explains the steps involved in implementing RPT, including the calibration of radiation sources inside the column. Post-processing of data and the generation of a distance count map are discussed, along with the principles associated with the Montecarlo algorithm used in the process. The main focus of this chapter is the utilization of RPT on a pulsed sieve plate column (PSPC), providing insights into its application and findings.

2.1 Introduction

The design and scale-up of pulsed sieve plate extraction columns, which utilize liquid-liquid mixing and separation, have traditionally relied on empirical correlations that are limited to a narrow range of operating conditions. This limitation underscores the significance of understanding the dynamic properties, such as main velocities and volume fraction, for achieving improved design and scale-up accuracy. These parameters play a pivotal role in determining the performance of the reactor. To investigate multiphase flow reactors effectively, it is essential to employ sophisticated measurement techniques capable of providing comprehensive information across the entire flow field. This includes both global (time-averaged) and local measurements at multiple scales. Such data not only serve as independent information for developing design and scale-up strategies but also contribute to validating phenomenological flow models and computational fluid dynamic (CFD) models. The validation of CFD models requires experimental investigations at multiple scales, extending beyond spatial and temporal averages. An overview of the various measurement techniques is given here in light of the importance of precise velocity measurements in liquid-liquid systems. These techniques play a vital role in acquiring the necessary data for design, scale-up, and model validation in multiphase flow systems. Generally, flow measurement techniques are divided in two groups, invasive and non-invasive. In invasive technique, a single or multiple probes/wires are inserted inside the flow and desired parameters are measured. Though such techniques are cost effective and most of the time provides direct measurements, the flow physics may change at the point of measurement itself. This affect the accuracy of the measurement and restrict the application of intrusive techniques in multiphase flow applications. In non-invasive technique, measurements are performed without disturbing the

flow and hence, it provides reliable data. Therefore, current thesis discusses the non-invasive techniques only.

2.2 Non-invasive flow measurement techniques in multiphase systems

Flow measurement techniques in multiphase flows are used to determine the flow behavior properties of two or more phases (e.g., gas-liquid, liquid-liquid, gas-solid-liquid) within a flow system. These techniques play a crucial role in various industries, including oil and gas, chemical processing, and environmental engineering. Sophisticated instruments such as electromagnetic flowmeters, ultrasonic flowmeters have been developed for measuring flow averaged velocities in various ways. In the case of electromagnetic flow meters, they operate by using Faraday's law of electromagnetic induction to measure the flow rate of conductive fluids. The meter consists of a pipe with a pair of electrodes that generate a magnetic field across the fluid. As the conductive fluid flows through the pipe, it induces a voltage in the electrodes, which is proportional to the velocity of the fluid. Ultrasonic flow meters, on the other hand, utilize sound waves to measure the flow velocity. They emit ultrasonic signals into the flowing fluid and measure the time it takes for the signals to travel between transducers placed at different positions in the pipe. By comparing the upstream and downstream travel times, the velocity of the fluid can be determined. These well-developed, handy, and fully constructed instruments utilize different principles to provide accurate measurements of the average velocity of the flowing liquid. Both electromagnetic flow meters and ultrasonic flow meters offer the advantage of noninvasiveness, as they do not require physical probes or elements to be inserted into the flow path. This makes them suitable for a wide range of applications where the flow needs to be measured accurately without disturbing or altering the

flow characteristics. They offer practical solutions for determining the overall flow characteristics within a multiphase system.

However, when it comes to analyzing and understanding the detailed flow behavior, including the axial, radial, and azimuthal velocities, more advanced techniques are required. Four prominent noninvasive flow measurement techniques, namely Laser Doppler Anemometry (LDA), Particle Image Velocimetry (PIV), Radioactive Particle Tracking (RPT), and Positron Emission Particle Tracking (PEPT)are particularly significant in this regard. These techniques go beyond the capabilities of small, handheld instruments, as they involve complex algorithms and require larger constructions. They offer a more comprehensive and detailed understanding of the flow characteristics within multiphase systems. By utilizing these techniques, researchers can obtain measurements and conduct analyses that reveal the various components of velocity, enabling a thorough examination of the flow dynamics in a multiphase system. A detailed explanation of all of these measurement techniques are given below.

2.2.1 Laser Doppler Anemometry (LDA)

Laser Doppler Anemometry (LDA) is a widely used technique for flow measurement in multiphase systems, particularly in gas-liquid and liquid-liquid flows where discrete phase fraction is low (<5%). It provides detailed information about the velocity distribution of the fluid by analyzing the Doppler shift in laser light scattered by small particles or droplets within the flow. Here is a detailed explanation of LDA and its formula for finding the three component velocities in liquid-liquid flows:

2.2.2 Principle of Laser Doppler Anemometry

LDA works on the principle of the Doppler effect, which states that the frequency of light changes when it interacts with moving objects. In LDA, a laser beam is split into two coherent

beams: the reference beam and the measuring beam. The measuring beam is directed into the flow, and as it interacts with the particles or droplets, it undergoes a frequency shift proportional to their velocity. The scattered light is collected and interferes with the reference beam, resulting in an interference pattern known as a Doppler signal. By analyzing the Doppler signal, the velocity distribution of the particles or droplets in the flow can be determined.

In liquid-liquid flows, the three-dimensional velocity vector can be decomposed into three components: the axial (u), radial (v), and azimuthal (w) velocities. The LDA system measures the axial velocity (u) based on the frequency shift of the scattered light. However, to determine the radial (v) and azimuthal (w) velocities, additional techniques or assumptions are required.

One common approach for obtaining the three component velocities is to use a cylindrical coordinate system, where the axial direction corresponds to the z-axis, the radial direction corresponds to the r-axis, and the azimuthal direction corresponds to the θ-axis. By assuming certain flow symmetries or using additional measurements, the radial and azimuthal velocities can be estimated. The formula for finding the axial velocity (u) using LDA is given by:

$u = -\lambda \Delta f / (2\pi \cos(\theta) \nu)$,

where:

λ is the laser wavelength,

Δf is the Doppler frequency shift,

θ is the angle between the laser beam and the flow direction,

ν is the refractive index of the fluid.

It is important to note that the accuracy of LDA measurements in liquid-liquid flows can be affected by factors such as particle size, particle concentration, and the refractive index

mismatch between the two liquids. Calibration and careful experimental setup are necessary to obtain accurate and reliable velocity measurements. By combining LDA measurements with complementary techniques or assumptions, such as flow symmetry or knowledge of the flow geometry, it is possible to estimate the radial and azimuthal velocities and obtain a more comprehensive understanding of the velocity distribution in liquid-liquid multiphase flows. Overall, Laser Doppler Anemometry is a powerful tool for studying fluid dynamics in multiphase systems, providing detailed velocity information that is valuable for various industrial and research applications.

2.2.3 Particle Image Velocimetry (PIV)

Particle Image Velocimetry (PIV) is a non-intrusive optical flow measurement technique used to analyze fluid motion in various applications, including multiphase systems such as liquid-liquid flows. PIV provides valuable insights into the velocity distribution and flow patterns within a given region of interest. The principle behind PIV involves capturing sequential images of tracer particles suspended in the flow. These particles can be either naturally occurring or artificially introduced into the fluid. Illumination, typically using a laser, is used to generate a light sheet that illuminates the region of interest. The tracer particles within this illuminated plane are then captured by a high-speed camera, which records their positions. To determine the velocity of the fluid, the images are analyzed using cross-correlation techniques. The displacement of the tracer particles between consecutive image frames is measured, providing information about the fluid's motion. The correlation analysis involves dividing the image frames into smaller interrogation regions or subregions. Within each subregion, the software calculates the cross-correlation function to determine the displacement vector, which corresponds to the fluid velocity at that location. In multiphase liquid-liquid flows, the PIV technique can be extended to measure the three components of the flow velocity: axial, radial,

and azimuthal velocities. To achieve this, multiple camera views or multiple laser planes can be employed to capture the velocity components in different directions. By using appropriate calibration techniques, the three-dimensional velocity field of the multiphase flow can be reconstructed. The formula for finding the three component velocities in liquid-liquid flows using PIV depends on the specific setup and calibration procedures employed. Generally, the process involves calibrating the PIV system by correlating the particle displacements in the images with known distances. The calibration allows for the conversion of pixel displacements into physical units, such as millimeters or meters. Once the calibration is established, the measured displacements in the images can be used to calculate the velocity components. The specific formulas used may vary depending on the coordinate system and orientation chosen for the flow analysis. However, the general principle involves converting the measured displacements into velocities by considering the time interval between image frames and the spatial dimensions of the flow field. It is worth noting that the accurate determination of the three component velocities in liquid-liquid flows using PIV can be challenging due to factors such as particle seeding, particle concentration, and potential optical distortions caused by refractive index variations between the phases. Careful experimental setup, calibration procedures, and data processing techniques are crucial to obtain reliable velocity measurements in multiphase systems using PIV.

2.2.4 Tracer based techniques

2.2.4.1 Positron Emission Particle Tracking (PEPT)

Positron Emission Particle Tracking (PEPT) is an advanced non-invasive flow measurement technique used to study the motion of individual particles in multiphase systems, including liquid-liquid flows. PEPT utilizes positron-emitting radioactive tracers that are introduced into the flow to track the motion of the phase of interest. It provides valuable insights into the

velocity distribution and flow patterns at a particle level within the system. The principle behind PEPT involves the emission of positron particles by a radioactive isotope, typically fluorine-18. The radioactive tracer is attached to a small particle suspended in the flow. When the positrons emitted by the tracer encounter electrons within the medium, they undergo annihilation, resulting in the emission of two back-to-back gamma-ray photons which are 180° apart. These gamma-ray photons can be detected using specialized detectors surrounding the flow region which can be post processed to get the tracer particle location. By analyzing the time difference between the two successive location of the tracer particle velocity of the tracer can be found. By tracking the position of the particle over time, its velocity and trajectory within the flow can be calculated. In multiphase liquid-liquid flows, PEPT can be used to determine the three component velocities: axial, radial, and azimuthal velocities. The formula for finding these velocities depends on the specific experimental setup and calibration procedures employed. To determine the axial velocity, the time difference between the emission of the two gamma-ray photons is used to calculate the displacement of the tracer particle along the flow direction. Dividing this displacement by the time interval between the emissions provides the axial velocity of the particle. For the radial and azimuthal velocities, additional detectors or specialized detector configurations are used. By determining the position of the tracer particle in the radial and azimuthal directions based on the gamma-ray photon emissions, the radial and azimuthal displacements can be calculated. Dividing these displacements by the corresponding time intervals provides the radial and azimuthal velocities, respectively. It is important to note that PEPT requires careful calibration to convert the detected gamma-ray photon positions into physical coordinates within the flow field. Calibration procedures involve the use of known reference points or calibration objects to establish the relationship between the detected positions and the actual particle positions.

Additionally, the accuracy and resolution of PEPT measurements depend on factors such as the positron range, detector positioning, background noise, and the time resolution of the detection system. Optimizing these parameters and employing advanced data analysis techniques are necessary to obtain accurate and reliable velocity measurements in liquid-liquid multiphase flows using PEPT.

While PEPT is a more expensive technique, LDA and PIV require transparent systems and are suitable for measuring systems with low phase fraction. ERT also has its own limitations. Considering these factors, the choice of RPT for the liquid-liquid system is justified, as it offers a non-invasive solution that can measure the three components of the marker phase's velocity. In our current study on PSPC, we have chosen to utilize RPT due to its advantages, as it allows us to gather valuable data regarding fluid velocity in the multiphase system while minimizing any disruption to the flow dynamics. Selection of RPT with its principle of working is detailed in section 1.3.

2.2.4.2 Radioactive Particle Tracking (RPT)

RPT is noninvasive flow measurement technique. In RPT, the motion of a single radioactive tracer particle (which is the marker of the phase of interest) is tracked by using the scintillation detectors which are placed strategically around the vessel of interest. In case of liquid tracking, the tracer particle is made neutrally buoyant while in case of solid tracking, the size, shape and density of the tracer particle is kept same as of the solid present in the flow. During the experiment, the intensity of radiation (count) emitted by the radioactive particle is recorded by detectors. The intensity recorded by each detector depends on the distance between tracer particle and detector, phases present between them, wall material and solid angle made by tracer particle on the detector. Radioactive particle releases energy in the form of photons. The number of photons received by the detector is measured by taking the distance between the

radioactive particle and detector as the radius of a sphere whose centre is the actual detector position and surface is particle location. The intersection point of these surfaces, corresponding to different detectors, is the position of the particle. Three detectors are sufficient to determine particle position, but to measure particle position with the change of time, a minimum of four detectors are required. The increased number of detectors increases the accuracy of the measurement. Therefore, a number of detectors are placed outside the column, from top to bottom, to track the whole path of the moving tracer particle.

Unlike PEPT this technique needs calibration prior to the experiment. During calibration, the tracer is placed at various known locations and the counts recorded on each detector are noted down. This gives a distance count map for each detector. Then, the actual experiment is performed where the tracer is placed inside the column with other moving particles. After the experiment, the position of the tracer is reconstructed by comparing the experimentally obtained count with calibrated one. It gives the Lagrangian position time series of the tracer particle. Time differentiation of two successive Lagrangian positions gives the instantaneous velocity of the tracer. This data is further processed to get mean velocities, fluctuating velocities, rms velocities, turbulent kinetic energy and turbulent quantities.

The main advantage of RPT is that it is a versatile technique as it can be used in both transparent and opaque techniques. It can be implemented for both dense and dilute systems with the similar accuracy. Further, it can be implemented at different scales without any major issues. The drawback of RPT is that it needs calibration. RPT can provide a spatial resolution of less than 1 mm at 50 Hz (Upadhyay et al., 2010) and temporal resolution up to 200 Hz (Bhusarapu et al., 2006).

2.3 RPT implementation and developments

Radioactive Particle Tracking (RPT) is a versatile technique that finds applications in various multiphase systems, including gas-solid, gas-liquid, and liquid-liquid systems. Its employment in these systems has contributed to significant advancements in understanding their hydrodynamics and flow characteristics.

In gas-solid multiphase systems, RPT has been employed to investigate particle behavior, such as particle trajectories, velocities, and concentration distributions. This information is crucial in industries such as pharmaceuticals, chemical processing, and powder handling, where efficient particle transport and control are essential. RPT enables the tracking of individual particles, providing insights into phenomena like particle dispersion, mixing, and segregation. It has also been used to study fluidized beds, pneumatic conveying, and granular flows, aiding in the optimization and design of related processes.

In gas-liquid multiphase systems, RPT has been utilized to study phenomena such as bubble dynamics, liquid-solid interactions, and gas-liquid mixing. It enables the tracking of gas bubbles or liquid droplets, allowing for the determination of their trajectories, velocities, and residence times. This information is valuable in industries like chemical engineering, oil and gas, and environmental engineering, where gas-liquid interactions play a crucial role. RPT has been employed to understand gas-liquid contacting devices, bubble columns, stirred tanks, and multiphase reactors, aiding in process optimization and scale-up.

In liquid-liquid multiphase systems, RPT has found applications in studying phenomena like liquid-liquid dispersion, emulsion formation, and phase separation. It enables the tracking of droplets or bubbles within the liquid-liquid system, providing valuable information about their movement, coalescence, and breakup. RPT has been employed in

industries such as food processing, pharmaceuticals, and chemical engineering, where precise control of liquid-liquid systems is crucial. It has been used to investigate liquid-liquid extraction processes, liquid-liquid dispersion in mixing tanks, and emulsion stability, facilitating process optimization and product development. The development of RPT as a technique has evolved over time. Researchers have focused on improving the accuracy, sensitivity, and resolution of the detection systems used in RPT. Advances have been made in scintillation detectors, photomultiplier tubes, and pulse processing units to enhance the measurement capabilities. Calibration methods and algorithms have been refined to improve position determination and data analysis. Additionally, computational techniques, such as Monte Carlo simulations, have been employed to enhance the understanding of the tracking process and optimize the measurement parameters. Continuous developments in RPT have led to its successful application in a wide range of multiphase systems. The technique continues to evolve, driven by the need for better understanding and control of complex flow phenomena. With its ability to provide detailed information about the behavior of individual particles or droplets, RPT holds promise for further advancements in multiphase flow research, process optimization, and product development in various industries. RPT literature survey and developments and employment of RPT in various systems is described in Table 2.1

Table 2.1: Literature on experimental methodology and employment of RPT in various systems

S No.	Authors	Experimental Details	Material used	Remarks
1	Kondukov et al. (1964)	Gas-Solid Fluidized bed	Six scintillation detectors used to track the motion of gamma ray tracer particle.	The concept of RPT first introduced by Kondukov et al. (1964). Studied only qualitative information could be done to the lack of sufficient data acquisition system.
2	Meek et al. (1972)	Liquid-solid Fluidized bed	Six scintillation detector used to track the solid motion in a turbulent liquid.	Detector were positioned on an axially moving carriage which was designed to move with the solid particle.
3	Lin (1981), Lin et al. (1985)	Gas-solid cylindrical fluidized bed	Tracer particle was prepared from epoxy coating on scandium particle. They used twelve scintillation detectors keeping four detectors in a staggered manner at three different heights.	Solid motion was measured using two sizes of tracer particle. They used weighted linear regression method for reconstruction of tracer position to measure solid velocities.

4	Moslemian et al. (1989), Moslemian et al. (1992)	Gas-solid cylindrical fluidized bed	They used sixteen scintillation detectors keeping four detectors in a staggered manner at four different heights.	They concluded that convection has significant effect on mixing process and the axial dispersion coefficient is greater than radial dispersion coefficient.
5	Devanathan et al. (1991)	Gas-liquid Bubble column	They used scandium-46 cylindrical particle to inject inside a polypropylene ball to make tracer. They used sixteen scintillation detectors.	Introduced RPT first time for gas-liquid system. Developed the modified version of RPT. They employed weighted linear regression method to process the data.
6	Yang et al. (1992)	Gas-liquid Bubble column	16 scintillation detectors were used.	Measured liquid motion using same data processing method as Devanathan et al. (1991).
7	Larachi et al. (1995)	Three phase fluidized bed reactor	8 scintillation detectors were used.	They introduced Monte Carlo method in which photon intensity counts detected by scintillation detector for known position of particle. Significant development of particle reconstruction method.

8	Cassanello et al. (1995), Cassanello et al. (2001)	Three phase fluidized bed and bubble column	8 scintillation detectors were used	They measured flow field of solid in three phase bed and studied liquid motion in a bubble column.
9	Degaleesan et al. (1997)	Gas-liquid Bubble column	Scandium-46 was inserted in to a polypropylene ball to prepare tracer.	Investigation of bubble column for different conditions and for different diameters. They investigated liquid velocities and various turbulence parameters.
10	Godfroy et al. (1997)	Three phase fluidized bed, gas spouted bed and liquid fluidized bed	Sc-46, Mo-99 and Au-198 particle used as tracer.	Developed an artificial neural network (ANN) algorithm to process the data obtained from the detectors. They investigated solid movement in three types of fluidized bed.
11	Roy et al.(2000)	Liquid-solid circulating fluidized bed	They used scandium isotope in a 2.5 mm diameter aluminum ball and encapsulated this particle using quartz to make tracer	Introduced RPT first time for continuous flow system. Measured solid velocities and various turbulence parameters.

12	Rammohan et al. (2002)	Liquid and Gas-liquid STR	Sc-46 radioactive particle used as tracer particle and sixteen NaI scintillation detector used.	Studied the flow behavior in stirred tank reactor both for single and multiphase flow. Concluded dynamic bias error for high velocity system for RPT technique.
13	Limtrakul et al. (2005)		An embedded scandium particle in an aluminium particle as tracer	They measured solid velocity, hold up and different turbulence parameters.
14	Bhusarapu et al. (2005)	Gas-solid riser of a circulating fluidized bed	Sc-46 having same size as that of fluidizing particle has been used as tracer.	They studied flow and mixing pattern of solid in the bed.
15	Doucet et al. (2008)	Solid-Solid V-blender		Implementation of RPT for irregular moving boundaries flow domain.
16	Khanna et al. (2008)	Conical fluidized bed dryer	Prepared tracer particles of 1.33 mm and 2.54 mm diameter by mixing gold powder with epoxy resin and used 12 scintillation detectors for the experiment.	Studied solid phase motion.
17	Sanaei et al. (2010)	Gas-Solid	Scandium oxide radioactive particle used.	Used RPT at elevated temperatures (25-600°C)

		Bubbling fluidized bed		
18	Upadhyay (2010)	Gas-liquid Bubble column	Scandium oxide salt used as tracer particle.	Measure liquid motion and various turbulence parameters.
19	Jain et al. (2014)	Liquid-solid fluidized bed	Sc-46 radioactive particle used and eight scintillation detector used.	Investigation of liquid solid fluidized bed for two different sizes of particle. Quantified the effect of liquid velocity and particles size on bed hydrodynamics.
20	Kamalanathan et al. (2016)	Gas-Solid Circulating fluidized bed	Sc-46 radioactive particle used as tracer particle and fourteen scintillation detector has been used.	Implementation of RPT first time for high velocity system. Studied the flow behavior of gas-solid circulating fluidized bed for laboratory scale as well as pilot plant scale.
21	Sharma et al. (2017)	Liquid, liquid-liquid and gas-liquid	Sc-46 radioactive particle used as tracer particle	Implementation of RPT technique for measurement of Time of Flight (TOF) and Volume Fraction (VOF).

		Coiled tube geometry		
22	Yadav et al. (2017)	Liquid-vapour Bubble column with internals	Sc-46 radioactive particle used as tracer particle to track the liquid phase, and twelve scintillation detector used.	Investigation of liquid phase hydrodynamics and mixing characteristics of bubble column equipped with sparse to dense internal over the wide range of superficial gas velocities and liquid velocities.

The subsequent sections provide a comprehensive explanation of the step-by-step implementation of Radioactive Particle Tracking (RPT). These sections cover the selection of tracer, radiation sensing and photon measuring equipment, photon counting methodology, hardware requirements, performance parameters (resolution and sensitivity study), and post-processing variables associated with RPT.

2.3.1 Utilization of single radioactive particle as tracer

Radioactive particles can be stored within lead pots to ensure containment and provide radiation shielding. Lead, being a dense material, effectively absorbs and blocks radiation. To further minimize direct contact, the radioactive particles are typically enclosed in glass vials, which are then placed inside the lead pots. This arrangement helps reduce the potential for direct exposure to the radioactive material. Image of lead storage pot is shown in figure 2.1(a).

Various sealed sources are employed for radioactive particle tracking, with examples including cesium-137 (Cs-137), cobalt-60 (Co-60), and scandium-46 (Sc-46). These sources emit gamma radiation, which can be detected and tracked using suitable detection systems. The energy of the gamma radiation emitted by a scandium source varies depending on the specific isotope used. In the case of scandium-46 (Sc-46), it emits gamma radiation with an energy of approximately 889 kiloelectron volts (keV). The half-life of Sc-46 is approximately 83.79 days. Due to its relatively shorter half-life compared to cobalt and cesium, scandium is commonly utilized for radioactive particle tracking applications. In the context of radioactive particle tracking, smaller-sized sources are typically preferred to enable precise tracking of individual particles. The choice of radioactivity for these sources depends on desired radiation intensity levels and the specific characteristics of the particles under observation. In radioactive particle tracking (RPT) applications, commonly used sizes for the glass beads containing scandium sources range from a few millimeters to a few centimeters in diameter. The size is chosen based

on the specific requirements of the tracking system, including the scale of the particles being tracked and the desired sensitivity of the measurement. Various sizes of radioactive particles are shown in Figure 2.1 (b).

In the creation of sealed sources for radioactive particle tracking, a small amount of scandium-46 is carefully enclosed within glass beads. These glass beads act as protective coatings, effectively preventing the release of radioactive material while enabling the emission of gamma radiation. These sealed sources are utilized safely in radioactive particle tracking applications, where the emitted radiation is detected and employed to monitor particle movement within the system. The process of encapsulating scandium sources in glass beads within a nuclear reactor involves specific techniques. Initially, a suitable form of scandium material, such as scandium oxide or scandium chloride, is prepared. This scandium material is then combined with a glass-forming compound. The mixture is subjected to high temperatures, causing the glass and scandium compound to melt and blend together. Once the desired composition is achieved, the molten mixture is transformed into small beads using methods like droplet formation or rapid cooling. As the mixture solidifies, the scandium becomes embedded within the glass matrix, resulting in the creation of glass beads containing the scandium source. To activate the scandium source, it is placed within the nuclear reactor and exposed to neutron irradiation. Neutrons interact with the scandium nuclei, leading to the activation of the scandium and the subsequent emission of gamma radiation. The thickness of the glass coating surrounding the scandium source can vary depending on the application and the desired level of radiation shielding. It is engineered to ensure adequate containment, minimizing the potential release of radioactive material, while allowing the emitted gamma radiation to pass through for detection. Determining the optimal thickness of the glass coating is often accomplished through calculations and simulations to enhance the overall performance

of the RPT system. Schematic of encapsulation of scandium source(core) in glass bead (shell) is shown in Figure 2.1I).

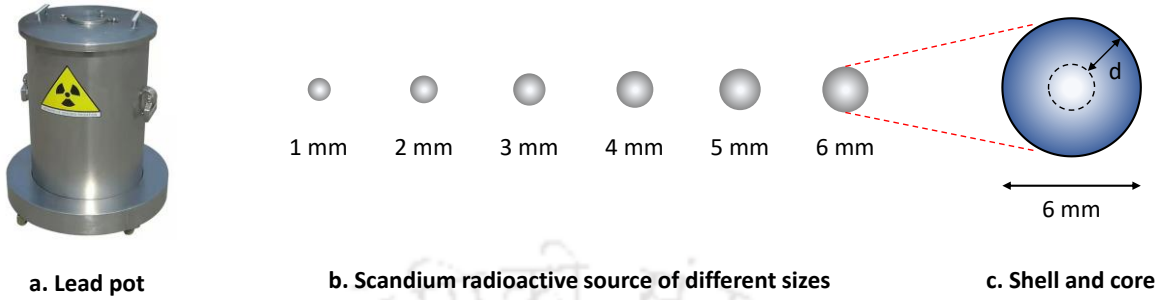

Figure 2.1: Radioactive particles of different sizes

2.3.2 Radiation sensing and data processing hardware

NaI scintillation detectors work by using a crystal of sodium iodide doped with thallium to convert gamma radiation into visible light flashes. The photomultiplier tube amplifies the light signals and converts them into electrical pulses. These pulses, along with pulse processing hardware such as SCAs, MCAs, and MIDAS, enable the detection, discrimination, and analysis of gamma radiation in radioactive particle tracking applications. Detailed working principle of radiation detection and photon counting unit is explained here.

2.3.2.1 Scintillation detector

In the RPT measurement technique, the radiation sensing units are typically NaI scintillation detectors. These detectors are designed to detect gamma radiation emitted by the radioactive particles in the system. NaI stands for sodium iodide, which is the scintillating material used in these detectors. The construction of NaI scintillation detectors involves a crystal of sodium iodide doped with a small amount of thallium (NaI(Tl)). When gamma radiation enters the detector, it interacts with the sodium iodide crystal, transferring its energy to the atoms within the crystal. This energy deposition causes the atoms to become excited from their ground state. As the excited atoms return to their ground state, they release the excess energy in the form of

photons, specifically photons of visible light. These emitted photons carry information about the energy of the gamma radiation that originally interacted with the crystal. In NaI scintillation detectors, the scintillator crystal and a photomultiplier tube (PMT) are the main components. The scintillator crystal is responsible for converting the energy from gamma radiation into visible light flashes. When the gamma radiation interacts with the crystal, it generates bursts or flashes of visible light photons. The photomultiplier tube (PMT) detects and amplifies the light signals emitted by the scintillator crystal. It consists of a vacuum-sealed tube containing a photocathode and a series of dynodes. When the light photons strike the photocathode, they cause the ejection of electrons through the photoelectric effect. These emitted electrons are then accelerated and multiplied as they pass through the dynodes, resulting in a significant amplification of the electrical signal. The output of the PMT is an electrical pulse whose amplitude is directly proportional to the energy of the gamma radiation that initially interacted with the NaI scintillation detector. This electrical pulse can be further processed and analyzed to obtain information about the radiation. In the context of radioactive particle tracking, NaI scintillation detectors serve as the radiation sensing units. They detect the gamma radiation emitted by the radioactive particles and convert it into electrical pulses. These pulses can be processed and analyzed to track the movement and behavior of the particles within the system. Summated photomultiplier detector output is transmitted to a single channel/multichannel pulse height analyser. Schematic of scintillation detector is shown in Figure 2.2.

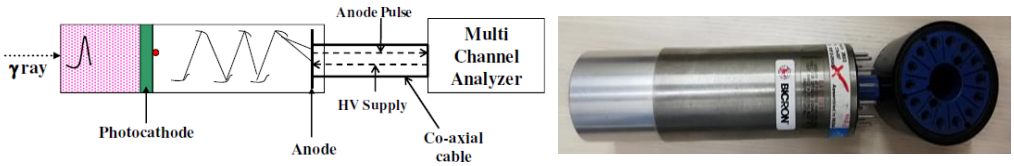

Figure 2.2: Scintillation detector

The pulse processing hardware used in radioactive particle tracking includes various components such as single channel analyzers (SCA), multi-channel analyzers (MCA), and multi-input data acquisition systems (MIDAS).

2.3.2.2 Single channel analyzer

A single channel analyzer (SCA) is a device used in radioactive particle tracking (RPT) to process the electrical pulses generated by a scintillation detector. Its main purpose is to count the number of photons received by the detector within a specific energy range and filter out undesirable pulses while reducing electronic noise. Unlike a multi-channel analyzer (MCA) that produces an energy spectrum, the SCA focuses on counting photons that fall within predetermined upper and lower energy thresholds. The SCA helps establish a window of acceptable energy levels for photon counting. Any pulses that fall within this energy window are considered valid photon counting events. When the scintillation detector records a photon counting event within the specified energy range, the SCA generates a TTL-compatible pulse. This pulse indicates that an input pulse falls between the base lI (E) level and the base line pulse window (E+ΔE) level. On the other hand, input pulses that fall outside of this energy band do not produce an output pulse. The SCA serves as a differential analyzer, the input pulses relative to a baseline level. Its primary function is to reduce electronic noise and eliminate undesirable pulses from the detection signal. By employing the SCA, the RPT system can improve the data quality by focusing on relevant photon counting events within the desired energy range. In earlier versions of RPT, only a low-level discriminator was applied to filter out unwanted pulses. However, in more recent configurations, both low-level and high-level discrimination have been utilized to further enhance the quality of the acquired data. This means that the SCA establishes both upper and lower energy thresholds to ensure that only

pulses within the desired energy range are counted and considered for analysis in the RPT system. Image of single channel analyser is shown in Figure 2.3

Figure 2.3: Single channel analyzer

2.3.2.3 Multi-channel analyzer

A multi-channel analyzer (MCA) is an important component in radioactive particle tracking (RPT) that is used for photon energy discrimination. Its primary function is to separate incident photons based on their energies, enabling the analysis of energy spectra. The MCA achieves this by converting analog signals from the photomultiplier tube (PMT) into digital data that can be processed and analyzed. The MCA operates on the principle of transforming continuous analog signals into their digital equivalents. By performing this conversion, the MCA enables the storage and display of digital information, specifically pulse height spectra, which is essential for recording and analyzing the energy distribution of the detected photons. An essential part of the MCA is the analog-to-digital converter (ADC). The ADC takes the analog signals produced by the PMT, which represent the energy levels of the detected photons, and converts them into discrete digital values. Image of ADC is shown in Figure 2.4.

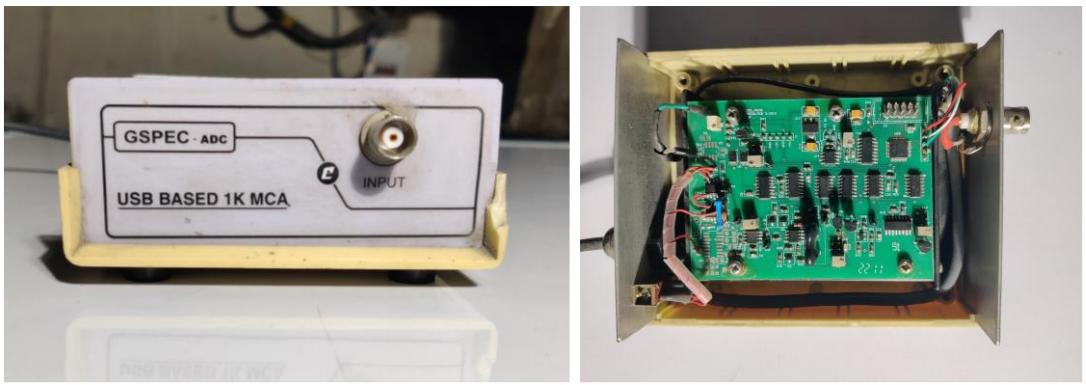

Figure 2.4: Analogue to digital converter (ADC)

These digital values are then stored in the memory of a computer, which has addressable locations corresponding to the maximum number of channels into which the spectrum can be divided based on energy. To achieve energy discrimination, the MCA requires a statistically significant number of photons over an extended period of time, resulting in a clear and well-defined energy spectrum. This means that the MCA performs best when it receives a large number of photons, allowing for accurate analysis of the energy distribution. However, it should be noted that the MCA's time resolution may be inadequate due to the need for a sufficient number of photons for accurate energy discrimination.

2.3.2.4 Multi-Input Data Acquisition System (used for photon acquisition)

MIDAS, in the context of radioactive particle tracking (RPT), refers to a specific unit designed for data acquisition from gamma radiation. It serves as a crucial interface between the RPT detectors and a computer system. The MIDAS unit facilitates the transfer of acquired data from the detectors to the computer's hard disk through a USB2 port. The MIDAS unit consists of several key components:

1. Power supply: This component is responsible for providing the necessary power to the entire assembly of RPT detectors. It is designed to offer a parallel circuit configuration,

enabling the supply of high voltage to each individual module. Typically, the power supply delivers +5V and ±15V outputs to meet the requirements of the system.

2. High voltage supply: The high voltage supply is a part of the Pulse Processing Unit (PPU) within the MIDAS unit. It utilizes a transformer to convert the provided voltage from the power supply into a higher voltage level known as the High Voltage (HV). The HV is essential for proper functioning of the detectors and the subsequent processing of the detected radiation signals.
3. Amplifier: The amplifier within the MIDAS unit is responsible for amplifying the weak electrical signals generated by the detectors in response to gamma radiation. The amplifier enhances the signal strength, making it easier to process and analyze the data.
4. Interface unit: This component acts as the interface between the MIDAS unit and the computer system. It enables the transfer of data from the MIDAS unit to the computer's hard disk through a USB2 port. The interface unit manages the communication and data transfer protocols, ensuring seamless integration between the RPT detectors and the computer system. Image of MIDAS used for current study is shown in Figure 2.5

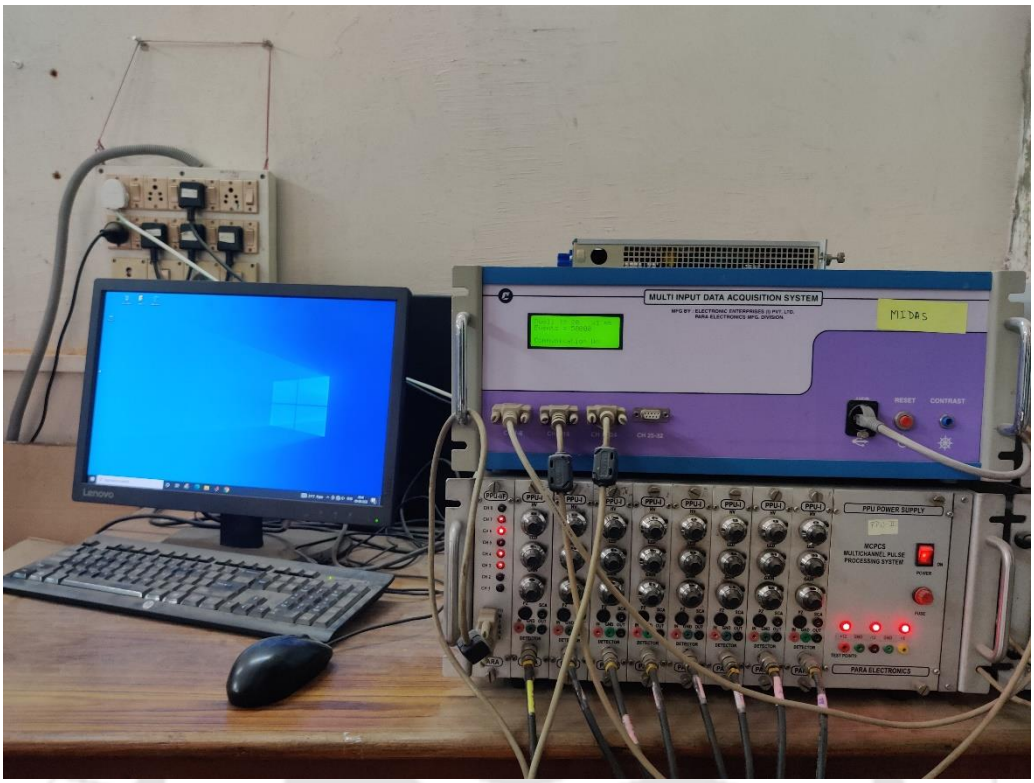

Figure 2.5: Multi input data acquisition system (MIDAS)

2.3.3 Resolution and sensitivity analysis

Resolution and sensitivity are important parameters in Radioactive Particle Tracking (RPT) measurement technique. They play a significant role in determining the accuracy and precision of particle tracking results. Prior to RPT implementation this analysis is performed. Resolution and sensitivity study determines the performance of RPT. In RPT, resolution refers to the ability to distinguish between individual particles and accurately measure their positions, while sensitivity refers to the capability of detecting and tracking low-intensity radioactive particles.

Resolution

It is the measure of uncertainty in locating the tracer particle

$$O_r = \sigma_c \frac{\partial r}{\partial C}$$

The detector's sensitivity is also defined as ratio between the change in recorded counts and the differential change in the position of the tracer particles.

Sensitivity

It is the measure of the ability of the detector to record a change in tracer particle location

$$S_r = \frac{1\partial c}{c\ \partial r}$$

The process of achieving resolution and sensitivity involves considering the number of detectors, the plane of detectors, and the alignments and orientations of detectors in each plane.

1. Number of Detectors: The number of detectors used in RPT affects both resolution and sensitivity. Increasing the number of detectors improves resolution by providing more data points for particle localization. It allows for a higher spatial resolution and reduces the ambiguity in particle tracking. Similarly, a greater number of detectors enhances sensitivity as it increases the chances of capturing radiation emitted by particles, especially when dealing with low-intensity sources. However, adding too many detectors can also increase the complexity of data processing and analysis.
2. Alignments and Orientations of Detectors in Each Plane: The alignment and orientation of detectors within each plane significantly impact the resolution and sensitivity of RPT. Proper alignment ensures that the detectors are accurately positioned relative to each other and the particle flow path. Aligning detectors in a straight line or grid pattern helps in precisely localizing particles in a plane. The orientation of detectors, such as their tilt or angle, can be adjusted to optimize the detection efficiency and improve sensitivity.

Schematic of different numbers of detects in two different configurations of orientations are shown in Figure 2.6.

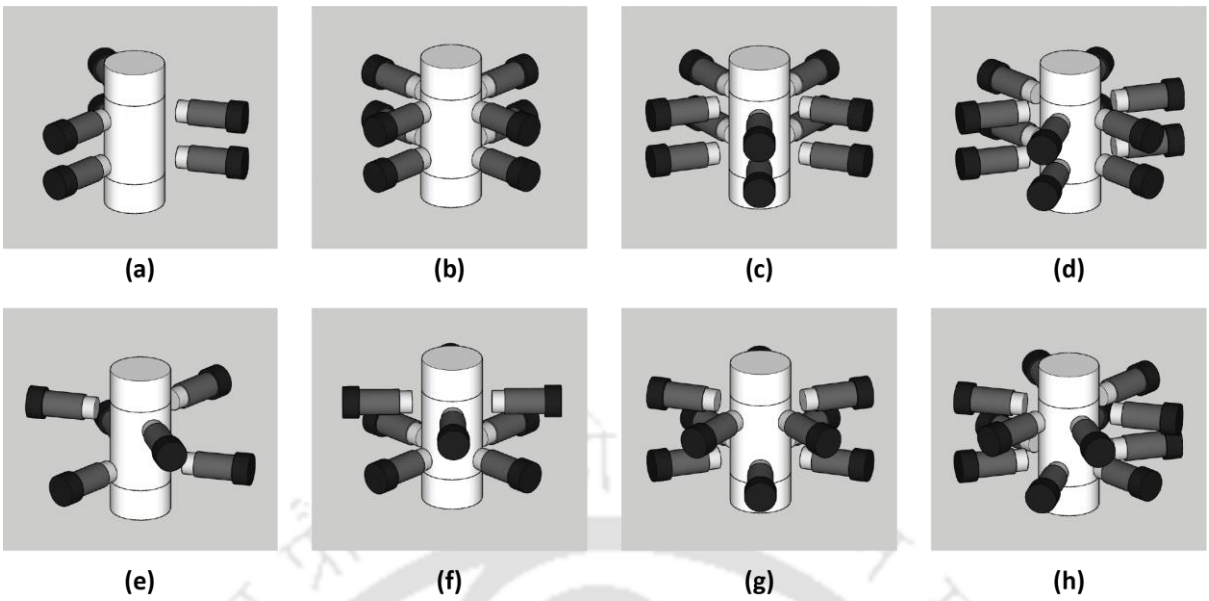

Figure 2.6: (a) Inline alignments of 3 detectors (b) Inline alignments of 4 detectors (c) Inline alignments of 5 detectors (d) Inline alignments of 6 detectors (e) Staggered alignments of 3 detectors (f) Staggered alignments of 4 detectors (g) Staggered alignments of 5 detectors (h) Staggered alignments of 6 detectors

3. Plane of Detectors: The arrangement of detectors in planes is crucial for achieving good resolution and sensitivity in RPT. Placing detectors in multiple planes along the column or flow path enables 3D tracking of particles. This three-dimensional information helps in accurately determining the position and trajectory of particles. Having detectors in different planes allows for the identification of particle movement in various directions, enhancing the overall resolution. The arrangement of planes should be carefully designed based on the specific system and flow characteristics.

In our current experimentation of RPT implementation, these four configurations are carried out and the calibration curves are checked

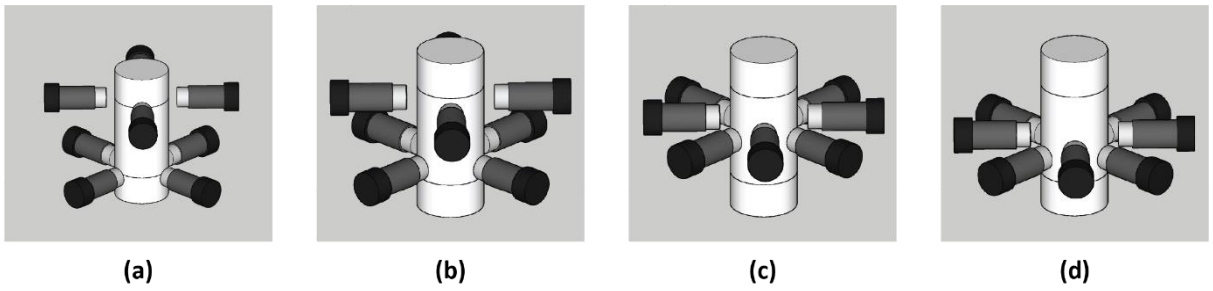

Figure 2.7: staggered alignments of 4 detectors in two planes (a) Two planes with center of detectors facing the sieve plate (b) Edges of detector faces configured between plates (c) close alignments with shortest distance between two plates in midst of two plates (d) close alignments with shortest distance between two plates slightly above bottom plate

4. Distance from wall of column: In RPT experiments, the accurate positioning of detectors is crucial. The selection of this distance is influenced by factors such as the strength of the radiation source and the diameter of the column. If the detectors are positioned too close to the wall of the column, they may become saturated with radiation, resulting in a loss of discrimination capability. This saturation can hinder the ability to accurately track and differentiate particles, leading to reduced resolution. On the other hand, if the detectors are placed too far from the wall, they may not effectively detect and discriminate particles located towards the center of the column. This can lower the sensitivity of the RPT system, as particles closer to the center may not be detected with sufficient accuracy. Therefore, the distance between the detectors and the wall of the column needs to be carefully chosen based on the specific conditions of the system, including the activity of the radiation source and the diameter of the column. Finding the right balance is crucial to ensure optimal performance and maximize the resolution and sensitivity of the RPT measurements.

In our current RPT implementation experimentation, we have also considered additional configurations and performed calibration curve checks. These configurations involve specific

setups and arrangements to assess the performance of the RPT system. The calibration curves are essential for relating the measured signals to the corresponding distances or positions within the system. By carrying out these additional configurations and calibration curve checks, we ensure that our RPT implementation is accurately calibrated and provides reliable and precise results. This helps validate the performance and effectiveness of the RPT technique in our experimental setup and enhances the overall quality of the data obtained from the system. The schematic of configurations varied for best calibration are shown in Figure 2.8

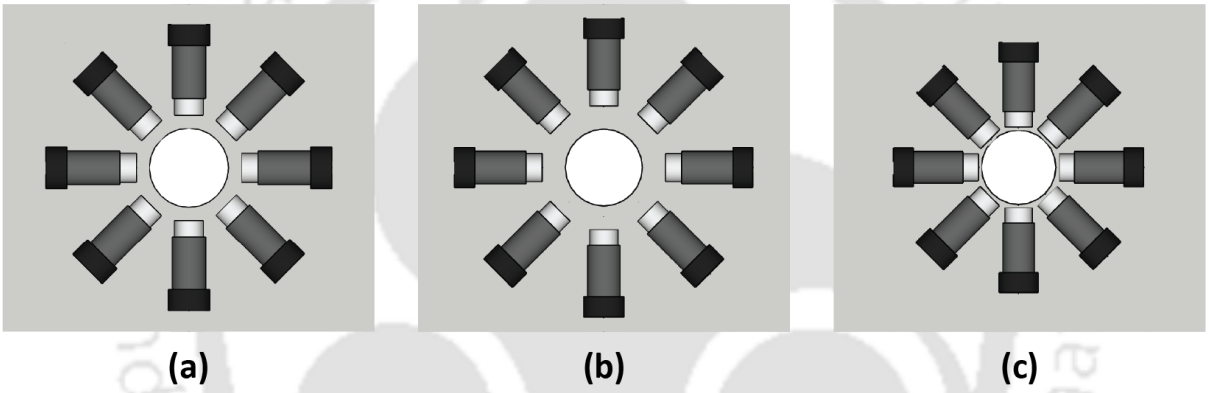

Figure 2.8: staggered alignments of 4 detectors in two planes (a) Reference distance of d between the face of detector and the column wall (b) Configuration of increased distance from the wall (c) Configuration of decreased distance from the wall

By carefully considering these parameters, the resolution and sensitivity of RPT can be enhanced. The appropriate number of detectors, well-planned arrangement of detector planes, and accurate alignments and orientations of detectors within each plane contribute to improved tracking precision and the ability to detect and track low-intensity radioactive particles. In the spatial domain, where RPT is performed, optimal results require a high resolution and a high sensitivity.

2.4 RPT Implementation steps

The implementation of the RPT (Radioactive Particle Tracking) technique in multiphase flow measurements refers to the application of RPT as a method for tracking and studying the behavior of radioactive particles within systems involving the flow of multiple phases. In multiphase flow, such as the flow of gas and liquid or the flow of different liquid phases, understanding the interactions, distribution, and movement of the phases is crucial for various industrial processes, research, and development. RPT offers a non-intrusive and accurate way to track the movement of radioactive particles within these complex flows. By introducing a small quantity of radioactive tracer particles into the system, the RPT technique allows researchers to monitor and analyze the behavior of these particles as they move through the multiphase flow. The particles emit gamma radiation, which can be detected using scintillation detectors or other radiation sensing devices. The emitted radiation is then processed and analyzed to obtain information about the particle trajectories, velocity, concentration, and other parameters of interest. The implementation of RPT in multiphase flow measurements provides valuable insights into the hydrodynamics, mixing, and flow characteristics of the different phases. It helps researchers understand the flow patterns, identify any bottlenecks or regions of poor mixing, optimize process parameters, and validate computational models or simulations. The step wise flow chart of RPT measurement is explained in detail here.

1. The flowchart of the RPT process, starting from setting the reference frame, utilizing a scintillation detector as the photon counting device, and using MIDAS as the pulse processing unit, can be outlined as follows:
2. Set the reference frame: Establish a fixed reference frame within the system, typically aligned with the column or vessel being studied. This frame serves as a spatial reference for tracking the movement of radioactive particles.

3. Scintillation detector as the photon counting device: Position the scintillation detector(s) at predetermined locations within the system. These detectors will capture the emitted photons from the radioactive particles and convert them into electrical pulses.
4. Utilize MIDAS as the pulse processing unit: Connect the scintillation detector(s) to the MIDAS unit, which serves as the pulse processing unit. MIDAS converts the analog electrical pulses from the detector(s) into digital data for further analysis and processing.
5. Post-process distance from the generated count using calibration: Use calibration data, such as a lookup table, to establish a relationship between the detected counts and the corresponding distances or positions. This calibration process ensures accurate mapping of the particle positions based on the detected photon counts.
6. Monte Carlo optimization algorithm: Apply the Monte Carlo optimization algorithm to refine and optimize parameters such as source strength, decay constant, and wall attenuation constant. This algorithm utilizes the calibrated data for known positions to simulate and generate counts, allowing for the optimization of these parameters to improve accuracy and reliability.
7. Reconstruction process and algorithm: Implement a reconstruction process and algorithm to interpret the optimized counts and estimate the particle positions within the system. This algorithm takes into account the optimized parameters, calibration data, and the geometry of the system to reconstruct the particle trajectories and locations.

By following these steps in the RPT process, from setting the reference frame to utilizing the scintillation detector, MIDAS as the pulse processing unit, post-processing the distance using calibration, applying the Monte Carlo optimization algorithm, and employing the reconstruction process and algorithm, we can accurately track and analyze the movement of radioactive particles within the system. These steps ensure reliable and precise results in understanding the hydrodynamics and behavior of multiphase flows in various applications.

In short the easier understanding can be made using three steps as shown in Figure 2.9

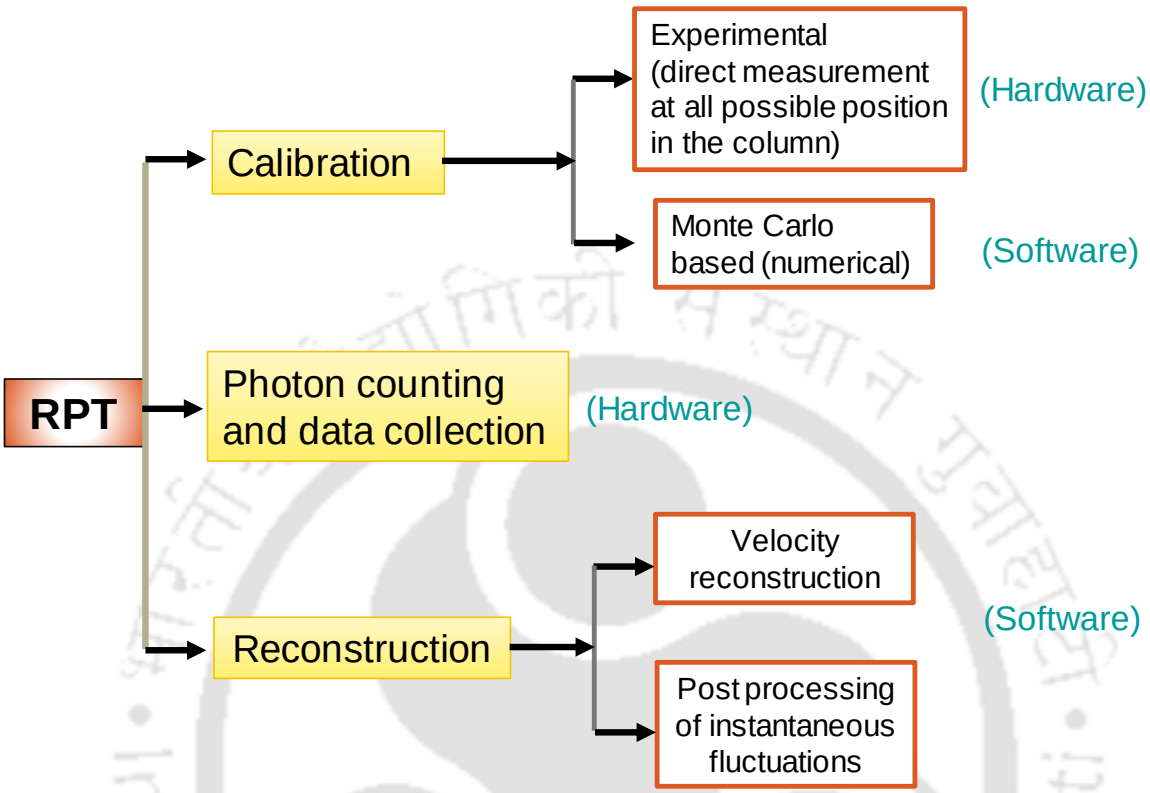

Figure 2.9: Steps in RPT

2.4.1 Experimental calibration

Calibration in radioactive particle tracking (RPT) in liquid systems is a crucial step that involves establishing a relationship between the measured signals from the detectors and the physical quantities of interest, such as particle position, velocity, and concentration. Calibration ensures accurate and reliable measurements and allows for the interpretation of experimental data. After ensuring best resolution and sensitivity of the sensors the source is calibrated. In this step the position of the crystal of detectors and the distance of those from the centre of column and from the wall of the column are ensured for best mapping. The calibration process in RPT typically involves the following steps:

2.4.1.1 Source calibration

1. Experimental Setup: A representative system is prepared, consisting of the liquid medium in which the particles will be tracked. The system can be a laboratory-scale setup or an industrial process, depending on the application.
2. Tracer Particle Selection: A suitable radioactive tracer particle is chosen to be introduced into the system. The tracer particle should have characteristics that enable it to mimic the behavior of the particles of interest in the flow. For example, the size, density, and surface properties of the tracer particle should closely match those of the particles being tracked.
3. Particle Injection: The tracer particle will be injected into system. In liquid system the particle will be made neutrally buoyant and will be introduced in to system to mimic the flow of continuous phase as marker phase.
4. Detector Calibration: The radiation sensing detectors, such as scintillation detectors, are calibrated using standardized procedures. This involves determining the detector response to a known quantity of radiation and establishing a calibration curve relating the measured counts or signals to the actual radiation intensity.
5. Signal Processing: The signals detected by the radiation sensing detectors are processed using appropriate pulse processing units, such as MIDAS (Modular Intelligent Data Acquisition System). The signals are converted into digital data and stored for further analysis.
6. Data Collection: The system is operated under various flow conditions, and data is collected by monitoring the signals from the detectors over time. The data includes the counts or intensities of radiation detected at different detector locations.
7. Analysis and Calibration Curve Generation: The collected data is then used to generate calibration curves or lookup tables that relate the measured signals to the desired physical quantities, such as particle position or velocity. This is done by correlating the measured

radiation counts with known reference positions or velocities obtained from other measurement techniques or simulations.

The process of making the source particle neutrally buoyant for mimicking the flow of the continuous phase (water) as a marker phase involves ensuring that the density of the tracer particle closely matches that of the continuous phase. This is important because if the tracer particle is denser or lighter than the continuous phase, it may not accurately represent the behavior of the particles in the flow. To achieve neutral buoyancy, the density of the tracer particle can be adjusted by using additives or coatings. For example, the particle can be coated with a thin layer of a material that alters its density, bringing it closer to the density of the continuous phase. By adjusting the coating thickness or composition, the density of the tracer particle can be finely tuned to match that of the continuous phase. The neutrally buoyant tracer particles behave similarly to the particles in the continuous phase, allowing for accurate tracking and characterization of the flow. This is particularly important in multiphase flow systems where the interactions and behavior of the particles are influenced by their buoyancy and settling characteristics. By mimicking the behavior of the continuous phase, the neutrally buoyant tracer particles enable a more realistic representation of the flow dynamics and provide valuable insights into the overall flow behavior.

Calibration is done prior to experiment where the tracer particle is placed at various known locations and its intensity (count rate) is recorded at each detector. This is achieved by calibration plate and the requirements and functioning of this plate is detailed in here. The intensity recorded by each detector depends on the distance between the particle and detector. The intensity of radiation recorded at each detector decreases exponentially with increase in the distance between the tracer particle and detector. Using these information calibration curves is plotted which relates the intensity of radiation recorded at a detector to the distance between the tracer and detector. A calibration plate is made to ensure positioning of the radioactive

source inside different places of interest. This detailed procedure of applications of calibration plates allows us to understand the significance of calibration data and its significance in confirmation of ideal reference frame.

2.4.1.2 Calibration device

In radioactive particle tracking (RPT), a calibration plate plays a crucial role in positioning the radiation source at precise and predetermined locations within a multiphase system, typically involving water as the continuous phase. This specialized apparatus serves as a reference point for the validation and calibration of the tracking system. The calibration plate is typically made of solid or transparent materials, such as acrylic or glass, and features multiple strategically placed holes or slots arranged in a specific pattern. These holes or slots act as target locations for the radiation source, allowing for accurate positioning. To utilize the calibration plate, several steps are followed. First, the plate is prepared by manufacturing or fabricating a suitable material with the desired hole or slot pattern, ensuring compatibility with the radiation source and the multiphase system being studied. The calibration plate is then positioned within the multiphase system, ensuring proper alignment and secure placement. Depending on the experiment's objectives, the plate may be located at specific positions within the system, such as near the walls or at the center. Next, the radiation source, typically a radioactive tracer particle, is carefully inserted into each hole or slot of the calibration plate. It is crucial to securely position and align the source with the plate to achieve accurate tracking and reliable measurements. The system is operated, and radiation sensing detectors, such as scintillation detectors, are used to measure the radiation emitted by the source at different positions. These detectors capture the signals and convert them into digital data for further analysis. The collected data is then compared to the known positions of the radiation source provided by the calibration plate. This comparison enables the calibration of the tracking system by establishing

the relationship between the measured signals and the actual source positions. Additionally, it serves to validate the accuracy and reliability of the tracking system. Utilizing a calibration plate in RPT allows for the accurate determination of the radiation source positions within the multiphase system. This calibration process enables the conversion of measured signals into meaningful spatial information, such as particle trajectories, velocities, and concentrations. The calibration plate acts as a reliable reference for validating the performance of the tracking system, ensuring precise and accurate measurements in multiphase flow experiments involving water or other continuous phases. Currently used calibrated plate and one set data of calibration of source are explained below.

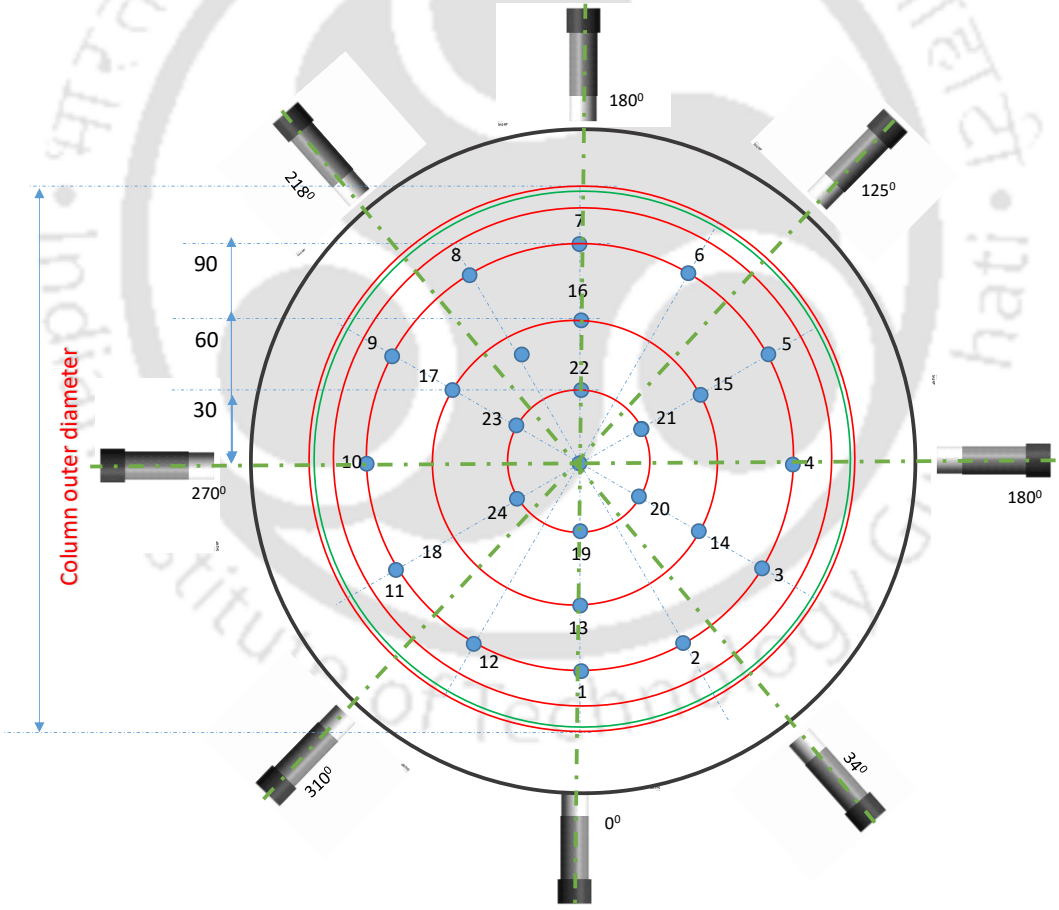

Figure 2.10: Arrangement of detectors

The particle is made neutrally buoyant. A radioactive scandium source is pasted on the tip of a rod and is placed inside column using calibration plate as shown in Figure 2.10. Twenty-four ports are chosen on calibration plate for inserting radioactive source at 240 known locations with a change of 1 cm in axial direction. The particle is kept at every location and the count is acquired in three iterations for consistency. Figure 2.11 describe the count vs distance map of first detector. Ports 6 and 8 are symmetric at same distance from detector 1 and the count is nearly similar in pattern. These ports are far from detector 1 so the count associated with is because the distance is high. Port 1,2 and 12 are closest to detector 1 and hence the count is showing high. Port 7,16 and 22 are straight behind the rod hence they have fringe behaviour slightly away from the exponential nature of distance vs count map. Same effective distance from the detector 1 shows the equivalent same count as we can see from the Figure 2.11. Similar count map will be recorded and act as look up table. From the known 240 positions count is generated for lakhs of points using Monte Carlo interpretation algorithm by optimising SS, tau, wallmue parameters.

The algorithms associated with the reconstruction stage are detailed in below sections in RPT post processing step.

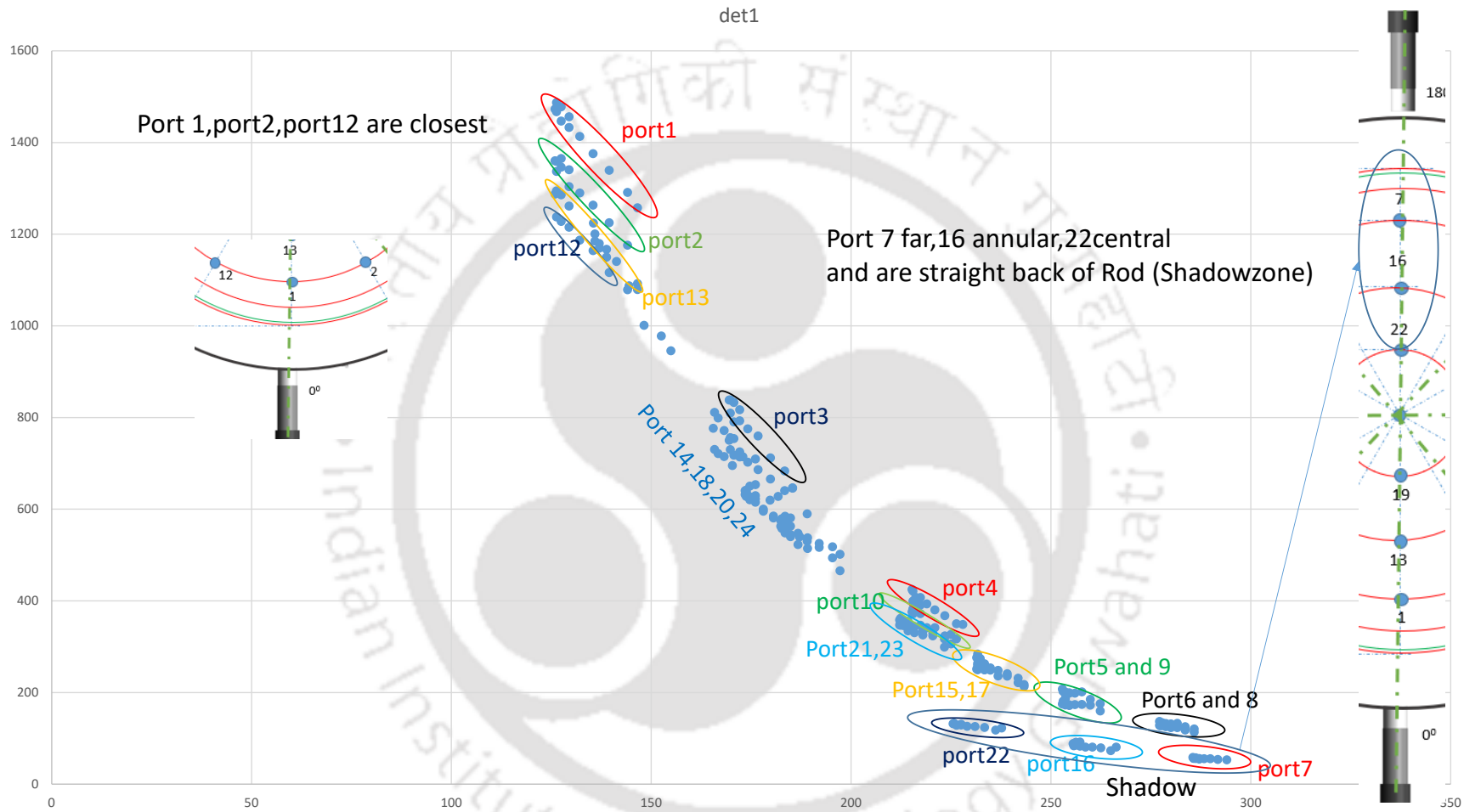

Figure 2.11: Count vs distance map for detector 1

2.4.2 Reconstruction algorithms (Development of algorithm)

As the particle move inside the column it changes its position with time, so algorithms are used for position reconstruction of particle inside the column. The different algorithms used are Monte Carlo method, Weighted Least Square Regression method, Feed Forward Neural Network method and Cross Correlation method.

2.4.2.1 The weighted least square algorithm

In this method the distance between the detector and particle is expressed by a polynomial function of the number of counts (Lin et al., (1981); Devanathan et al. (1990); Yang et al. (1992); Degaleesan (1997) etc.). The polynomial is fitted to the data obtained during calibration. As the particle is small it is assumed to be a point source. At least four detectors are adequate to provide the coordinates of the particle. The numbers of detectors are increased to reduce error due to fluctuation of signals. The uniform distribution of detectors around the bed also reduces error generation. The result of this method depends on the proper introduction of weighting function. This approach has a disadvantage of low accuracy and resolution in dense flows when the detector is far from the column wall.

2.4.2.2 Monte Carlo Method

As the particle moves inside the entire column its occurrence near the front face of the detector is lesser than the side face. So the side face of the detector receives more counts than the front face. Monte Carlo method is used in RPT technique for generating photon counts (Roy, 2002). The number of photo peak photon counts recorded by a detector can be calculated by using equation (Larachi et al., 1994; Roy, 2000).

$$C = \frac{T\nu A\varepsilon_{abs}\phi}{1+\tau\nu A\varepsilon_{abs}\phi} \tag{2.14}$$

Where, T = sampling time (s)

ν = Number of gamma ray photons emitted per disintegration

A = Source strength (Ci)

ε_{abs} = Absolute efficiency of detector

ϕ = Photo peak fraction

τ = Detector dead time (s)

The absolute efficiency ε_{abs} is calculated by equation (Larachi et al., 1978; Roy, 2000).

$$\varepsilon_{abs} = \oiint_{\Omega} \frac{\vec{r}.\vec{n}}{r^3} \exp\left(-\sum_{j=1}^{N} \mu_j l_j\right)\left(1-\exp\left(-\mu_D d\right)\right) d\Sigma \tag{2.15}$$

Where, $\vec{n}$ is the radius vector from source to detector

$\vec{r}$ is the unit normal vector to the curved surface of the detector

μ_D is the mass attenuation coefficient of the detector crystal material

d is the penetration depth of photons in the detector crystal

μ_j is the mass attenuation coefficient of all the materials that comes in the path of photons between the source and the detector

In equation three parameters are unknown, they are dead time, source strength and medium attenuation coefficient. To know these unknown parameters experiment is conducted where the

radioactive particle is placed at different known location so that they can be used in Monte Carlo algorithm. Figure 2.11 shows the schematic diagram of positioning of source and detector when the source is outside detector flat face and within the detector flat face. Electronic settings in RPT are kept same for two scales of application. To capture changes of pulsation we need to use 20 hz (5 milli seconds). Gain need to set as low as possible so that before the pulsation cycle changes data need to be acquired.

2.4.3 RPT Post Processing (Distance count Map)

After acquiring the data of tracer position with respect to time many parameters will be calculated. The time differentiations of these positions give instantaneous velocities of the particle. For determining mean velocity, the column will be divided in to a number of sampling compartments. As the experiment progress for a long time, the particle passes through one compartment several times. From this number of occurrences of the particle in a specific compartment the ensemble average velocity is calculated. The column is discretized with equal volume of compartment. Different parameters need to be calculated using the following equations. Quantities calculated from RPT experimental data are explained in detail. The instantaneous velocities in r, θ and z direction is given by equations

Instantaneous velocity

$$v_r = \frac{2}{\Delta t}\left[r_2 \cos\left(\theta_2 - \theta\right) - r\right] \tag{2.1}$$

$$v_\theta = \frac{2}{\Delta t}\left[r_2 \sin\left(\theta_2 - \theta\right)\right] \tag{2.2}$$

$$v_z = \frac{\Delta z}{\Delta t} \tag{2.3}$$

Where,

$$r = \frac{1}{2}\sqrt{r_1^2 + r_2^2 + 2r_1 r_2 \cos\left(\theta_1 - \theta_2\right)} \tag{2.4}$$

The average velocities measurements are given by below equations

Ensemble average velocity

$$\left\langle v_q\left(i,j,k\right)\right\rangle = \frac{1}{N\left(i,j,k\right)}\sum_{n=1}^{N(i,j,k)} v_{q,n}\left(i,j,k\right) \tag{2.5}$$

Fluctuating velocity component

$$v_q\left(i,j,k\right) = v_q\left(i,j,k\right) - \left\langle v_q\left(i,j,k\right)\right\rangle \tag{2.6}$$

Azimuthal average velocity component

$$\left\langle v_q\left(i,k\right)\right\rangle^{az} = \frac{\sum_{j=1}^{T_{\dim}(i)} \left\langle v_q\left(i,j,k\right)\right\rangle N\left(i,j,k\right)}{\sum_{j=1}^{T_{\dim}(i)} N\left(i,j,k\right)} \tag{2.7}$$

RMS velocity

$$\left\langle v_q\right\rangle^{RMS} = \sqrt{\left\langle v_q^{'2}\right\rangle} \tag{2.8}$$

The stress and kinetic energy is given by equation below equations

Stress

$$\tau_{qs} = \rho_p \left\langle v_q^{'}\left(i,j,k\right) v_s^{'}\left(i,j,k\right)\right\rangle \tag{2.9}$$

Fluctuating kinetic energy per unit volume

$$KE = \frac{1}{2}\rho_p \left[\left\langle v_r'^2 \right\rangle + \left\langle v_\theta'^2 \right\rangle + v_z'^2 \right] \tag{2.10}$$

Total kinetic energy per unit mass

$$K = \frac{1}{2}\left[\left\langle v_r'^2 \right\rangle + \left\langle v_\theta'^2 \right\rangle + v_z'^2 \right] \tag{2.11}$$

Several works have been done on RPT with wide variety of experimental setup. Brief review of the key work on RPT is given in literature section. Step wise algorithm of evaluation of measurement parameters are explained here using the above formulae

The step wise process of RPT quantities using calibration data, experimental counts from individual detectors, and various derived parameters involves the following steps:

i. Calibration Data: The process begins with obtaining calibration data using a calibration plate, as discussed earlier. This data provides the relationship between the measured signals and the known positions of the radiation source.

ii. Experimental Counts: The radiation sensing detectors, such as scintillation detectors, capture the radiation counts from the source at different positions within the multiphase system. These experimental counts are recorded and stored for further analysis.

iii. Instantaneous Position: Using the calibration data and the measured counts, the instantaneous position of the radiation source is determined. This provides information about the location of the source at a particular instant in time.

iv. Ensemble Average Velocity: By analyzing the position data over multiple instances, the ensemble average velocity of the radiation source can be calculated. This parameter gives an average measure of the source's velocity within the system.

v. Azimuthal Average Velocity: In systems with rotational symmetry, such as cylindrical columns, the azimuthal average velocity is calculated. This parameter considers the average velocity of the source around the column's circumference, providing insights into the flow pattern.

vi. Fluctuation Velocity: The fluctuation velocity represents the variability or fluctuations in the source's velocity. It is obtained by analyzing the deviations from the ensemble average velocity, reflecting the turbulent nature of the flow.

vii. RMS Velocity: The Root Mean Square (RMS) velocity is a measure of the overall magnitude of the velocity fluctuations. It quantifies the intensity of the turbulence within the system.

viii. Turbulent Kinetic Energy: The turbulent kinetic energy represents the energy associated with the turbulent motion within the system. It is derived from the velocity fluctuations and provides information about the turbulence intensity.

ix. Reynold Stress: The Reynold stress is a measure of the correlations between velocity fluctuations in different directions. It characterizes the interactions between different components of the flow and provides valuable information about the turbulent flow dynamics.

These parameters contribute to a comprehensive understanding of the multiphase system and assist in analyzing its hydrodynamic behavior. The glimpse of flow chart from the above algorithm is shown in Figure 2.12.

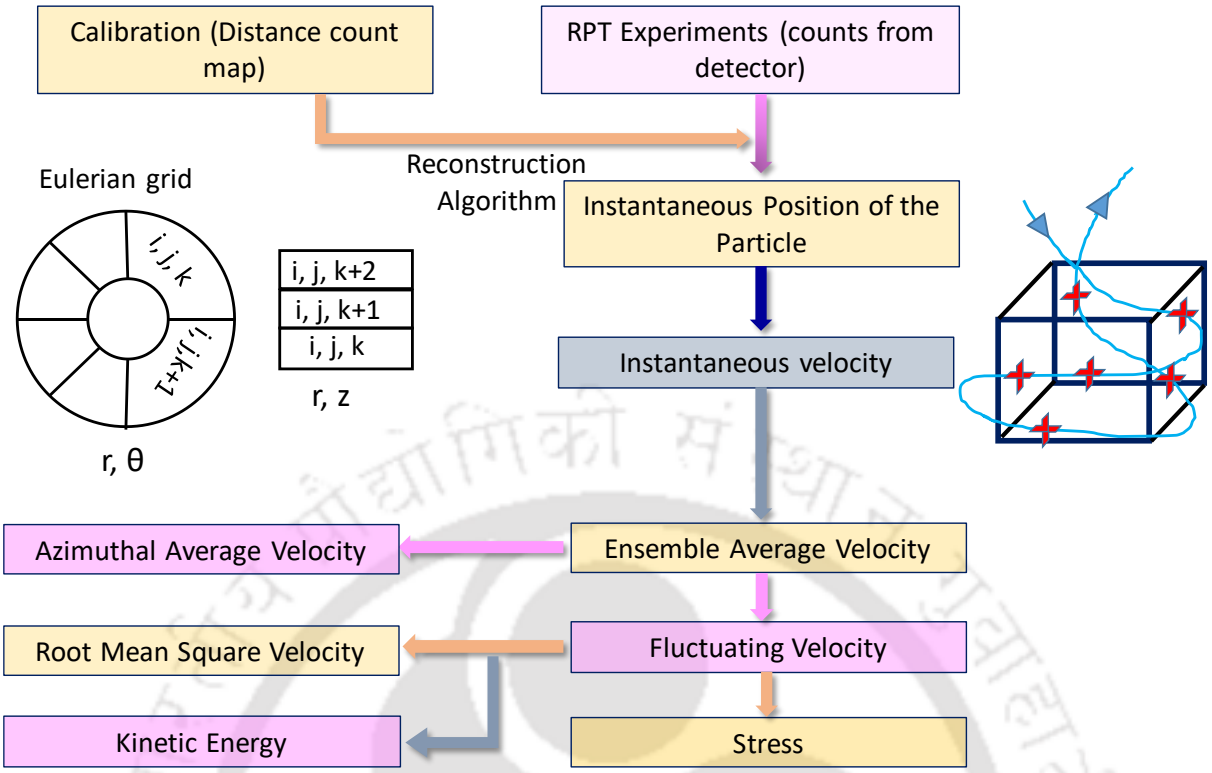

Figure 2.12: Flowchart of Radioactive particle tracking tique

2.5 Experimentation glimpse: The laboratory-scale pulsed sieve plate column employed in the current study features a column of diameter (D) 75 mm, height (H) of 600 mm, and a plate spacing (h) of 100 mm. The holes in the sieve plates have a diameter of 3 mm, contributing to a fractional free area (α) of 17%. Six plates are used as internal in the laboratory scale column with a plate spacing of 10 cm. Two types of geometric configurations are used namely sieve plate and slotted plate with similar FFA for the RPT experimentation further details of plates are explained in the chapter. For experimental investigations, the unit between the third and fourth plates is chosen so as to ensure that the flow is free from the exit and end effects.

Six scintillation detectors are strategically arranged in two planes around the column, ensuring coverage of all zones within the space. The r, theta, and z positions of the center of scintillation detectors is provided in the table.

Table 2.2: Crystal positions of detectors:

Detector	**r**	**theta**	**z**
Det 1	71	0	289
Det 2	60	90	289
Det 3	83	180	289
Det 4	79	270	289
Det 5	80	315	330
Det 6	80	135	336

Table 2.3: calibration grid:

r	**theta**	**z**	**r**	**theta**	**z**	**r**	**theta**	**z**	**r**	**theta**	**z**	**r**	**theta**	**z**
0	0	260	18	0	260	18	90	260	18	180	260	18	270	260
0	0	270	18	0	270	18	90	270	18	180	270	18	270	270
0	0	280	18	0	280	18	90	280	18	180	280	18	270	280
0	0	290	18	0	290	18	90	290	18	180	290	18	270	290
0	0	300	18	0	300	18	90	300	18	180	300	18	270	300

0	0	310	18	0	310	18	90	310	18	180	310	18	270	310
0	0	320	18	0	320	18	90	320	18	180	320	18	270	320
0	0	330	18	0	330	18	90	330	18	180	330	18	270	330
0	0	340	18	0	340	18	90	340	18	180	340	18	270	340
0	0	350	18	0	350	18	90	350	18	180	350	18	270	350

Utilizing a top calibration plate, a Sc^{46} radiotracer of 1.6 mm diameter and a density of 2.85 g/cm^3 is affixed at various r, theta, and z positions using a one-meter long rod. The rod, with the attached radiotracer, is inserted through the calibration plate, placing the tracer at 170 distinct positions, some of the positions are mentioned in above table Detectors are triggered to acquire counts at an acquisition frequency of 20 milliseconds. These 6 detectors systematically monitor the gamma rays emitted by the source at various positions, forming a comprehensive look-up table. As it is impractical to place particles in every spatial location, the Monte Carlo algorithm is employed to generate detector counts based on the solid angle using the beam et al. algorithm. Different detectors subtend different solid angles relative to the reference positions of the source (top, front, angular). Leveraging known six detector positions and 170 calibrated counts, counts are generated for 1,40,400 positions across the volume between the third and fourth plates (finest grid).

Under experimental conditions, the particle, enclosed in a 3.2 mm bead, is made neutrally buoyant and placed between the third and fourth plates. Note that the particle diameter is chosen bigger than the hole diameter in the sieve plate so as to ensure that the particle always remains between the plates. Changes in system dynamics over time may necessitate periodic recalibration for accounting decay constant. Phase-specific recalibration is not needed because

we are tracking the aqueous phase all the time but time-specific calibration is needed. For this purpose, calibration is performed before and after the experiment for the laboratory scale column and for the bigger scale column calibration is performed thrice. The exact location, alignment, and size of the detectors are shown in Fig. 2.10. The neutrally buoyant particle covers all positions in the chosen zone, divided into fine grids.

In the current laboratory-scale study, the Stokes number of the neutrally buoyant particle is determined to be 0.14. For all experiments in this study, the frequency is 1 Hz, and any variation in pulsation velocity (Af) is solely caused by variations in pulsation amplitude. The amplitude of the pulsation ranges between 20 to 40 percent of the column diameter. The column is operated at four different pulsation velocities: 1.7 cm/s, 2.2 cm/s, 2.7 cm/s, and 3.3 cm/s. The amplitude of the liquid column's pulsation is controlled by regulating the pulsation amplitude of the air column in the pulse leg. All the files are acquired at 50 hz frequency.

Uncertainty and Reproducibility analysis of the particle position and velocity:

Initially, calibration was performed with known locations, with the exception of a few inaccessible ones, using a calibration plate. Count data was then generated for the entire 3D space using optimization techniques. In the subsequent stage, the particle was placed at a known position different from those used during count generation, and its position reconstruction was cross-checked using the generated count data. This process served to confirm the accuracy of the position reconstruction. Later, the predicted position of the particle was determined. Visually, the particle was placed on the plate and subjected to pulsation at a velocity of 1 cm/s. Observations of the particle's behaviour were made visually, and its velocity was then post-processed using the calibrated data and the experimental count registered. It was confirmed that the visual observations for the operating condition matched the z velocity

through RPT post-processing. This validation process ensured the accuracy and reproducibility of the analysis.

Reference

Bhusarapu, S., 2005, "Solids flow mapping in gas-solid risers", D.Sc. thesis. Washington University in Saint Louis, Missouri, USA.

Chen, J., Kemoun, A., Al-Dahhan, M. H., Dudukovic, M. P., Lee, D. j., Fan, L. S., 1999, "Comparative hydrodynamics study in a bubble column using computer-automated radioactive particle tracking (CARPT)/computed tomography (CT) and particle image velocimetry (PIV)", *Chem. Eng. Sci.* 54, 2199–2207. https://doi.org/10.1016/S0009-2509(98)00349-2.

Chaouki, J., Larachi, F., and Dudukovic, M.P., 1997, "Non-invasive monitoring of multiphase flows", Elsevier, New York

Degaleesan, S., 1997, "Fluid dynamic measurements and modelling of liquid mixing in bubble columns", D. Sc. Thesis. Washington University, St. Louis.

Devanathan, N., 1991, "Investigation of liquid hydrodynamics in bubble columns via computer automated radioactive particle tracking", D.Sc. thesis. Washington University, Missouri, USA.

Devanathan, N., Moslemian, D., Dudukovic, M. P., 1990, "Flow Mapping in Bubble Columns", *Chem. Eng. Sci.* 452285–2291.

Dudukovic, M. P., 2000, “Opaque Multiphase Reactors: Experimentation, Modeling and Troubleshooting”, *Oil Gas Sci. Technol.* 55, 135–158. https://doi.org/10.2516/ogst:2000008.

Degaleesan, S., Dudukovic, M. P., Pan, Y., 2002, “Application of wavelet filtering to the radioactive particle tracking technique”, *Flow Measurement and Instrumentation*, 3(1-2), 31-43.

Dudukovic, M. P., 2003, “Use of gamma Ray computed tomography (CT) and computer aided radioactive particle tracking (CARPT) in multiphase reactors”. *Hem. Ind.* 57, 249–261. https://doi.org/10.2298/hemind0306249d.

Fraguío, M. S, Cassanello, M. C., Degaleesan, S., Dudukovic, M., 2009, “Flow regime diagnosis in bubble columns via pressure fluctuations and computer-assisted radioactive particle tracking measurements”, *Ind. Eng. Chem. Res.* 48, 1072–1080. https://doi.org/10.1021/ie800549d.

Jain, V.; Kalo, L.; Kumar, D.; Pant, H. J.; Upadhyay, R. K., 2017, “Experimental and numerical investigation of liquid-solid binary fluidized beds: Radioactive particle tracking technique and dense discrete phase model simulations”, Particuology. 33, 112-122. https://doi.org/10.1016/j.partic.2016.07

Kamalanathan, P.; Kalo, L.; Pant, H. J.; Upadhyay, R. K., 2017, “Effect of dynamic bias on accuracy of radioactive particle tracking (RPT) technique at different data acquisition frequencies”, *Appl. Radiat. Isot.* 128, 13-21. https://doi.org/10.1016/j.apradiso.2017.06.034.

Kalo, L.; Kamalanathan, P.; Pant, H. J.; Cassanello, M. C.; Upadhyay, R. K. 2019, "Time series analysis of a binary gas-solid conical fluidized bed using radioactive particle tracking (RPT) technique data", *Chem. Eng. J.* 377, 119807. https://doi.org/10.1016/j.cej.2018.08.193

Kalo, L., Kamalanathan, P., Pant, H. J.; Cassanello, M. C., Upadhyay, R. K., 2019, "Mixing and regime transition analysis of liquid-solid conical fluidized bed through RPT technique". *Chem. Eng. Sci.* 207, 702–712. https://doi.org/10.1016/j.ces.2019.07.005.

Kondukov, N.B., Kornilaev, A.N., Skachko, I.M., Akhromenkov, A.A. and Kurglov, A.S., 1964, "An investigation of the parameters of moving particles in a fluidized bed by a radioisotope method", *Int. Chem. Eng.*, 4, 43-47.

Kunii, D. and Levenspiel, O., 1991, "Fluidization engineering", Butterworth- Heinemann series in Chemical Engineering, Ch.8.

Larachi, F., G. Kennedy, G., Chaouki, J., 1994. "A γ-ray detection system for 3-D particle tracking in multiphase reactors", *Nucl. Inst. Methods Phys. Res. A.* 338, 568–576. https://doi.org/10.1016/0168-9002(94)91343-9.

Larachi, F., Chaouki, J., Kennedy, G., Dudukovic, M. P., 1997, "Radioactive particle tracking in multiphase reactors: principles and applications", in Non-Invasive Monitoring of Multiphase Flows, J. Chaouki, F. Larachi, and M. P. Dudukovic, Eds., Elsevier, New York.

Levenspiel, O., Bischoff, K. B., 1963, "Patterns of flow in chemical process vessels", *Advan. Chem. Eng.*, 4, 95-198.

Levenspiel, O., 1999, “Chemical reaction engineering”, John Wiley & Sons, Third Ed.

Lin, J.S., Chen, M.M., and Chao, B.T., 1985, “A novel radioactive particle tracking facility for measurement of solids motion in gas fluidized beds”, *AIChE J.*, 31, 465-473.

Moslemian, D., 1987, “*Study of solids motion, mixing and heat transfer in gas-fluidized beds*”, Ph.D Dissertation, University of Illinois at Urbana-Champaign, Urbana, Illinois.

Rammohan, A., Kemoun, A., Al-Dahhan, M. and Dudukovic, M., 2001, “A Lagrangian description of flows in stirred tanks via computer automated radioactive particle tracking (CARPT)”, *Chem. Engg. Sci., 56,* 2629-2639.

Roy, S., Kemoun, A., Al-Dahhan, M. H., Dudukovic, M. P., 2005, “Experimental investigation of the hydrodynamics in a liquid-solid riser”. *AIChE J.* 51, 802–835. https://doi.org/10.1002/aic.10447.

Roy, S., Larachi, F., Al-Dahhan, M. H., Dudukovic, M. P., 2002, “Optimal design of radioactive particle tracking experiments for flow mapping in opaque multiphase reactors, *Appl. Rad. Isot.* 56, 485–503. https://doi.org/10.1016/S0969-8043(01)00142-7.

Upadhyay, R. K.; Pant, H. J.; Roy, S., 2013. “Liquid flow patterns in rectangular air-water bubble column investigated with Radioactive Particle Tracking”, *Chem. Eng. Sci.* 96, 152–164. https://doi.org/10.1016/j.ces.2013.03.045.

Wang, T., Lin, Z.J., Zhu, C.M., Liu, D.C. and Saxena, S.C., 1993, “Particle velocity measurements in a circulating fluidized bed”, *AIChE J.*, 39, 1406-1410.

Xu, G., Sun, G., Nomura, K., Li, J. and Kato, K., 1999, "Two distinctive variational regions of radial particle concentration profiles in circulating fluidized bed risers", *Powder Tech.*, 101, 91-100.

Yang, Y., Jin, Y., Yu, Z., Wang, Z. and Bai, D., 1991, "The radial distribution of local particle velocity in a dilute circulating fluidized bed", *Circulating Fluidized Bed Technology III*, P.Basu, M.Horio and M.Hasatani, Eds., Pergamon Press, New York, 201-206

Zhou, J., Grace, J.R., Lim, C.J. and Brereton, C.M.H., 1995, "Particle velocity profiles in a circulating fluidized bed riser of square cross-section", *Chem. Eng. Sci.*, 50-2, 237-244.

CHAPTER-3

Single Phase Investigation in Laboratory Scale- Pulsed Sieve and Slotted Columns

Chapter 3 : Single Phase Investigation in Laboratory Scale-Pulsed Sieve and Slotted Columns

Graphical abstract

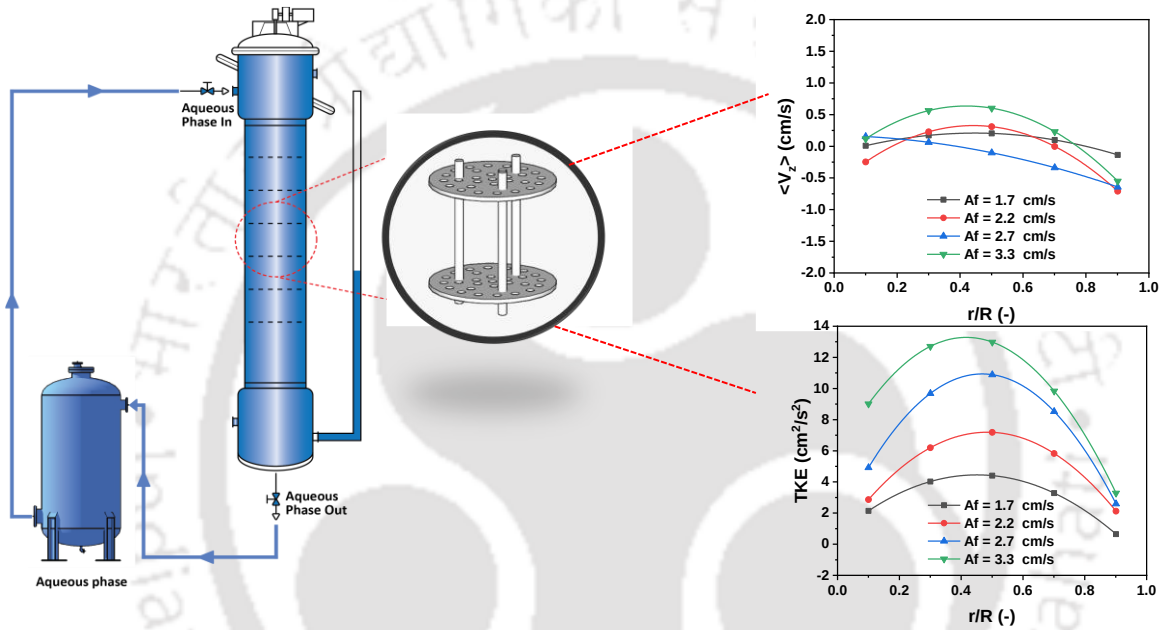

Abstract

The chapter describes the details of the laboratory scale experimental setup. The uses of the auxiliary equipment of the laboratory PSPC are discussed. The details of the internal plate cartridges and the operational management of the column are briefed. This chapter discuss the single-phase investigation of velocity field using two different plates. As multiphase is a complex scenario initially the experiments are conducted stage wise. The experimental procedure is discussed in detail. This chapter also details the column operation at no flow and single-phase flow by variation of pumping rates and pulsation velocities and corresponding turbulence parameters are postprocessed using the RPT methodology explained in chapter 2.

3.1 Introduction

Pulsed columns can be categorized as pulsed disc-and-doughnut (PDDC) or pulsed sieve-plate (PSPC) columns based on their internals. In PDDC, the internals consist of alternately ordered discs and doughnuts, whereas in PSPC, the internals comprise perforated sieve plates. The liquid in a PSPC passes through the sieve perforations, whereas liquid in PDDC follows a tortuous flow path. Each of these columns has its own advantages and disadvantages. Several studies have reported the pressure drop, longitudinal dispersion, drop size distribution and dispersed phase hold-up in PSPC and PDDC. PDDC is employed for uranium recovery and purification at the front end, while PSPC is employed for back-end processes of the nuclear fuel cycle. Both columns play crucial roles in nuclear industry applications and have been studied extensively by researchers for their respective purposes. Fluid dynamics in pulsed columns are governed by geometric parameters like plate opening area also referred to as fractional free area (FFA), plate/ column diameter, inter-plate spacing, structure of the plate opening, and operational parameters such as phase flow rates, pulsation amplitude, pulsation frequency. Flow studies available in the literature are primarily performed using CFD. Charton et al. (2012) reported longitudinal dispersion studies in PDDC. Sourav et al. (2018) made a comparative hydrodynamic study between PSPC and PDDC. Experimental longitudinal dispersion studies have been performed using radiotracers. Apart from a sieve plate, a coalescence dispersion plate has also been used as a column internal. The coalescence dispersion plate is another form of perforation plate with half-punched surfaces. Xiaojin et al. (2011) reported a two-phase experimental and numerical study on a coalescence dispersion pulsed sieve plate extraction column.

For process intensification, a pulsatile or oscillatory flow baffled columns have also been used as a reactor for single and two-phase reactions. Such a reactor is known as an oscillatory baffled reactor (OBR). While maintaining plug flow-like circumstances, the interaction of baffles with the oscillatory motion of the fluid leads to improved transport rates and uniform mixing. Brounald et al. (1988) reported the impact of sharp edges of baffles on energy and flow patterns loss for oscillatory flow in rectangular and cylindrical U-tubes. Central disc and helical baffles have shown inferior mass transfer performance than single-orifice baffles. Multi-orifice baffles have shown similar performance for longitudinal dispersion when scaled up from single-orifice baffles. Multi-orifice baffles are more suitable for multiphase applications as compared to single-orifice baffles as they can generate smaller droplets.

The schematics of different internals used in pulsed columns and oscillatory baffled columns are shown in Figure 3.1. Pulsed columns are reported to incorporate sieve plates, disk and doughnut internals, as well as coalescence plates. Single orifice, multi orifice (sieve, central disk), disk and doughnut, and helical internals have been used in OBRs.

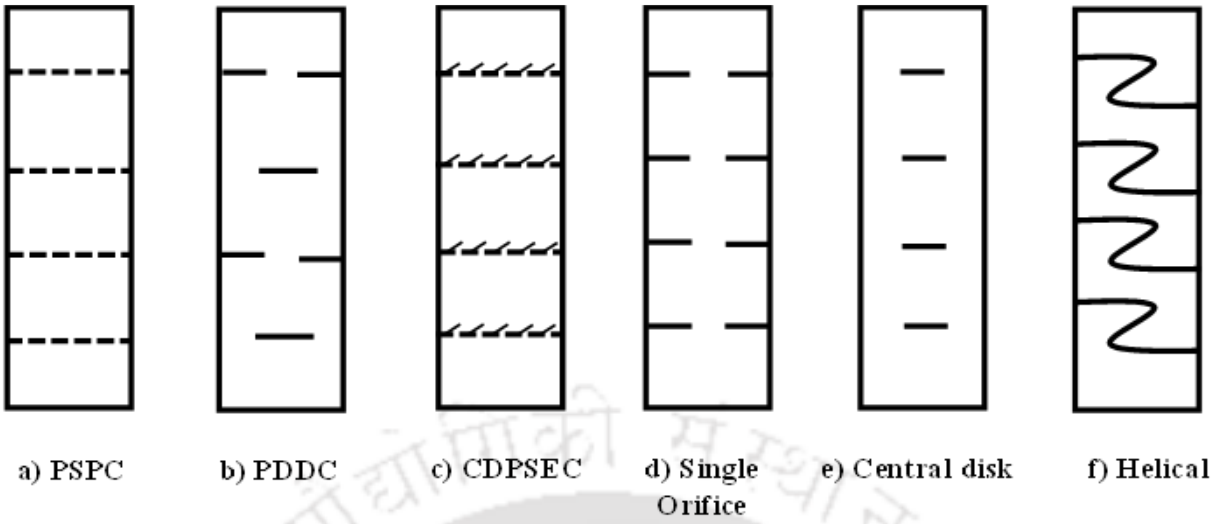

Figure 3.1: Different internals (a) Pulsed sieve plate column (PSPC), (b) Pulsed disc and doughnut column (PDDC) (c) Coalescence dispersion pulsed sieve plate column (CDPSEC), (d) Single orifice baffle plates, (e) Central disks and (f) Helical inserts.

Experimental flow field studies in these columns are reported by very few investigators. Bhujalski et al. (2006) investigated the fluid flow characteristics of a single-phase flow in a PDDC using Particle Image Velocimetry (PIV) and Laser Doppler Velocimetry (LDV). Amocrane et al. (2014) conducted PIV measurements in PDDC and validated the results obtained from CFD modelling. Drumm et al. (2011) performed a PIV experiment to study both single-phase flow and two-phase flow in a Rotary Disc Column (RDC). In our previous works we have reported the experimental measurement of the local velocity field in PSPC. Each of these internals causes a different flow field in the column which leads to different extraction efficiency. To improve the performance of pulsed columns under different, new internals are designed. It is critical to evaluate the local flow field caused by the new internal. A novel internal slotted plate was designed for the single-phase pulsed column. The present work aims to study the local flow characteristics using the slotted plate through the implementation of the

RPT technique. A series of experiments were conducted under two conditions: no net flow and single-phase flow. The average velocity in the longitudinal direction, along with root mean square (RMS) velocities of both longitudinal and lateral directions, and turbulent energy are performed to examine the flow field inside the column. The present work aims to study the local flow characteristics using the two plates through the implementation of the RPT technique. A series of experiments were conducted and the experimental procedure is explained in next section in detail.

3.2 Experimental procedure

Figure 3.2a shows the schematic diagram of the experimental setup. The experimental setup consists of an active column section (glass), top and bottom disengagement sections, pulse leg, three-way valve along with a timer to induce pulsation, air compressor, pumps, rotameter, and storage tank. Tap water is fed from the top of the column through a centrifugal pump. The flow rate is controlled using a rotameter. The inner diameter of the active PSPC is 0.075 m and height is 0.7 m. A cartridge consisting of 8 sieve plates (3.2 mm sieve holes and 17% open area) is used as an internal. The sieve plates are placed 0.1 m apart from each other. Figure 3.2b shows the schematic of the sieve plate internal used in the current study. The sieve plates are placed 0.1 m apart from each other.

The 3-way valve is used to induce pulsation in the column. During the “ON” cycle of the valve, air from the compressor enters the pulse leg and pushes up the liquid in the column while during the “OFF” cycle, the pulse leg pressure is exhausted which allows the liquid in the column to fall down due to hydraulic head. Periodic repetition of this causes a periodic pulsation inside the column. The pulse amplitude can be controlled by increasing the pressure of the air coming

into the pulse leg while the frequency can be altered by altering the ON and OFF timings of the valve through the timer. It should be noted that in the current work pulsation frequency is kept constant at 1 Hz for all the cases. Hence, pulsation velocity (Af), which is multiplication of pulse amplitude (A) and pulse frequency (f), is varied by varying the pulse amplitude. The column is operated at different pulsation velocities to find the effect of the pulsation velocity on the flow field. The experiments are performed under no flow and single phase flow conditions. Table 3.1 shows the flow conditions for which experiments are performed in the current work.

Table 3.1: Experimental matrix

Flow Condition	**Pulsating Velocity (Af) [cm/s]**	**Aqueous Phase Flow rate (Q) [LPH]**	**Corresponding superficial velocity**
No net flow	1.7, 2.2, 2.7, 3.3	-	-
Single phase flow	1.7, 2.2, 2.7, 3.3	120	**0.8**
	2.7	70, 100, 120, 160	**0.4, 0.6, 0.8, 1**

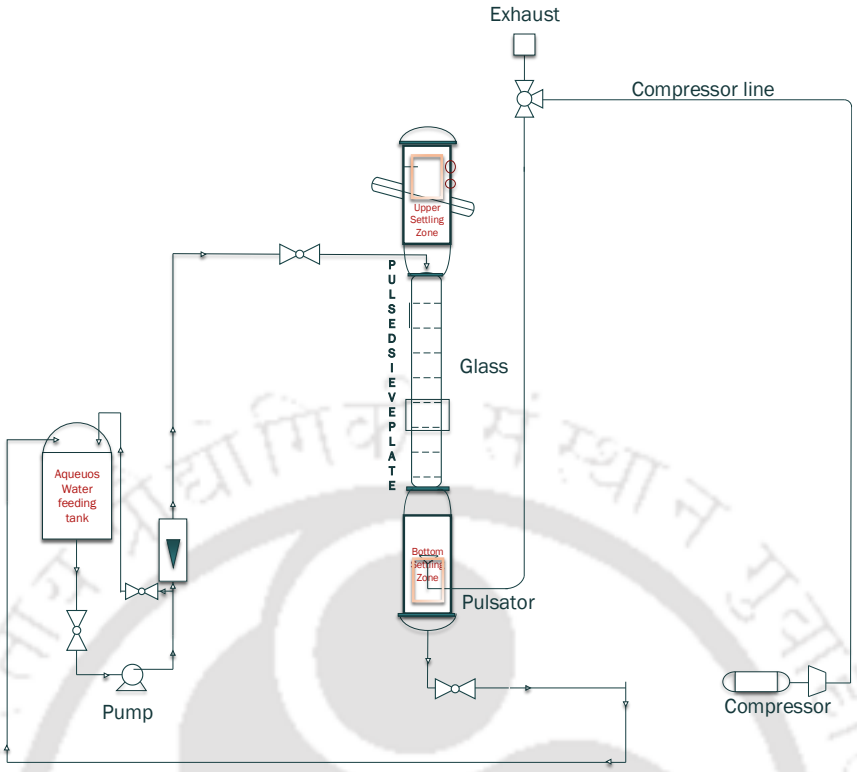

(a)

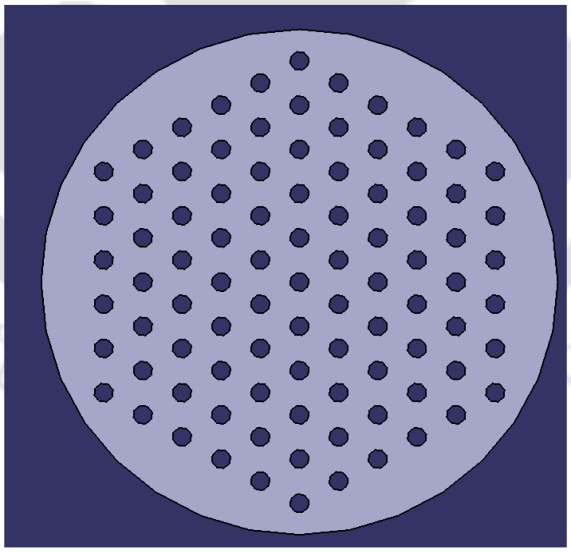

(b)

Figure 3.2: (a) Schematic diagram of pulse sieve plate column (b) Sieve plate design

For each case, the liquid flow field is mapped by using the radioactive particle tracking technique. A single neutrally buoyant radioactive particle is used as a tracer to map the flow field. The size of the tracer particle is kept slightly bigger than the sieve plate hole diameter i.e. 3.2 mm. To prepare the neutrally buoyant tracer particle a small particle of Sc-46 is encapsulated inside the polystyrene bead. The density of the tracer particle is maintained by trapping a small amount of air while sealing the polystyrene bead after inserting the Sc-46 particle. The details of the tracer particle preparation has been explained by Devnathan et al. It should be noted that the tracer particle motion is restricted between the two consecutive sieve plates and the motion between these two sieve plates is only observed. In the current work, the liquid flow field is studied between the third and fourth plates from the bottom. Total six NaI (Tl) detectors are placed around the column between the two sieve plates to track the motion of the tracer particle. For each condition the experiments are performed for 5 hours and data are acquired continuously with a frequency of 25 Hz. The counts recorded on each detector is used to locate the instantaneous tracer particle position time series. The same is used to calculate instantaneous velocities, mean velocities, axial and radial rms velocities, turbulent kinetic energy, and turbulent intensity by using the suitable post-processing which is explained in detail our previous contributions. Post processing variables are shown in table 3.2.

Table 3.2: Postprocessing Equations

Variable	Formulation
Ensemble average velocity	$\langle V_q(r,\theta,z)\rangle = \frac{1}{N(r,\theta,z)} \sum_{n=1}^{N(r,\theta,z)} V_{q,n}(r,\theta,z)$
Fluctuating velocity component	$V'_q(r,\theta,z) = V_q(r,\theta,z) - \langle V_q(r,\theta,z)\rangle$
RMS velocity component	$\langle V_q(r,\theta,z)\rangle^{RMS} = \sqrt{\langle V_q'^2(r,\theta,z)\rangle}$
Turbulent Kinetic energy	$TKE = \frac{1}{2}(\langle V_r'^2\rangle + \langle V_\theta'^2\rangle + \langle V_z'^2\rangle)$
Turbulence Intensity	$TI = \sqrt{\frac{1}{3}(\frac{(\langle V_r'^2\rangle + \langle V_\theta'^2\rangle + \langle V_z'^2\rangle)}{(\langle V_r\rangle^2 + \langle V_\theta\rangle^2 + \langle V_z\rangle^2)}}$

3.3 Results and Discussion

3.3.1 With sieve plate as internal

Experiments are performed in PSPC for mainly two cases: no flow and single-phase flow conditions. For both the cases, experiments are performed for four different pulsation velocities of 1.7, 2.2, 2.7, 3.3 cm/s. The pulsation frequency is kept constant as 1 Hz for all the cases. Hence, the change in pulsation velocity (Af) is implemented by changing pulsation amplitude. This section is mainly divided in two parts: no flow and single-phase flow conditions. In no flow condition, liquid is filled inside the PSPC and tracer particle is placed between the two successive sieve plates. In this case, the tracer particle moves only due to the pulsation that is

generated by using the compressed air in pulse leg via three-way valve as explained in above section. It should be noted that in this case liquid is in batch. The experiments are performed for different pulsation velocities to understand the effect of the pulsation on liquid flow field. In single phase flow condition, liquid flows from top to the bottom. The tracer particle is placed between the two successive sieve plates as in no flow case and effect of both pulsation velocities and liquid velocities on the flow field are investigated. The results will help to understand the contribution of liquid velocity and pulsation velocity on the flow field. To the best of our knowledge no such data is reported in the literature for PSPC column.

3.3.1.1 Effect of Pulsation Velocity at no flow condition

Figure 3.3 shows the radial variation of the mean axial velocity of the liquid for different pulsation velocities (Af) at no flow condition. The mean axial velocity ($<V_z>$) of the liquid is close to zero for low Af values. This should ideally be the case as for no flow condition the particle moves up and down around a baseline where the particle is kept at the time of injection. Hence, for no flow condition, the mean axial velocity of the liquid should be zero or very close to zero. These results verify that RPT is able to predict the basic features of the velocity field. For higher Af values, the mean axial velocity is found to be slightly positive for r/R values in the range of 0.2-0.6 and slightly negative near the wall (r/R>0.6). However, the values are very low (a few mm/s). This clearly shows the presence of recirculation (fluid going down through the wall and moving up through the regions where r/R is in between (0.2-0.6). Such recirculatory flow patterns is also reported for two-phase flow) in CFD/CFD-PB based numerical models for 0.075 m PSPC by Sen et al.[26,27]. Moreover, experimental results indicated that the extent of recirculation intensifies as pulsing velocity is raised. At this stage, it may be mentioned that the reason for such a recirculatory pattern is the interaction of the pulse with

the sieve plate. As the number of holes in the region of r/R = 0.2-0.6 is more than those at the center (r/R<=0.1), the liquid moved upward in presence of pulsation. As r/R increases further, the number of holes also increases but at the same time presence of the wall starts influencing the flow field. Thus, near the wall (r/R ~ 0.8-0.9), the liquid starts to flow down to ensure the mass balance. It should be noted that for all the Af values, no significant radial mean velocity is observed.

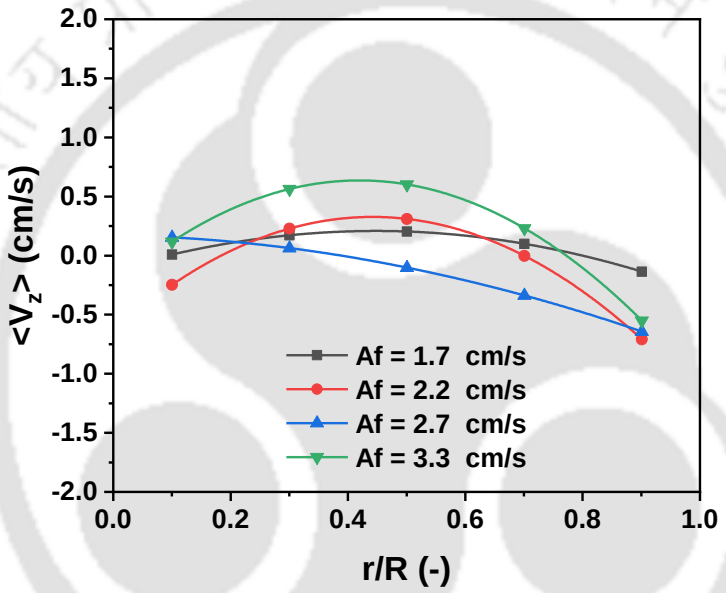

Figure 3.3: Radial variation of mean axial velocity of liquid at no flow condition

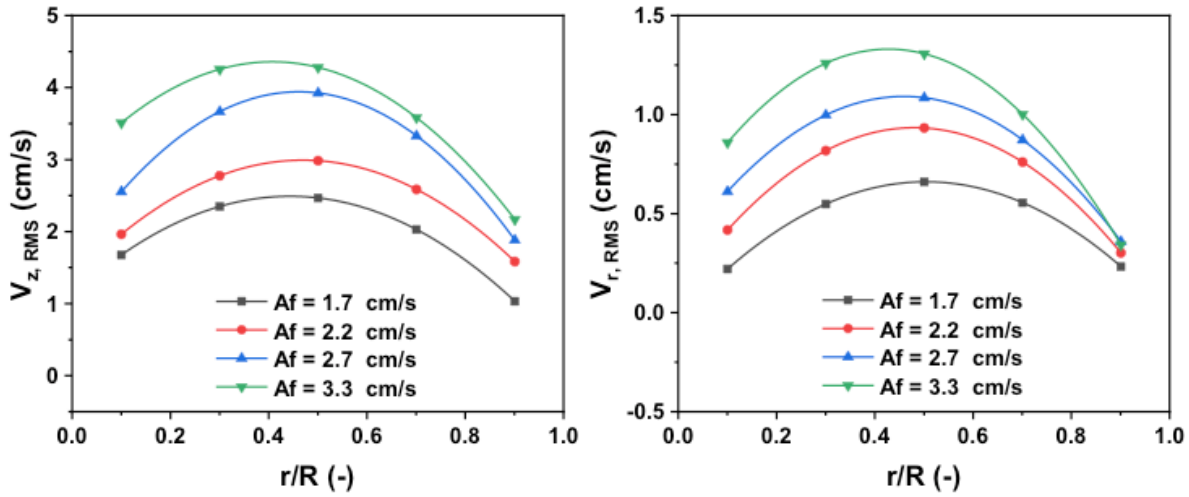

Figure 3.4: Radial variation of (a) axial rms velocity (b) radial rms velocity for different pulsation velocities at no flow condition

Figure 3.4a shows the radial variation of axial rms velocity (*Vz,rms*) of the liquid at no flow condition for different pulsation velocities. Unlike mean axial velocity, significant axial rms velocity is observed for no flow conditions for all the pulsation velocities. The axial rms velocity is found to be higher in the region of r/R 0.2-0.8 for all the pulsation velocities. At the center of the column (i.e. r/R <= 0.1) axial rms velocities are lower due to the lower number of holes at the center of the sieve plate in the column (see Figure 3.2b). Hence, as also mentioned earlier, the quantity of liquid moving upward/downward at the center (r/R<=0.1) is less. This results in lower fluctuation velocity at the center of the column. Due to the no-slip boundary condition, the velocity of the liquid is zero at the wall (r/R=1). Hence, the fluctuation is also low. The higher number of holes in the region having 0.2< r/R<0.8 means that the bulk of the liquid moves up and down in this region which in turn leads to higher axial rms velocities. The magnitude of the axial rms velocities shows that pulsation generates a significant degree of axial mixing. In fact, such a high degree of axial mixing is detrimental to the mass transfer

performance of the column. Moreover, as expected, an increase in pulsing velocity causes an increase in the values of axial rms velocities which means that mixing also increases with an increase in Af.

Figure 3.4b shows the radial rms velocity (*Vr,rms*) for different pulsation velocities at no flow condition. Though the mean radial velocity is observed to be very low, significant radial rms velocity is observed for all the pulsation velocities. This is mainly due to the hole at the sieve plate which induces a certain degree of radial motion as the fluid jets come out of it during the upstroke of the pulse. It is pertinent to note that if this effect is averaged across all sieve holes for statistically long periods of time the overall effect would be negligible as the radial components of velocity generated due to jetting at one hole would cancel out that at the next hole. This is precisely the reason why mean radial velocities are almost zero. However, in terms of rms values, these contributions would not cancel as is seen in Figure 3.4(b). The radial rms velocity is also higher in the region of $0.2<r/R<0.8$ due to the larger number of holes in the sieve plate in that region. At the wall ($r/R\sim1$), due to the no-slip condition radial rms velocity is also lower. Similar to the observation made for axial rms velocity, radial rms velocity also increases with an increase in the pulsation velocity. An increase in the intensity of the jetting effect at higher pulsation velocity is responsible for this. It should be noted that for all pulsation velocities studied in this work value of axial rms velocity is approximately 2-3 times higher than the radial rms velocity. This signifies that the fluctuations in the axial direction are more dominant than those in the radial direction.

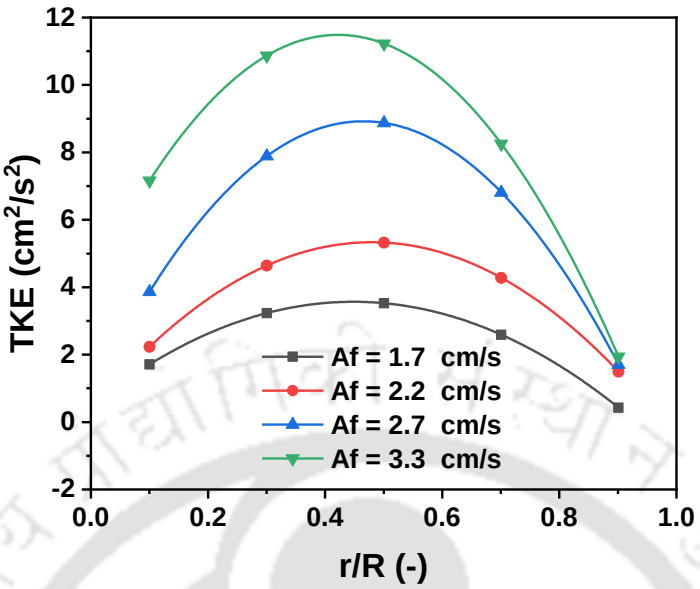

Figure 3.5: Radial variation of turbulent kinetic energy (TKE) at no flow condition

Figure 3.5 shows the radial variation of the turbulent kinetic energy (TKE) for all the pulsation velocities. The turbulent kinetic energy is also higher in the region having 0.2<r/R<0.8 due to higher values of rms velocities. The turbulent kinetic energy is seen to increase with an increase in the pulsation velocity. An increase in the pulsation velocity would increase velocity gradients across sieve holes which essentially lead to the generation of the higher degree of turbulence. This reflects as an increase in rms velocities (Figure 3.4) as well as an increase in turbulent kinetic energy. Figure 3.6 shows the radial variation of the turbulent intensity for all the pulsation velocities. The turbulent intensity is defined as the square root of the ratio of average fluctuation velocity to the mean velocity (as shown in table 3.2).

The turbulent intensity trend is similar to TKE. Interestingly, a significantly high value of turbulent intensity is found for all the pulsation velocities. This is mainly due to the significantly low mean velocities and higher fluctuation velocities. The higher value of

turbulent intensity signifies enhanced mixing in PSPC, which increases with increase in pulsation velocity.

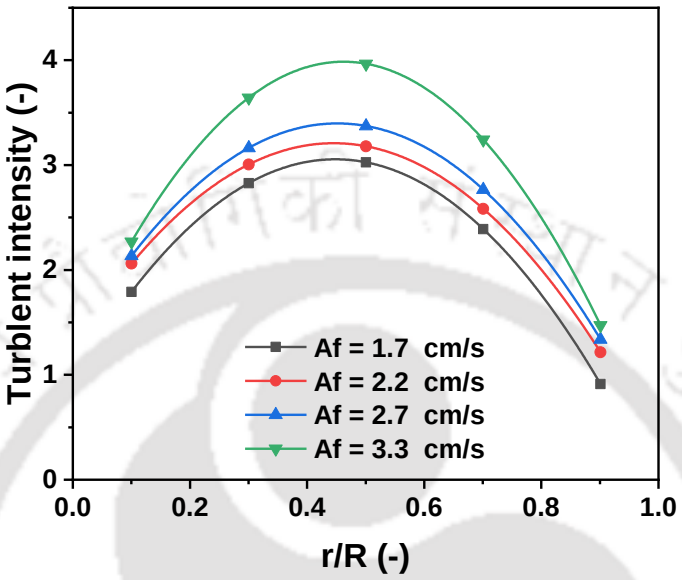

Figure 3.6: Radial variation of turbulence intensity at no flow condition

Experiments are further performed for the single-phase flow condition. Water is fed from the top of the column and it flows downward along the column. The effect of pulsation velocity (Af) and flow rate (Q) on mean axial velocity, axial rms velocity, radial rms velocity, turbulent kinetic energy, and turbulent intensity are studied using the RPT technique. It should be noted that in this case also the tracer particle motion is restricted between the third and fourth sieve plates.

3.3.1.2 Effect of pulsation velocity at a constant liquid flow rate of single-phase flow

Figure 3.7 shows the radial variation of mean axial velocity for liquid flow rate of 120 LPH at different pulsation velocities. Results show that even in the case of single-phase flow, the mean

axial velocity of the liquid is close to zero for all the pulsation velocities. It should be noted that in current case the liquid motion is measured between the two successive sieve plates i.e., the tracer particle motion is restricted between two plates even though the fluid could pass through the sieve holes. Hence, for long term time average mean velocity values are expected to be close to zero similar to no flow condition. In fact, this represents the only limitation of the current experiments where the correct values of mean axial velocities near the sieve holes cannot be captured. It should be noted that in the case of single-phase flow also no significant radial mean velocity is observed for all the pulsation velocities. Further, at higher pulsation velocities a recirculatory flow pattern is observed which is similar to the no flow condition and also reported in the literature.

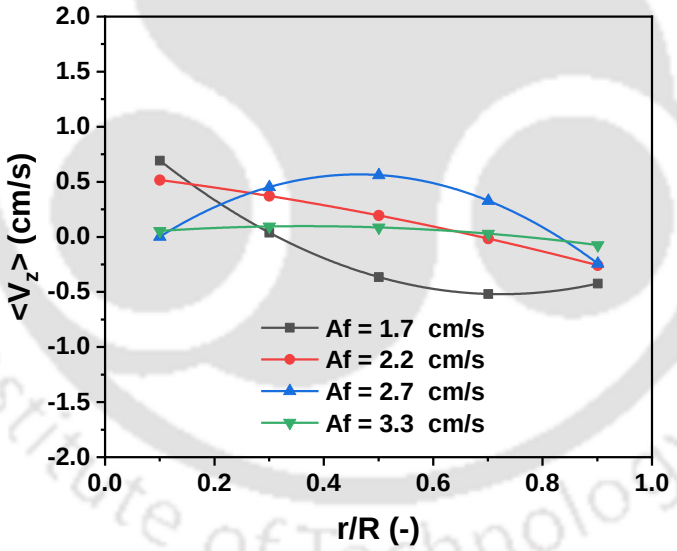

Figure 3.7: Radial variation of mean axial velocity at liquid flow rate of 120 LPH at different Af

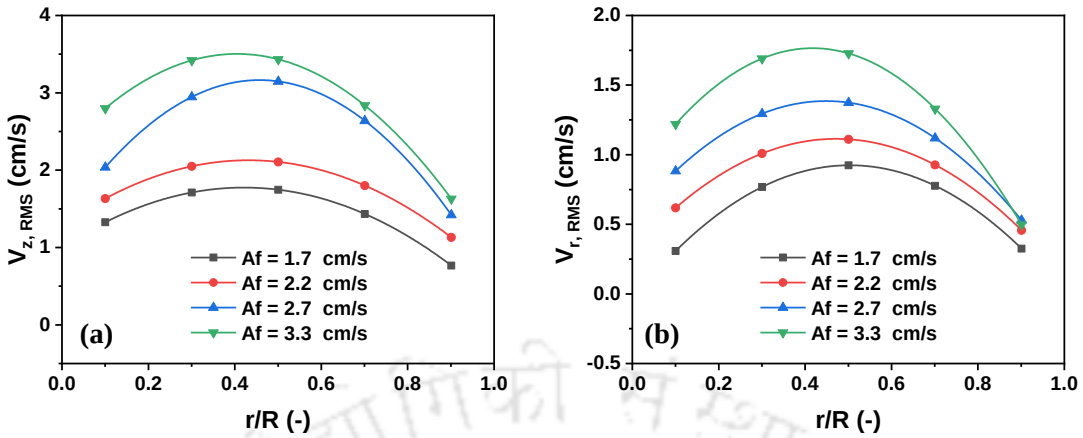

Figure 3.8: Radial variation of (a) axial rms velocity (b) radial rms velocity for different pulsation velocities at liquid flow rate of 120 LPH

Figure 3.8a shows the axial rms velocities of the liquid at a flow rate of 120 LPH for different pulsation velocities. The axial rms velocity is once again higher in the region where r/R is in between 0.2 to 0.8 for all pulsation velocities as the number of sieve holes is higher in this part of the column cross-section. Relatively lower fluctuations at the wall could be attributed to the no-slip condition on the wall. Another interesting observation is that the values of axial rms velocities in the case of single-phase flow are lower compared to the case of no net flow condition for all the pulsation velocities (see Figure 3.8 and Figure 3.4). This suggests that instantaneous velocity fluctuation introduced due to the pulsation is attenuated by the net flow of liquid from top to bottom. However, the reduction is not significant. An increase in the pulsation velocity causes an increase in the axial rms velocity. This is because at higher pulsation velocity the velocity gradient across the sieve holes would be more.

Figure 3.8b shows the radial rms velocity for single phase flow at different pulsation velocities. Similar to the no flow condition, radial rms velocity for single phase flow is also higher in the

region where r/R in the range of 0.2-0.8. This is again due to the greater number of holes in this region. As with the case of no flow condition the radial fluctuations are generated due to the jetting action at the sieve holes as the fluid is ejected out of them during the upstroke of the pulse. However, unlike axial rms velocity, a marginal increase in radial rms velocity is observed for single phase flow case compared to no flow condition. Furthermore, for single phase flow the axial rms velocity is about 1.5-2 times higher than the radial rms velocity. However, for no flow condition the ratio of axial to radial rms velocities is in the range of 3-4. These observations clearly show that the fluctuating motion is primarily in the axial direction in case of both single phase and no flow conditions. A net downward flow of the liquid leads to marginal increase in the radial fluctuating flow components generated by the jetting action at the sieve holes.

Figure 3.9 shows the radial variation of turbulent kinetic energy (TKE) at liquid flow rate of 120 LPH. The trend of the kinetic energy of turbulence for single phase flow is similar to that seen for no net flow condition. The maximum kinetic energy of turbulence is observed in the region where r/R is in between 0.2 to 0.8 for all the pulsation velocities. Furthermore, with an increase in the pulsation velocity, TKE increases for the single phase also. This is due to the increase in energy input to the system at higher pulsing velocities. However, similar to axial rms velocity, the turbulent kinetic energy is also lower for the single-phase flow when compared with the no flow condition for all the pulsation velocities. This is mainly due to the damping of the axial fluctuations in presence of a net downward flow of the liquid.

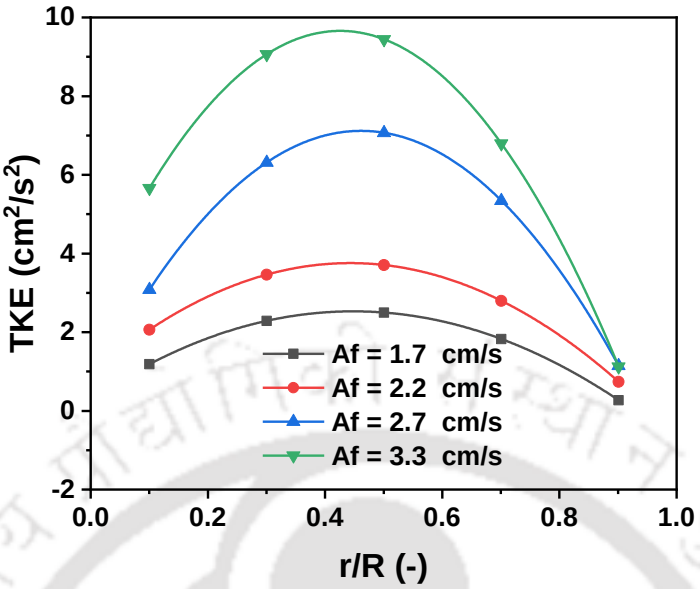

Figure 3.9: Turbulent kinetic energy (TKE) at a liquid flow rate of 120 LPH for different pulsation velocities

Figure 3.10 shows the turbulent ijntensity at a liquid flow rate of 120 LPH for different pulsation velocities. As for the no flow condition, the trend of turbulent intensity is similar to that for TKE. The turbulent intensity increases with an increase in pulsation velocity. This shows that higher pulsation velocity provides enhanced mixing in case of single-phase flow also. However, the turbulent intensity in case of single-phase flow is found to be lower than that in no flow condition. This further confirms that net downward motion of liquid attenuates the fluctuation created by the pulsation. However, it should be noted that the turbulent intensity is still significantly higher compared to that in the conventional extractor. This confirms that PSPC provides better local mixing.

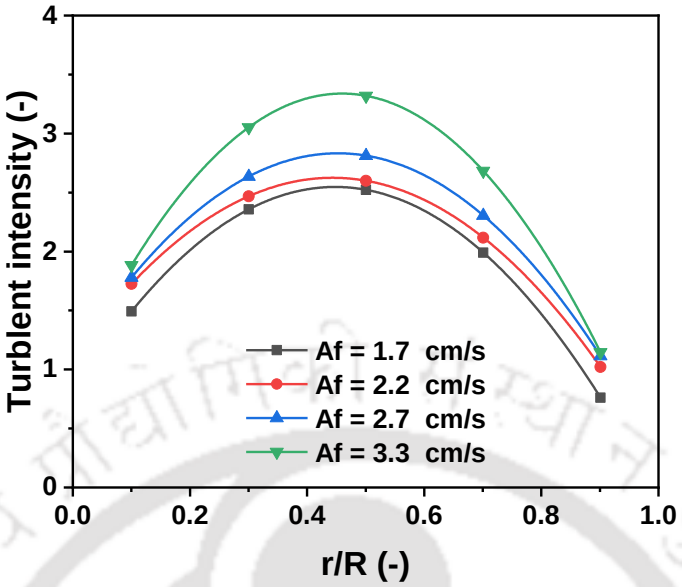

Figure 3.10: Turbulent intensity for different pulsation velocities at a liquid flow rate of 120 LPH

3.3.1.3 Effect of flow rate at constant pulsation velocity of single-phase flow

To study the effect of flow rate on liquid flow field in PSPC, experiments are performed for different flow rates, (70, 100, 120, 160 LPH), at a constant pulsation velocity of 2.7 cm/s. Figure 3.11 shows the radial variation of mean axial velocity for different liquid flow rates at a constant pulsation velocity. The mean velocity of the liquid is almost zero for all the cases. This is once again because of the fact that the motion of the particle is restricted between the two successive sieve plates. Hence, for a long time average, any condition will lead to a scenario that would be similar to the case with no flow condition as far as mean velocity is concerned. It should be further noted that for all the liquid flow rates no significant radial mean velocity is observed.

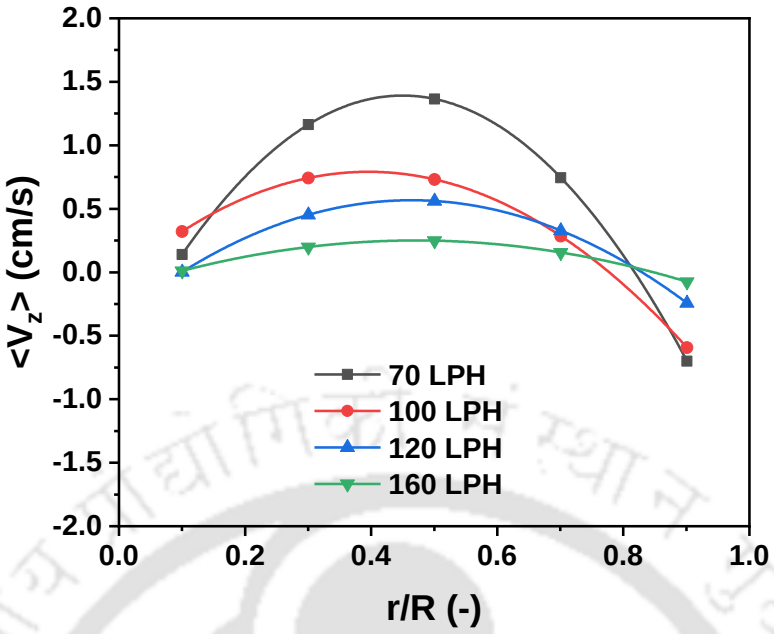

Figure 3.11: Radial variation of mean axial velocity at Af = 2.7 cm/s for different liquid flow rates

Figure 3.12a shows the radial variation of axial rms velocity for a constant pulsation velocity of 2.7 cm/s at different liquid flow rates. Similar to the other cases, the axial rms velocities for all the flow rates are higher in the region where r/R in between 0.2 and 0.8 due to the design of the sieve plate. The axial rms velocity is lower near the wall due to the no slip condition that reduces the fluctuations near the wall. Further, it is observed that axial rms velocity decreases with an increase in the liquid flow rate. This shows and reinforces the idea that an increase in the flow rate attenuate the turbulence generated due to the pulsation and hence, the axial rms velocity. Further, for all the values of the liquid flow rates, axial rms velocity is lower compared to the case of no net flow. This confirms that in the case of single phase flow the turbulence generated due to the flow is indeed lower due to the damping effect.

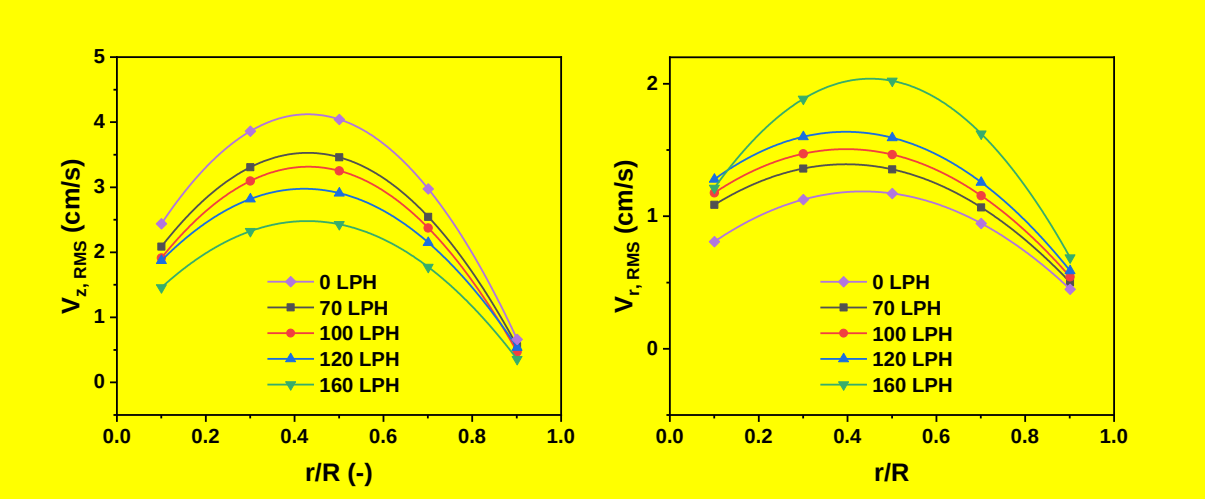

Figure 3.12: Radial variation of (a) axial rms velocity (b) radial rms velocity (c) azimuthal rms velocity for different liquid flow rates at Af = 2.7cm/s

Figure 12b shows the radial rms velocity for different liquid flow rates. In this case also radial rms velocities are higher in the region where r/R is in between 0.2 and 0.8 due to the design of the sieve plate. For all the cases radial rms velocity is significantly lower when compared with the axial rms velocity. Furthermore, compared to the no net flow condition (Figure 3b), radial rms velocity is higher for all the liquid flow rates and increases with increase in the flow rate. As explained earlier this is because of the net down flow of liquid through the sieve hole, which generates enhanced fluctuation in radial direction.

Figure 13 shows the radial variation of turbulent kinetic energy for different liquid flow rates. The TKE follows the same trend as that of axial rms velocity. Results show that the kinetic energy of turbulence decreases with an increase in the liquid flow rates. This is due to the higher dampening effect at a higher flow rate. Hence, it can be concluded that the turbulence is mainly caused by pulsation in PSPC. Figure 3.14 shows the turbulent intensity at different liquid flow rates for constant pulsation velocity of 2.7 cm/s. Similar to the other cases turbulent intensity trend is same as of the TKE. This shows that turbulence is primarily in the axial direction for

all the cases. The turbulent intensity decreases with increase in liquid flow rate. This shows that for higher liquid flow rate attenuate in fluctuation generated due to the pulsation is also high. However, even at maximum liquid flow rate the turbulent intensity is significantly higher. Hence, higher degree of mixing is observed in PSPC for all the condition compared to conventional sieve plate column. Therefore, it can be concluded that for all the conditions studied in current work PSPC provides higher degree of mixing and hence enhanced mass transfer.

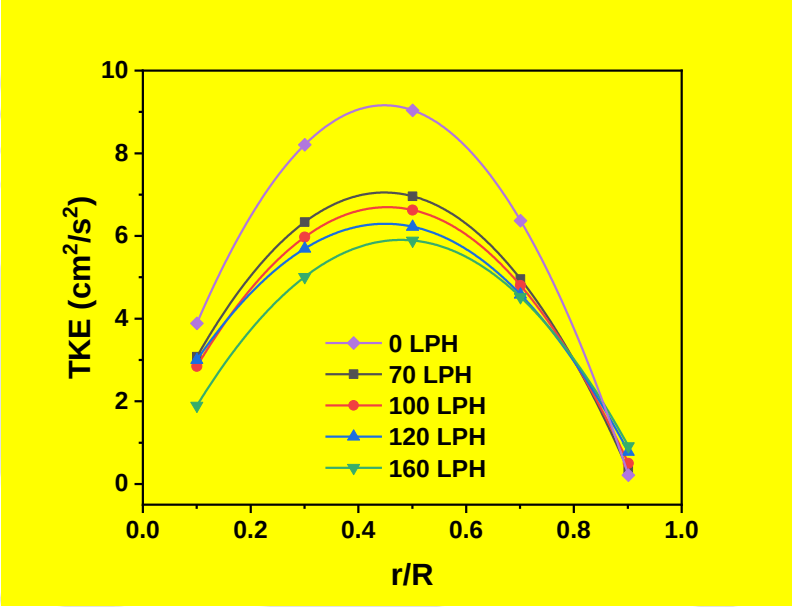

Figure 3.13: Turbulent kinetic energy for different liquid flow rates at Af = 2.7 cm/s

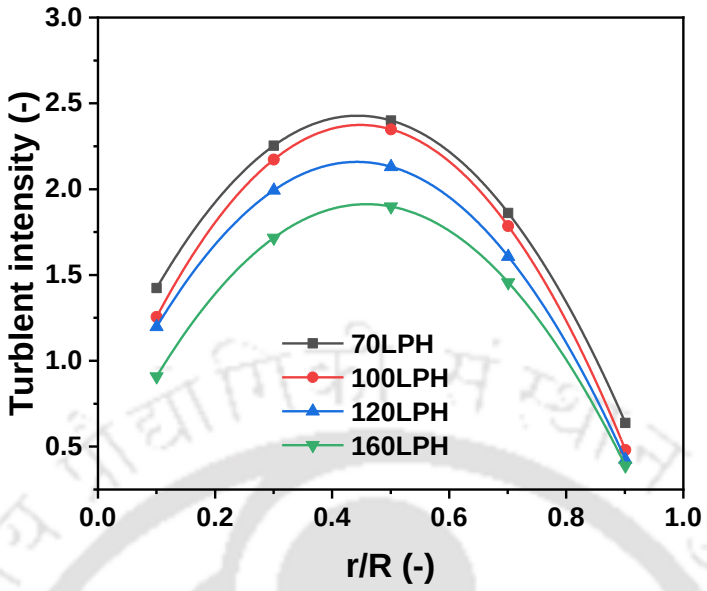

Figure 3.14: Turbulent intensity for different liquid flow rates at Af = 2.7 cm/s

This section of the study delved into an extensive examination of the local hydrodynamics occurring within single-phase pulsed columns featuring sieve plates as internal components. The utilization of sieve plates as internals has garnered substantial attention within the research community due to their widespread adoption in various industrial applications, such as mineral processing, nuclear fuel processing, and pharmaceutical industries. Despite their prevalent usage, it is worth noting that there exists a scope for enhancing the design of sieve plate structures to achieve more favourable mixing profiles. To address this potential for improvement, we have pursued an in-depth investigation in this direction and subsequently devised a novel plate structure that holds promise for enhancing the mixing profile within these columns. The forthcoming section will provide a detailed exposition of this newly developed plate structure, shedding light on its unique features, potential benefits, and the expected impact on hydrodynamics within the column. A central aspect of our investigation involves subjecting

the designed structure to a comprehensive evaluation under various pulsatile flow conditions. We will carefully assess its performance, considering different pulsation intensities and water flow rates, all with a sharp focus on the single-phase hydrodynamics governing the system. By presenting our findings in the next section, we aim to contribute valuable insights that can drive advancements in the field of single-phase pulsed column design, particularly concerning the implementation of sieve plate internals and the optimization of mixing profiles for enhanced industrial applications.

3.3.2 With slotted plate as internal

The selection of a slotted groove plate design with three different segmentations of openings over a sieve plate with uniform openings in pulsed column extraction applications is based on specific considerations. The slotted groove plate design was planned to offer advantages in terms of its potential impact on fluid dynamics, and mixing behavior with more viscous fluid interactions. The three distinct segmentations of openings on the plate provide variations in flow patterns and dispersion characteristics, contributing to some unknown interesting facts. This experimental choice aims to explore and evaluate the benefits of a tailored design that introduces additional complexity to the plate structure, offering insights into its effects on the efficiency of pulsed column extraction systems. Experiments are conducted using novel plate and the experimentation is implemented as shown in figure 3.15

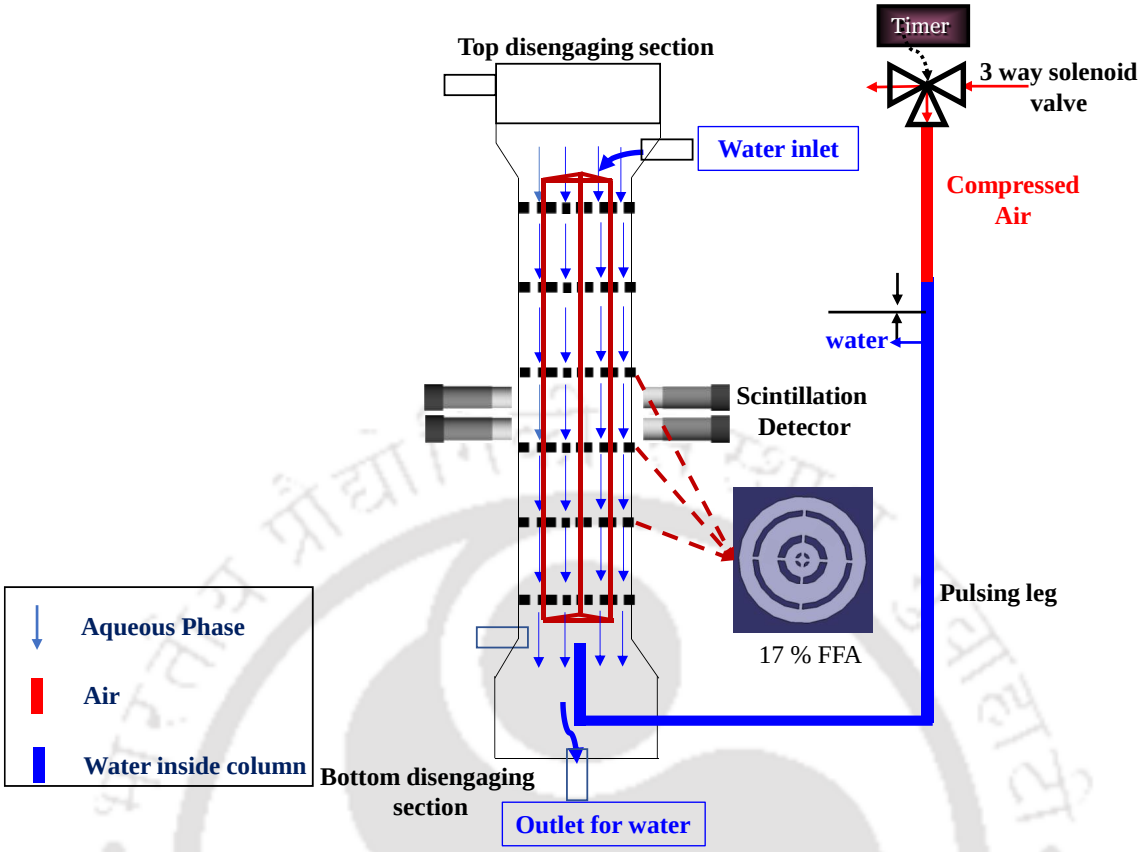

Figure 3.15: Schematic diagram of single-phase flow in pulsed slotted plate column (PSLPC).

In the previous section, we have thoroughly explained the implementation procedures. Now, in this section, we proceed to present the design of the slotted plate. A detailed comparison between both plate structures is also provided here, allowing for a comprehensive understanding of their respective features and characteristics. Figure 3.16 serves as a visual aid, displaying the schematic of zonal considerations utilized for mapping the similarity flow area. This Figure helps to illustrate and highlight the specific regions and patterns of flow similarity between the two plate structures under investigation. This section focuses on introducing the design of the slotted plate, discussing its attributes in relation to the conventional plate structure, and utilizing Figure 3.16 to facilitate a clearer grasp of the flow areas where similarities can be observed between the two designs. For the sieve plate, the central zone

comprises one hole with the area of opening 8.03 cm^2 and the central zone opening area in the slotted plate corresponds to 11.10 cm^2. The number of holes in the sieve plate annular zone are 6,12,18 in three hexagonal patterns as marked in the schematic i.e corresponds to an area of 289.38 cm^2, while the annular zone corresponds to an area of 274.86 cm^2 in the slotted structure. Finally, the peripheral zone in the sieve plate corresponds to an area of 434.07 cm^2 while the slotted stricture peripheral flow opening area is 519.78 cm^2. These are the local opening areas of the two structures. Though the peripheral area showed more opening area but the flow in these areas are hindered by no slip effect of the wall.

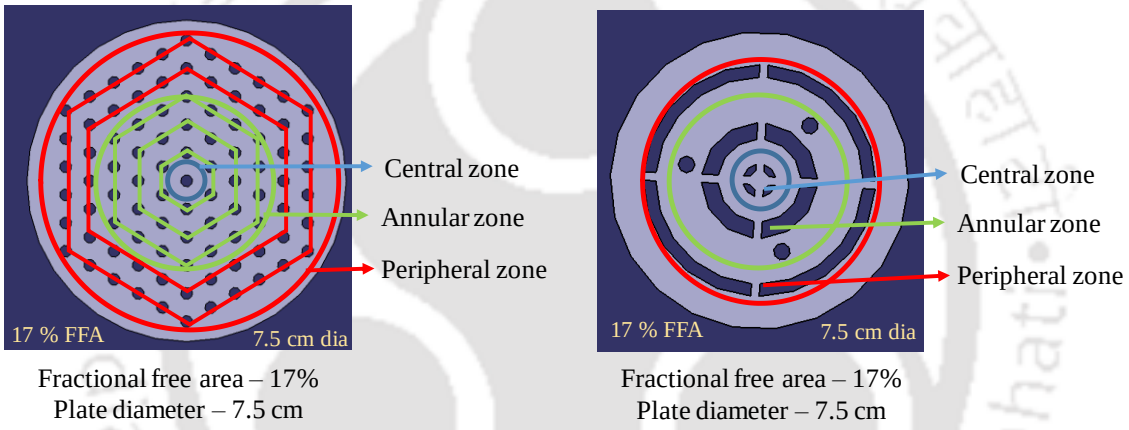

Figure 3.16: Zonal free area consideration for the similarity

Assuming approximation of parabolic velocity profile at inlet, the flow in the three peripheral areas are calculated and is shown in the Figure 3.17. This also showed that the flow in the annular regions is quite high with reference to that of peripheral and central zones. This makes us clear that in pulsed columns with the presence of slotted structure plates, the flow distribution is divided in such a way that the flow quantities will be higher in the annular zones. The corresponding local velocity distribution is also observed in same pattern.

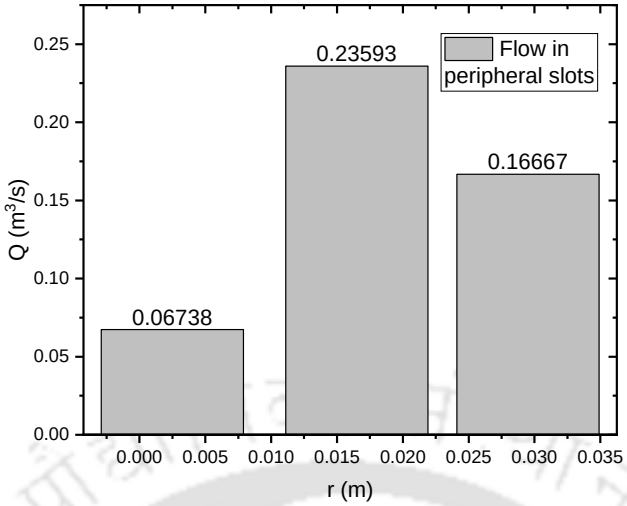

Figure 3.17: Zonal flow rates in the peripheral slots

Experiments have been performed for two conditions. In the first condition, there is no net flow through the column and only pulsation is provided to the liquid. The effect of pulsation velocity (Af) i.e. product of pulse amplitude (A) and frequency (f) is studied in this case. Second, a net flow of single-phase liquid (water) occurs from bottom to top along with the pulsation and the effect of pulsation velocity (Af) and flow rate on the local velocity field is investigated. The pulse frequency of 1 Hz is maintained in each case. All the flow conditions are listed in Table 3.3.

Table 3.3: Single pose slotted plate operating conditions

Flow Condition	**Pulsating Velocity (Af) [cm/s]**	**Aqueous Phase Flow Rate (U) [LPH]**
No net flow	**1.6, 2.2, 2.7. 3.3**	**-**
Single phase flow	**1.6, 2.2, 2.7. 3.3**	**120**

	2.7	**70, 100, 120, 160, 200**

Experiments are carried out for different pulsation velocities of 1.7, 2.2, 2.7, and 3.3 cm/s. The PSPC is filled with water and a tracer particle is introduced between two subsequent slotted plates while there is no flow. The only source of movement for the tracer particle is the pulsation brought about by the compressed air in the pulse leg via a three-way valve. Reynolds number based on the pulsation velocity and column diameter varies between 1275 and 2475. At a plane between the two plate, the velocity would be high at the centre and low near the wall. The exact nature of the velocity profile will depend on the Reynolds number as well as the frequency. During the upstroke, the liquid hits the slotted plate and the liquid jet comes out from the slots and spread radially. The jets coming out from the slots interact with each other. During the downstroke, the flow direction is reversed and the jets are directed downwards. As a result, an oscillatory flow field is developed in the liquid between two plates. Figure 3.18 shows the mean axial velocity profile. The mean axial velocity is highest in the annular region (r/R ~ 0.5) and lower near the centre as well as near the wall. This is because the flow rate is highest in the middle slot and lower in the central and near wall slots.

3.3.2.1 Effect of Pulsation Velocity at no flow condition

Figure 3.16 shows the variation of the mean axial velocity of the aqueous phase for four different pulsation velocities for no-flow condition. The magnitude of the mean axial velocity is about an order of magnitude less than the pulsation velocity (within ±0.25 cm/s) except in the near wall region where it is always negative and relatively higher than everywhere else in the column. The mean axial velocity in no-flow condition increases slightly with an increase

in Af value. In a cycle, the upward motion of the fluid occurs due to the upstroke only whereas during the downstroke the downward motion is because of the downstroke as well as due to gravity. This probably explains the negative value of mean axial velocity in the almost entire region at the smaller Af value of 1.7 cm/s. It is worth highlighting that none of the Af values exhibit any observable radial mean velocity in comparison to its axial velocity. This clearly suggests that the flow is predominant in axial direction. A similar velocity profile was observed in our previous work using sieve plate as internals. The velocity profile for Af = 1.7 cm/s using sieve plate is shown for comparison. The difference in the profiles can possibly be attributed to the different distribution of open area in the two internals.

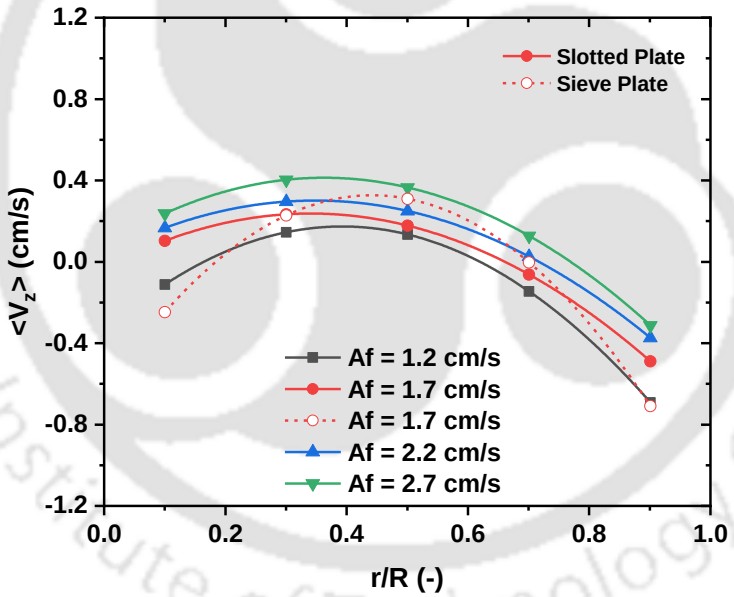

Figure 3.18: Radial variation of mean axial velocity of aqueous phase at no flow condition

As the flow of liquid occurs in the upward and downward direction alternately in a cycle, the mean axial velocity does not give a clear idea of the velocity magnitude. Therefore, the root

mean square (rms) values of the axial and radial velocities are plotted in Figure 3.19. The rms values of the axial and radial velocities using sieve plates as internals are also plotted for comparison. For the slotted plate, the axial rms velocity is maximum at r/R = 0.3 and value is slightly lower near the centre (r/R = 0.1). The fluid velocity is lowest near the wall because of the dominant viscous effects in the near wall region. With an increase in the Af value, the rms axial velocity increase. However, the profile of axial velocity remains qualitatively same. The maximum value of rms axial velocity is close to the Af value.

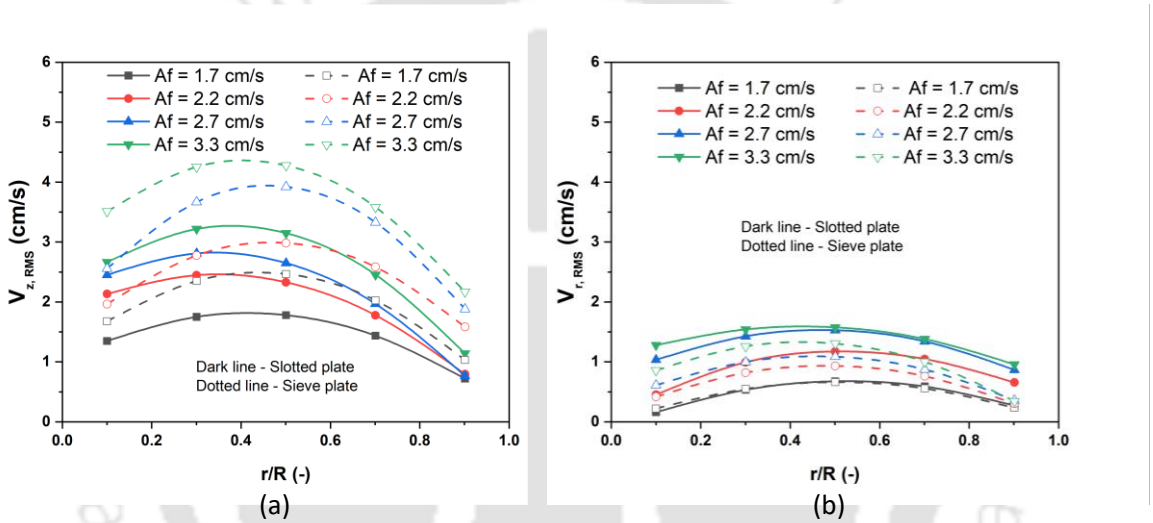

Figure 3.19: Radial variation of (a) axial rms velocity (b) radial rms velocity for different pulsation velocities at no flow condition with reference to sieve plate

For all four values of Af, the value of rms axial velocity is higher in case of sieve plates when compared with that for the slotted plate. Further, the maximum value for sieve plate occurs at r/R = 0.5. However, the rms value of radial velocity is higher than those for the sieve plates for the three higher pulsation velocities. For the lowest pulsation velocity of 1.7 cm/s, the profile of rms radial velocity is almost same for the slotted and sieve plates. The values of mean velocity are higher in the annular region for both plates. Though the flow area of the peripheral

or near wall zone is high, there is a reduction in the velocity magnitude due to the wall effect. All of the pulsation velocities have a significant radial rms velocity despite the fact that the mean radial velocity is fairly modest. This is because the direction of radial velocity keeps changing at a location in the upward and downward strokes. As the open area is relatively distributed in sieve plate, the jet coming out of holes does not spread as much as in the case of slotted plate. Figure 3.20 shows the radial variation of turbulent kinetic energy (TKE) which is a measure of the fluctuations in the flow. This also shows that the TKE is enhanced with increase in pulsation intensity and the annular zones show more mixing profiles in comparison to that of the wall zones. The profile of turbulent kinetic energy is same as that of rms velocities i.e. it is highest in the annular region and decreases towards the centre and near wall regions. TKE also increases with an increase in the Af value.

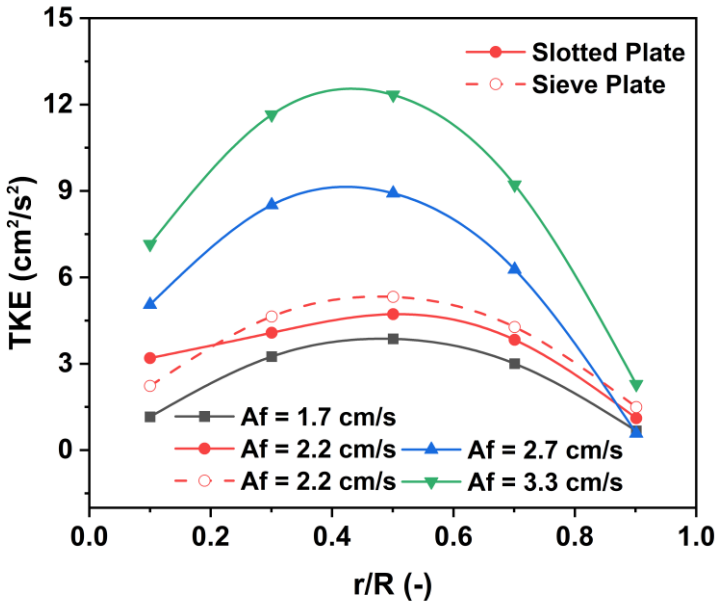

Figure 3.20: Radial variation of turbulent kinetic energy (TKE) at no flow condition

In single phase flow condition, a net flow of water through the column occurs. First, the effect of the pulsation velocity (Af) on the velocity profile is investigated at a constant flow rate of 120 LPH (a mean velocity of 0.75 cm/s) in the downward direction. Figure 3.21 shows the profile of mean axial velocity for all the four values of Af. In case of single-phase flow condition, the velocity can be thought of having a net downward velocity component and a pulsating velocity component. At the lowest Af value of 1.2 cm/s, the mean axial velocity decreases linearly from center to the wall unlike in the no-flow condition at the same frequency in which the mean axial velocity is highest in the annular region than at the center and wall.

For the three higher values of Af (1.7, 2.2 and 2.7 cm/s), the mean axial velocity is positive at almost the all the locations. The value of mean axial velocity for these af values is observed to be negative in the near wall region in the no-flow condition (see Figure 3.21).

During the upstroke, the water is swept through slots in a positive direction but there is a minimum effect of net downward force by the downward-flowing water in this condition. The up-stroke fluctuations due to the pulsation are much intensified in comparison to the downward-flowing water in this condition. The mean values are minimized in reference to that of the no-flow condition due to external downward force by flowing water.

3.3.2.2 Effect of pulsation velocity at a constant aqueous phase flow rate of single-phase flow

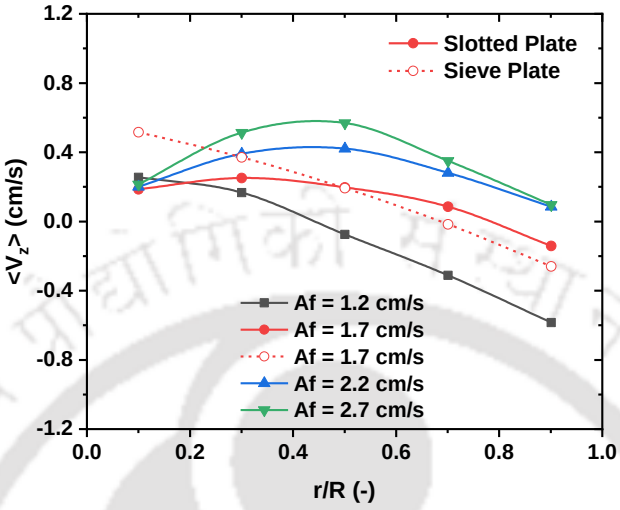

Figure 3.21: Radial variation of mean axial velocity at a flow rate of 120 LPH for four different pulsation velocities for slotted plate internals. The profile for sieve plate internal is also shown for the pulsation velocity of 1.7 cm/s for comparison

Figure 3.22 shows the radial variation of axial and radial RMS velocities for different pulsation velocities at a constant flow rate of 120LPH. The values of V_z RMS is found to be slightly lower when compared with those for the no flow condition for the same plate. The V_z RMS values in the annular zone are found to be more due to the effect of increased flowing zones. The V_r RMS values are found to be slightly more in comparison to that of corresponding sieve plate values at this condition as well. This shows that the groove structure has better radial mixing performance in reference to that of the corresponding sieve plate of the same FFA at all conditions. Though there is the external downward force by pumping of water, the pulsation velocity effect is dominant in comparison to that of flowing water velocity at this condition.

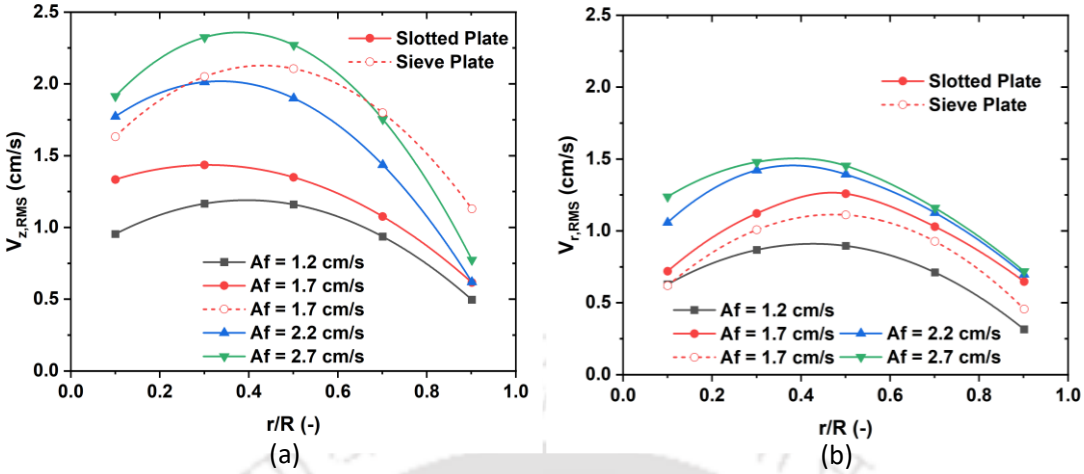

Figure 3.22: Radial variation of (a) axial rms velocity (b) radial rms velocity for different pulsation velocities at aqueous phase flow of 120 LPH

Figure 3.23 shows the radial variation of turbulent kinetic energy at 120 LPH pumping rate of water. As the pulsation velocity is increased the TKE is found to be increased but the net TKE values are shown to be nearly comparable to that of the sieve plate structure. In the sieve plate the axial RMS velocities are higher while in the slotted plate structure, the radial fluctuations are more. Hence, the net TKE of both plates showed comparable magnitudes at this condition.

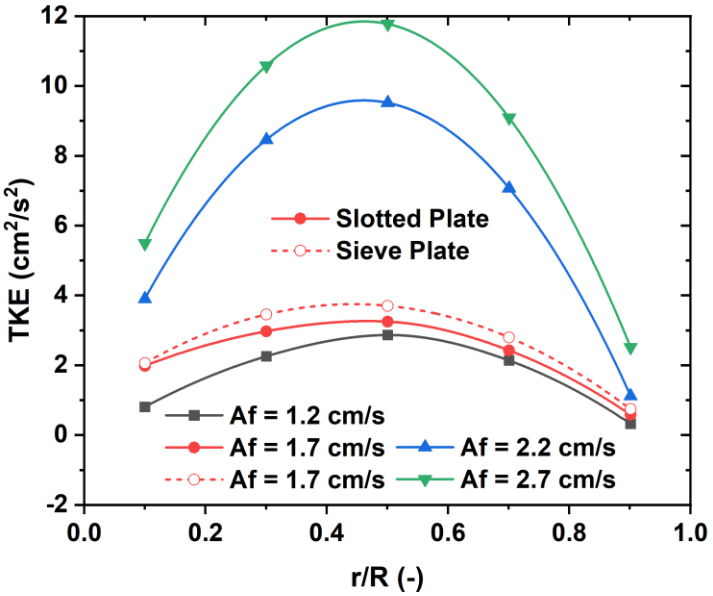

Figure 3.23: Turbulent kinetic energy (TKE) at aqueous phase flow of 120 LPH for different pulsation velocities

Next, the water pumping rates are varied keeping the pulsation intensity constant. The results are demonstrated in this section. Similar conditions are performed for the slotted plates in comparison to that of the conducted experiments in our previous article.

3.3.2.3 Effect of flow rate at constant pulsation velocity of single-phase flow

The column is operated at four different flow rates (70LPH,100 LPH,120LPH,160LPH) at constant pulsation intensity of 2.7 cm/s. Figure 3.24 shows the radial variation of mean axial velocity at four different flow rates of 70, 100, 120 and 160 LPH. When the pulsation is dominant (low flow rate), the mean velocity in the annular region is the highest. A sthe flow rate increase, the mean axial velocity in the annular region decreases. As the flow is from top to bottom, the mean axial velocity decreases (or becomes negative) with an increase in the flow

rate. The mean axial velocities are enhanced at this condition in comparison to that of no flow and single-phase flow conditions. There is more amount of liquid flowing in the peripheral zone with an increase in pumping rates, while the upstroke pulsation intensities are dominant in the central zones. Annular regions showed the enhanced effect of upstroke pulsation and the peripheral regions showed the enhanced effect of water flow rates.

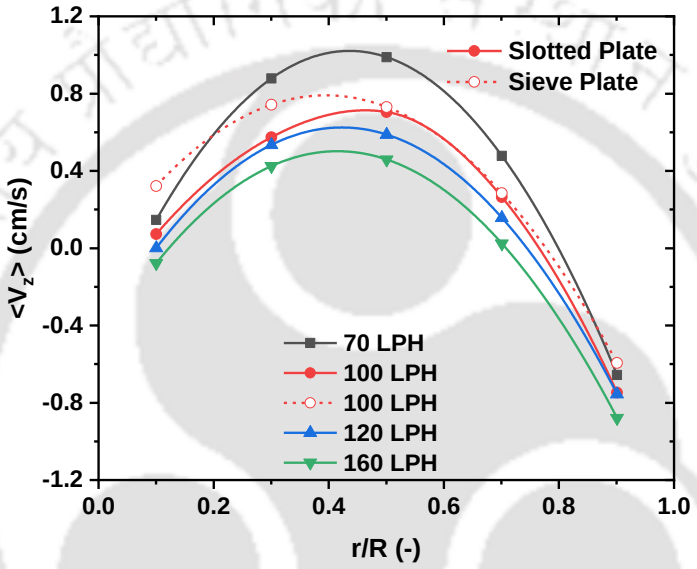

Figure 3.24: Radial variation of mean axial velocity at Af = 2.7cm/s for different aqueous phase flow rates

Figure 3.25 shows the radial variation of axial and radial RMS velocities for four different flow rates at a constant pulsation velocity of 2.7 cm/s. The radial RMS velocity is observed to be higher for slotted plate in comparison with those for sieve plate. Axial RMS velocity for sieve plate case is higher than for the slotted plate case and has higher value in the annular region. In a slotted plate the radial distance between slots is large and the jets have significant radial motion before they interact and radial velocity becomes zero. In contrast, the holes are

distributed in a sieve plate and the liquid jet coming out of a hole interact with the jets coming out from the nearby holes resulting in relatively low radial velocity.

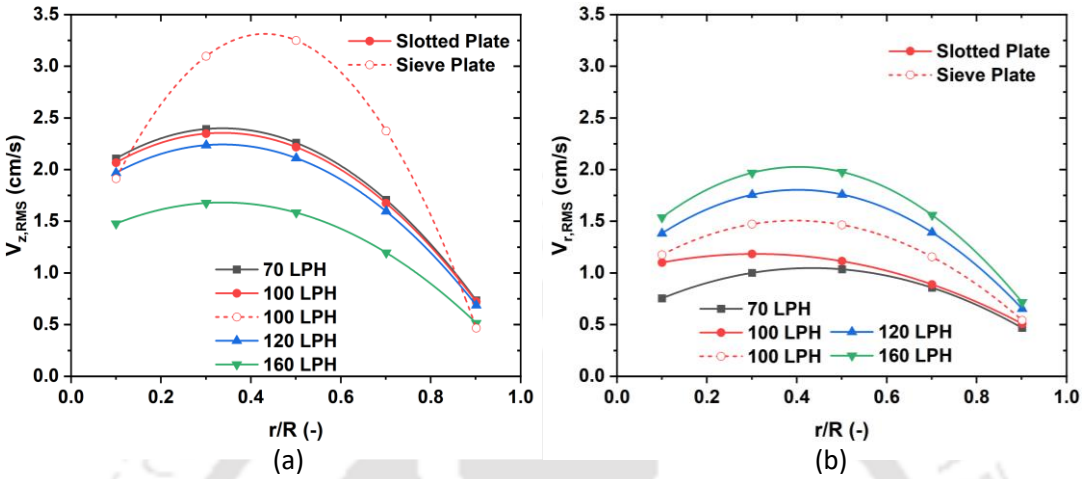

Figure 3.25: Radial variation of (a) axial rms velocity (b) radial rms velocity for different aqueous phase flow rates at Af = 2.7cm/s

Figure 3.26 shows the radial variation of TKE with different pumping rates. The flow effects enhanced the radial fluctuations while the axial fluctuations are diminished. In the net effect, the TKE values are high in reference to that of no flow condition. The employment of flow imposes more fluctuations and the results are clearly showing that fact.

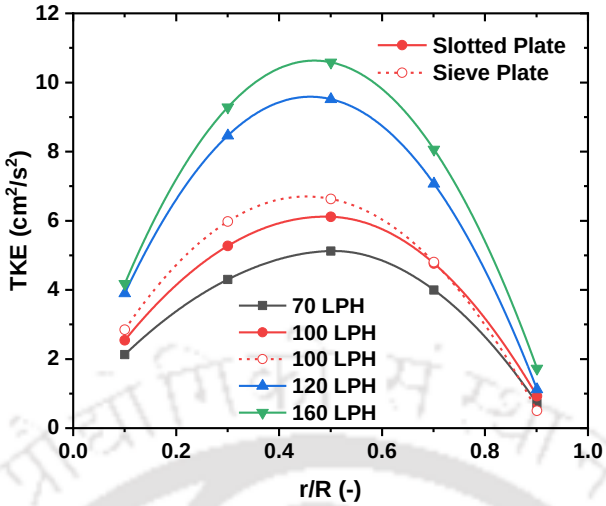

Figure 3.26 Kinetic energy of turbulence for different aqueous phase flowrates at Af = 2.7 cm/sec

3.4 Conclusions

Experiments were conducted in a 0.076 m diameter single-phase pulse sieve plate column, where Residual Pressure Technique (RPT) measurements were performed for both no flow and single-phase flow conditions. The study calculated various parameters, including mean velocity field, axial and radial RMS velocities, turbulent kinetic energy, and turbulent intensity, using single particle tracking data within two successive planes for all the conditions. For both no flow and single-phase flow conditions, the mean axial velocity showed a positive value at the center of the column and negative values at the walls, indicating the presence of recirculation of the continuous phase fluid between adjacent sieve plates. This recirculation was attributed to flow and non-flow regions, aligning with similar findings from literature using CFD simulations. The axial RMS velocity and turbulent kinetic energy were higher with increasing pulsing velocity for both no flow and single-phase flow conditions. However, in the

case of single-phase flow, fluctuations generated due to pulsation were attenuated by the net downflow of liquid, leading to lower axial RMS velocity compared to the no flow conditions. The radial fluctuation increased in the single-phase flow condition, although the increase in radial RMS velocity was marginal. Overall, the primary flow remained in the axial direction, resulting in lower turbulent kinetic energy for the single-phase flow condition compared to the no net flow case. Turbulent intensity values indicated a higher degree of mixing for all cases, with the highest turbulence observed in the no flow condition compared to the single-phase flow case. Despite this, the pulse sieve plate column exhibited better mixing and mass transfer compared to the conventional sieve plate column. Additionally, the slotted structure exhibited lower axial velocities than the sieve plate structure under corresponding no flow and single-phase conditions. The radial RMS values for the slotted structure were slightly higher than those of the Vr RMS values for the sieve plate structure. With increased pulsation velocity, fluctuations were boosted, particularly in the annular zone. However, wall effects in the peripheral zones reduced the intensity of fluctuation magnitudes. The new structure showed some hydrodynamic similarities to the sieve plate, and further two-phase studies are anticipated to provide more insights into structure selection.

Reference

Amokrane, A., Charton, S., Lamadie, F.; Paisant, J. F., Puel, F., 2014. "Single phase flow in a pulsed column: Particle Image Velocimetry validation of a CFD based model, *Chem. Eng. Sci.* 114, 40–50. https://doi.org/10.1016/j.ces.2014.04.003.

Amokrane, A., Charton, S., Lamadie, F., Paisant, J. F., Puel, F. 2014, "Single-phase flow in a pulsed column: Particle Image Velocimetry validation of a CFD based model", *Chem. Eng. Sci.* 114, 40–50. https://doi.org/10.1016/j.ces.2014.04.003.

Angelov, G., Gourdon, C., 2009, "Turbulent flow in pulsed extraction columns with internals of discs and rings: Turbulent kinetic energy and its dissipation rate during the pulsation". *Chem. Eng. Process. Intensif.* 48, 592–599. https://doi.org/10.1016/j.cep.2008.07.002.

Bahmnyar, H.;Nazari, L.; Jaber, S. Prediction of solute concentration changes along pulsed sieve column. *Chem. Engg. Comm.* **2009**, 196,1332-1347. https://doi.org/10.1021/i260031a016.

Bart, H.J., Drumm, C., Attarakih, M., 2008, "Process intensification with reactive extraction columns". *Chem. Eng. Process. Process Intensif.* 47, 745–754. https://doi.org/10.1016/j.cep.2007.11.005.

Benedict, M., Pigford, T.H., Levi H.W., 1981, Nuclear Chem.Eng. McGraw Hill Book Company.

Bhambal, S., Makasare, P., Uzagare, N., 2016, "Study of Enhancement of Heat Transfer using Helical Baffle" 6, 194–196.

Bhusarapu, S.,2005, “Solids flow mapping in gas-solid risers”, D.Sc. thesis, Washington University, Saint Louis, Missouri, USA.

Boyadzhiev, L., Spassov, M., 1982, “On the size of drops in pulsed and vibrating plate extraction columns”. *Chem. Eng. Sci.* 37, 337-340.

Brunold, R., Hunns, J.C.B., 1989. “Losses for Oscillatory”. *Chem. Eng*. 44, 1227–1244.

Bujalski, J. M., Yang, W., Nikolov, J., Solnordal, C. B., Schwarz, M. P., 2006, “Measurement and CFD simulation of single-phase flow in solvent extraction pulsed column”, *Chem. Eng. Sci.* 61, 2930–2938. https://doi.org/10.1016/j.ces.2005.10.057.

Bujalski, J. M., Yang, W., Nikolov, J., Solnordal, C. B., Schwarz, M. P., 2006, “Measurement and CFD simulation of single-phase flow in solvent extraction pulsed column”, *Chem. Eng. Sci.* 61, 2930–2938. https://doi.org/10.1016/j.ces.2005.10.057

Burkhart, L.E., 1956, “Extraction efficiency of a pulse column of varied geometry”, M.S. Thesis.

Caishan. J., Shuai. M., Qiong. S., 2013, “Mass transfer characteristics in a standard pulsed sieve-plate extraction column”, *Energy Procedia.* 39, 348–357. https://doi.org/10.1016/j.egypro.2013.07.222.

Charton, S., Duhamet, J., Borda, G., Ode, D., 2012, “Axial dispersion in pulsed disk and doughnut columns”. *Chem. Eng. Sci.* 75, 468–477. https://doi.org/10.1016/j.ces.2012.04.011.

Chen, J., Kemoun, A., Al-Dahhan, M. H., Dudukovic, M. P. Lee, D. j., Fan, L. S., 1999, "Comparative hydrodynamics study in a bubble column using computer-automated radioactive particle tracking (CARPT)/computed tomography (CT) and particle image velocimetry (PIV)", *Chem. Eng. Sci.* 54, 2199–2207. https://doi.org/10.1016/S0009-2509(98)00349-2.

Degaleesan, S. 1997, "Fluid dynamic measurements and modelling of liquid mixing in bubble columns", D. Sc. Thesis, Washington University, St. Louis.

Devanathan, N., 1991, "Investigation of liquid hydrodynamics in bubble columns via computer automated radioactive particle tracking", D.Sc. thesis, Washington University, USA.

Devanathan, N., Moslemian, D., Dudukovic, M. P., 1990, "Flow Mapping in Bubble Columns", *Chem. Eng. Sci.* 452285–2291.

Din, G. U., Khan, I. H., Chughtai, I. R., Inayat, M. H., Jin, J. H., 2013, "Radiotracer investigations to study the hydrodynamic characteristics of continuous phase in a pulsed sieve plate extraction column". *EPJ Web Conf.* 50, 01004. https://doi.org/10.1051/epjconf/20135001004

Din, G.U., Chughtai, I.R., Inayat, M.H., Khan, I.H., Qazi, N.K., 2010, "Modelling of a two-phase counter current pulsed sieve plate extraction column - A hybrid CFD and radiotracer RTD analysis approach". *Sep. Purif. Technol.* 73, 302–309. https://doi.org/10.1016/j.seppur.2010.04.017.

Drumm, C., Attarakih, M., Hlawitschka, M.W., 2010, "One-Group Reduced Population Balance Model for CFD Simulation of a Pilot-Plant Extraction Column". *Ind. Eng. Chem. Res.* 3442–3451. https://doi.org/10.1021/ie901411e.

Dudukovic, M. P., 2000, "Opaque Multiphase Reactors: Experimentation, Modeling and Troubleshooting", *Oil Gas Sci. Technol.* 55, 135–158. https://doi.org/10.2516/ogst:2000008.

Dudukovic, M. P., 2003, "Use of gamma Ray computed tomography (CT) and computer aided radioactive particle tracking (CARPT) in multiphase reactors". *Hem. Ind.* 57, 249–261. https://doi.org/10.2298/hemind0306249d.

Eid, K., Casamatta, G., Muratet, G., Gourdon, C., 1991, "Drop breakage sieve-plate column". *Chem. Eng. Sci.* 46, 1595–1608.

Fraguío, M. S, Cassanello, M. C., Degaleesan, S., Dudukovic, M., 2009, "Flow regime diagnosis in bubble columns via pressure fluctuations and computer-assisted radioactive particle tracking measurements", *Ind. Eng. Chem. Res.* 48, 1072–1080. https://doi.org/10.1021/ie800549d.

Ghadiri, M., Ashrafizadeh, S.N., Taghizadeh, M., 2014, "Study of molybdenum extraction by tri octylamine and tributyl phosphate and stripping by ammonium solutions". *Hydrometallurgy*, 144–145, 151–155. https://doi.org/10.1016/j.hydromet.2014.02.009

Godfrey, J. C., & Slater, M. J. (Eds.). 1994. "Liquid-liquid extraction equipment". New York: Wiley.

Goswami, S., Sen, N., Samantray, J. S., Dash, A., Sharma, V. K., Shenoy, K.T., Pant, H. J., 2017, "Investigation of flow dynamics of single phase in a pulsed sieve- plate column using radiotracer technique", *J. Radioanal. Nucl. Chem.* 313, 669–676. https://doi.org/10.1007/s10967-017-5373-0.

Jahya, A.B., Pratt, H.R.C., Stevens, G.W., 2005, "Comparison of the performance of a pulsed disc and doughnut column with a pulsed sieve plate liquid extraction column". *Solvent Extr. Ion Exch.* 23, 307–317. https://doi.org/10.1081/SEI-200045257

Jain, V., Kalo, L., Kumar, D., Pant, H. J., Upadhyay, R. K., 2017, "Experimental and numerical investigation of liquid–solid binary fluidized beds: Radioactive particle tracking technique and dense discrete phase model simulations", *Particuology*. 33, 112–122. https://doi.org/10.1016/j.partic.2016.07.011

Jones, S. C., 1963, Ph.D. dissertation, University of Michigan, Ann Arbor, Mich.

Kagan, S. Z., Aerov, M. E., Lonik V., Volkova T. S., 1965, "Some hydrodynamic and mass transfer problems in pulsed sieve-plate extractors", *Int. Chem. Eng*. 656-661.

Kalo, L., Kamalanathan, P., Pant, H. J., Cassanello, M. C., Upadhyay, R. K., 2019, "Mixing and regime transition analysis of liquid-solid conical fluidized bed through RPT technique. *Chem. Eng. Sci.* 207, 702–712. https://doi.org/10.1016/j.ces.2019.07.005.

Kalo, L., Kamalanathan, P., Pant, H. J., Cassanello, M. C., Upadhyay, R. K., 2019, "Time series analysis of a binary gas-solid conical fluidized bed using radioactive particle tracking (RPT) technique data", *Chem. Eng. J.* 377, 119807. https://doi.org/10.1016/j.cej.2018.08.193

Kamalanathan, P., Kalo, L., Pant, H. J., Upadhyay, R. K., 2017, "Effect of dynamic bias on accuracy of radioactive particle tracking (RPT) technique at different data acquisition frequencies", *Appl. Radiat. Isot.* 128, 13–21. https://doi.org/10.1016/j.apradiso.2017.06.034.

Khatir, Z., Hanson, B. C.; Fairweather, M., Heggs, P. J., 2016, "High-fidelity CFD simulations of pulsed sieve-plate extraction columns", *11th Int. ERCOFTAC Symp. Eng. Turbul. Model. Meas.*

Kolhe, N. S., Mirage, Y. H., Patwardhan, A.W., V.K. Rathod, V. K., Pandey, N. K., Mudali, U.K., Natarajan, R., 2011, "CFD and experimental studies of single-phase axial dispersion coefficient in pulsed sieve plate column. *Chem. Eng. Res. Des.* 89,1909–1918. https://doi.org/10.1016/j.cherd.2011.01.020.

Larachi, F., G. Kennedy, G., Chaouki, J. 1994, "A γ-ray detection system for 3-D particle tracking in multiphase reactors", *Nucl. Inst. Methods Phys. Res. A.* 338, 568–576. https://doi.org/10.1016/0168-9002(94)91343-9.

Lorenz, M., Haverland, H., Vogelphol, A., 1990, "Fluid dynamics of pulsed sieve plate extraction columns", Chem. Eng. Technol. 13, 411–422. https://doi.org/10.1002/ceat.270130156.

McDonough, J.R., 2018. Process development using oscillatory baffled mesoreactors. PQDT - UK Irel.

Mehrkesh, A., Tavakoli, T., Hatamipour, M.S., Karunanithi, A.T. Modeling and simulation of a rotating-disk contactor for the extraction of aromatic hydrocarbons from a lube-oil cut. *Ind. Eng. Chem. Res.* ***2013,*** 52, 9422–9432. https://doi.org/10.1021/ie303427m

Miyauchi, J., Oya, H., 1965, "Longitudinal dispersion in pulsed perforated-plate columns", AIChE J. 11, 395-402

N.S. Kolhe, N. S., Mirage, Y. H., Patwardhan, A. V., Rathod, V. K., Pandey, N. K., Mudali, U.K., Natarajan, R., 2011, "CFD and experimental studies of single-phase axial dispersion coefficient in pulsed sieve plate column". *Chem. Eng. Res. Des.* 89,1909–1918. https://doi.org/10.1016/j.cherd.2011.01.020.

Roy, S., Kemoun, A., Al-Dahhan, M. H., Dudukovic, M. P.,2005, "Experimental investigation of the hydrodynamics in a liquid-solid riser". *AIChE J.* 51, 802–835. https://doi.org/10.1002/aic.10447.

Roy, S., Larachi, F., Al-Dahhan, M. H., Dudukovic, M. P., 2002, "Optimal design of radioactive particle tracking experiments for flow mapping in opaque multiphase reactors, *Appl. Radiat. Isot.* 56, 485–503. https://doi.org/10.1016/S0969-8043(01)00142-7.

Sarkar, S., Singh, K. K., Shenoy, K. T., 2017, "CFD simulations of single-phase flow in pulsed disc and doughnut columns: Axial dispersion and pressure drop". *Sep. Sci. Technol.* 52, 2861–2875. https://doi.org/10.1080/01496395.2017.1375952.

Sehmel, G. A., Babb. A.L., 1963, "Holdup studies in a pulsed sieve-plate solvent extraction column". *Ind. Eng. Chem. Process Des. Dev.* 2,38–42. https://doi.org/10.1021/i260005a008.

Sen, N., Sarkar, S., Singh, K.K., Mukhopadhyay, S., Shenoy, K.T., 2018, “Regime Transition and Holdup in Pulsed Sieve- Plate and Pulsed Disc-and-Doughnut Columns: A Comparative Study Regime Transition and Holdup in Pulsed column”. *Solvent. Extr. Ion. Exch.* 36, 66–83. https://doi.org/10.1080/07366299.2017.1415672

Sen, N., Singh, K.K., Patwardhan, A.W., Mukhopadhyay, S., Shenoy, K.T., 2016 “CFD simulation of two-phase flow in pulsed sieve- plate column – Identification of a suitable drag model to predict dispersed phase hold up”. *Sep. Sci. Technol.* 51, 2790–2803. https://doi.org/10.1080/01496395.2016.1218895

Sen, N., Singh, K. K., Patwardhan, A. W., Mukhopadhyay, S., Shenoy, K. T., 2018, “CFD simulations to predict dispersed phase holdup in a pulsed sieve plate column”, *Sep. Sci. Technol.* 53,2587–2600. https://doi.org/10.1080/01496395.2018.1459702

Sen, N., Singh, K. K, Patwardhan, A. W., Mukhopadhyay, S., Shenoy, K. T., 2016, “CFD simulation of two-phase flow in the pulsed sieve-plate column – Identification of a suitable drag model to predict dispersed phase hold up”, *Sep. Sci. Technol.* 51,2790–2803. https://doi.org/10.1080/01496395.2016.1218895

Sen, N., Singh, K. K, Patwardhan, A. W., Mukhopadhyay, S., Shenoy, K. T., 2019, “CFD-PBM simulations of a pulsed sieve plate column”. *Prog. Nucl. Energy.* 111, 125–137. https://doi.org/10.1016/j.pnucene.2018.10.012.

Sen, N.; Singh, K. K; Patwardhan, A. W.; Mukhopadhyay, S.; Shenoy, K. T., 2020, “Computational Fluid Dynamics Modelling to Predict Axial Dispersion in Pulsatile

Liquid-liquid Two phase Flow in Pulsed Sieve Plate Columns". *Solvent Extr. Ion Exch.* 1–25. https://doi.org/10.1080/07366299.2020.1840030.

Shakib, B., Torkaman, R., Mostaedi, M.T., Asadollahzadeh, M., 2020, "The performance of pulsed scale-up column for permeable of selenium and tellurium ions to organic phase, case study: Disc and doughnut structure". *Chem. Eng. Process. - Process Intensif.* 157, 108042. https://doi.org/10.1016/j.cep.2020.108042

Smith, K.B., Mackley, M.R., 2006, "An experimental investigation into the scale-up of oscillatory flow mixing in baffled tubes". *Chem. Eng. Res. Des.* 84, 1001–1011. https://doi.org/10.1205/cherd.05054

Somkuwar, N., Kolhe, N., Rathod, V., 2014, "Hydrodynamics of a Pulsed Sieve Plate Extraction Column", *Indian Chem. Eng.* 56,235–257. https://doi.org/10.1080/00194506.2014.910707.

Sreenivasulu, K., D. Venkatanarasaiah, Y., Varma, B.G., 1997, "Drop size distributions in liquid pulsed columns", Bioprocess Eng. 17, 189–195. https://doi.org/10.1007/s004490050374.

Sun, Y., Gao, Y. H., Jiao, C., Zhou, Y., Zhang, M., 2019, "Study on droplet velocity in a pulsed sieve plate extraction column by four-sensor optical fiber probe". *Chem. Eng. Res. Des.* 144, 550–558. https://doi.org/10.1016/j.cherd.2019.02.031.

Tang, X., Chen, F., Luo, G., Wang, J., 2009, "Estimation of axial dispersion in pulsed-plate extraction columns". *Chem. Eng. Res. Des.* 87,1562–1566. https://doi.org/10.1016/j.cherd.2009.04.001.

Tang, X., Chen, F., Luo, G., Wang, J., 2009, Estimation of axial dispersion in pulsed-plate extraction columns. *Chem. Eng. Res. Des.* 87,1562–1566. https://doi.org/10.1016/j.cherd.2009.04.001.

Theobald, D.W., Hanson, B., Fairweather, M., Heggs, P. J., 2020, "Implications of hydrodynamics on the design of pulsed sieve-plate extraction columns: A one-fluid multiphase CFD model using the volume of fluid method", *Chem. Eng. Sci.* 221, 115640. https://doi.org/10.1016/j.ces.2020.115640.

Torab-Mostaedi, M., Ghaemi, A., Asadollahzadeh, M., Pejmanzad, P., 2011, "Mass transfer performance in pulsed disc and doughnut extraction columns". Brazilian J. Chem. Eng. 28, 447–456. https://doi.org/10.2298/CICEQ110123019T

Tsouris, C., Kirou, V.I., Tavlarides, L.L., Wang, C.Y., 1994, "Drop size distribution and holdup profiles in a multistage extraction column". *AIChE J.* 40, 407–418. https://doi.org/10.1002/aic.690400304

Upadhyay, R. K., Pant, H. J., Roy, S.,2013, "Liquid flow patterns in rectangular air-water bubble column investigated with Radioactive Particle Tracking", *Chem. Eng. Sci.* 96, 152–164. https://doi.org/10.1016/j.ces.2013.03.045.

Van Delden, M.L., Vos, G.S., Kuipers, N.J.M., de Haan, A.B., 2006, "Extraction of caprolactam with toluene in a pulsed disc and doughnut column - Part II: Experimental evaluation of the hydraulic characteristics". *Solvent Extr. Ion Exch.* 24, 519–538. https://doi.org/10.1080/07366290600760649.

Wang, Y., Mumford, K.A., Smith, K.H., Li, Z., Stevens, G.W. 2016, "Dispersed-Phase Holdup and Characteristic Velocity in a Pulsed and Nonplused Disk-and-Doughnut Solvent Extraction Column". *Ind. Eng. Chem. Res.* 55, 714–721. https://doi.org/10.1021/acs.iecr.5b02293

Xiaojin, T., Guangsheng, L. 2011, "CFD simulations of flow characteristics in pulsed-sieve-plate extraction columns", *Ind. Eng. Chem. Res.* 50 1110–1114. https://doi.org/10.1021/ie101788b.

Yadav, R. L., Patwardhan, A. W., 2008, "Design aspects of pulsed sieve plate columns". *Chem. Eng. J.* 138,389–415. https://doi.org/10.1016/j.cej.2007.06.015.

Yi, H., Smith, K. H., Fei, W., Stevens, G. W., 2020, "CFD Simulation of Two-Phase Flow in a Hybrid Pulsed Sieve-Plate Solvent Extraction Column: Prediction of Holdup and Axial-dispersion Coefficients". *Solvent Extr. Ion Exch.* 38, 88–102. https://doi.org/10.1080/07366299.2019.1691300.

Yung, K.K.L., Smith, C.D., Bowser, T., Perera, J.M., Stevens, G.W., 2012, "The use of an ionic liquid in a Karr reciprocating plate extraction column". *Chem. Eng. Res. Des.* 90, 2034–2040. https://doi.org/10.1016/j.cherd.2012.03.006

CHAPTER-4

Single Phase Flow Investigation in Pilot-Scale Pulsed Sieve Column

Chapter 4 : Single Phase Flow Investigation in Pilot-Scale Pulsed Sieve Column

Graphical abstract

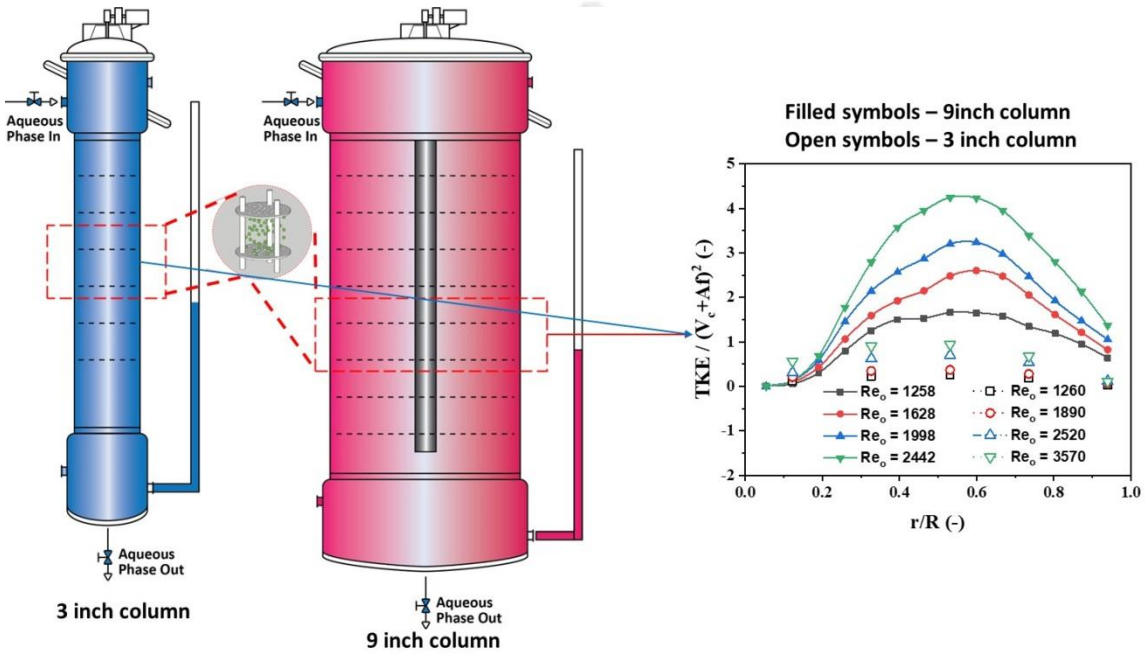

Abstract

This chapter describes the construction design and developments of the fabricated pilot scale system. There is lack of evidential investigation of flow behavior at pilot scale in pulsed column. This chapter is focused at the local field turbulence investigation using radiation based experimental measurement technique. Dimensional analysis and the choice of the conditions are explained in detail. The reporting variables are measured using gamma-based radiation using scintillation detectors (NaI). We have previously reported the local field investigation in laboratory scale column using different internals and different operational scenario. In the current chapter, the local velocity field information of velocities, eddy diffusivities and the turbulent kinetic energies using 23 percent sieve plates are discussed.

4.1 Introduction

Pulsed columns are commonly used for liquid-liquid extraction in the chemical processing industry (Sarkar et al., 2017). The performance of the pulsed column depends on the local hydrodynamics in the column which in turn, depends on the geometric and flow parameters (Sen et al., 2020; Kolhe et al., 2011; Somkumar et al., 2014; Yadav et al., 2008). Scaling up a chemical or biological process requires consideration of different types of similarities in the smaller and larger scale columns. The first step in the scale up is to increase the column capacity or volume while maintaining geometric similarity i.e. radius and height of the column are scaled up in the same proportion. The next step is to ensure kinematic and dynamic similarities as far as possible.

Flow phenomena occur at two different scales in a Pulsed Sieve Plate Column (PSPC). On the one hand, a jet of fluid emerges from each hole and interacts with the jets emerging from the surrounding holes. The hole diameter is the relevant length scale for this phenomenon. Whereas, for flow between two consecutive plates, column diameter is the relevant length scale. While scaling up, the diameter of the hole does not need to change so the flow behavior at the hole scale is same at the two scales. If the diameter of the holes in the scaled-up geometry is kept same, the related physical phenomena such as jet diameter and droplet diameter in case of two-phase flow would remain same at the two scales provided the local fluid velocity at the hole is same in the two cases. Further, the number of holes per unit plate area or fractional free area should ideally be same in both the scales. However, the column diameter changes and consideration for the flow similarity between the two scales needs to be considered. For the flow between the two consecutive plates, the geometric parameters of relevance are column dimeter (D), the distance between the two consecutive plates (h). Further, the flow parameters

of relevance for single phase flow are phase flow rate (Q), pulsation amplitude (A), pulsation frequency (f), acceleration due to gravity (g) along with the fluid density (ρ), viscosity (μ) for single phase flow. We combine pulsation amplitude (A) and frequency (f) to give a velocity scale representing the pulsation speed (Af). These seven variables can be combined to give four independent dimensionless groups $\frac{h}{D}, \frac{gD}{(Af)^2}, \frac{DAf\rho}{\mu}, \frac{Q\rho}{\mu D}$. The last two variables represent oscillatory (Re_O) and flow Reynolds numbers, respectively.

To the best of our knowledge, there are very few studies available in the literature on the scale up of PSPC. A variant of PSPC is also used as reactor, commonly known as oscillatory baffled reactor (OBR). The plates used in PSPC are called baffles in OBR. Depending on single or multiple openings in the baffles, they are named as single orifice or multi orifice baffle reactors. Smith et al., (2015) performed scale up studies in oscillatory baffled columns in columns of diameter 24 mm, 54 mm and 150 mm using a single orifice baffle by measuring axial dispersion (Smith et al., 2006; Mcdonough et al., 2015). They suggested oscillatory Reynolds number, net flow Reynolds number and Strouhal numbers as the relevant non-dimensional numbers for flow. They found axial dispersion to be same in the three columns when the non-dimensional numbers are same in the three cases. They also studied axial dispersion using multiorifice baffles in the 150 mm diameter column having the same orifice diameter as in a single orifice 24 mm diameter column. Interestingly, they found the axial dispersion to be same in the multiorifice and single orifice columns. Jian et al. (2005) reported a numerical study on the scale-up of single-orifice oscillatory baffled columns under batch condition (Ahmed at el., 2019). The study investigated the effect of increasing the size of column on flow behavior and mixing efficiency (Law et al., 2018). For a single orifice baffle, they observed a linear scale up behavior. The studies discussed above are focused on scale-up of a single orifice column.

Clearly, there is lack of literature for scale-up behavior of the multi-orifice oscillatory baffled reactors which typically have horizontal orientation as well as pulsed sieve plate columns which have a vertical orientation (Ardestani et al., 2021). Recently, we have investigated velocity field between two consecutive plates in a vertical pulsed sieve plate column of 76 mm (3 inch) diameter using radioactive particle tracking. In this work, we investigate the velocity field in a column of 210 mm (8.26 inch) diameter for single phase flow in no net flow and continuous flow in the upward direction. The velocity profiles obtained from the lab scale and pilot scale column are compared.

4.2 Experimental section

A pilot scale pulsed sieve plate column of 210 mm diameter and 800 mm height made up of glass is designed for the experiments. Figure 4.1 shows a schematic of the experimental set up along with the pilot scale column. The column has seven sieve plates each having 23% free area. The plates are evenly spaced with a distance of 100 mm between two consecutive plates and are supported by a 38 mm rod at the center. Support framework comprising spacer rods and shell structure for a plate system is used to ensure the accurate spacing between the sieve plates. It may be noted that the lab scale column from our previous chapters had three tie rods of 3 mm in triangular pattern in annular zone, whereas pilot column has only a central rod of 38 mm passing through the center of the column. The geometrical data of the lab scale and pilot scale columns are given in Table 4.1. Note that the hole diameter is same in both the columns. The outer diameter of the pilot scale column is 222 cm and the inner diameter is 210 mm which is approximately three time that of the lab scale column (Juela et al., 2022). For brevity and convenience, the lab scale column is referred as 3 inch column whereas the pilot

scale column is referred as 9 inch column throughout the dissertation. The design considerations suggest the inter-plate distance to be nearly half of the plate diameter and therefore are 100 mm in the pilot scale column. In the lab scale column, it was not possible to accommodate all the detectors within half column diameter (38 mm) and therefore a larger inter-plate distance of 100 mm (1.3 times the column diameter) was chosen in the lab scale column (Calero et al., 2016). The frequency of the oscillations is kept 1 Hz in all the cases in both the columns.

The values of the non-dimensional parameters are given in Table 4.2. The value of the corresponding pulsating velocities and/or flow rates for each type of column is also given in the Table. Experiments have been performed for three cases. One, when there is no net flow and only pulsation is provided to the column. Two, experiments are performed at a fixed flow rate and the effect of variation in pulsation velocity is studied. Third, experiments are performed for a fixed pulsation velocity and the effect of flow rate on the velocities is investigated (Saremi et al., 2021). As can be seen from the second row in Table 4.2, the values of oscillatory Reynolds number is same when the effect of pulsation velocity is studied in the first (no net flow) and second (constant flow rate) cases. Similarly, the flow Reynolds numbers are similar in case three (constant pulsation velocity) as can be seen in row 3 of Table 4.2. The dimensionless number representing the ratio of flow rate and pulsation flow rate is almost constant in all the cases and is close to 20% as can be seen from row 5 in Table 4.2. The dimensionless group which is a type of Froude number or its inverse has a difference of an order of magnitude in the two cases. However, it may be noted that the gravity does not affect the flow as the flow is not driven by gravity.

Table 4.1: Details of the geometry of the lab scale and pilot scale PSPC

Geometric Parameter	Laboratory scale	Pilot scale
Diameter of column (D), mm	75 mm	210 mm
Height of column (H), mm	600 mm	800 mm
Plate spacing (h), mm	100 mm	100 mm
Hole diameter	3 mm	3 mm
Fractional free area (α)	17%	23%

Table 4.2: Scale up study and dimensionless quantities comparison of PSPC of two different scales

Dimensionless parameters	Small Diameter Laboratory scale	Big Diameter Pilot scale
h/D	1.33	0.48
Re_o	1432 (Af= 1.7 cm/s) 2275 (Af= 2.7 cm/s) 2780 (Af= 3.3 cm/s)	1415 (Af= 0.6 cm/s) 2123 (Af= 0.9 cm/s) 2831 (Af= 1.2 cm/s) 4011 (Af= 1.7 cm/s)
Re_f	374 (70 LPH) 534 (100 LPH) 641 (120 LPH) 855 (160 LPH)	401 (210 LPH) 573 (300 LPH) 687 (360 LPH) 916 (480 LPH)

$\frac{gD}{(Af)^2}$	2543 1008 675	57167 25407 14292 7121
$\frac{Q}{Af(D)^2}$	0.21 0.22 0.22 0.24	0.22 0.21 0.19 0.18

For no net flow case, experiments are performed at four different pulsation velocities of 0.6, 0.9, 1.2 and 1.7 cm/s in the pilot scale column. The first three pulsating velocities correspond to equivalent cases for lab scale column for which the values of oscillatory Reynolds number (Re_o) is similar in both the cases. The condition of 1.7 cm/s is common in both the cases so that the results for a same pulsation velocity in two scales can be understood.

The flow between two adjacent plates becomes periodic except near the inlet and exit. Therefore, velocity measurements are made using radioactive particle tracking (RPT) in a periodic unit i.e. region between two consecutive plates. In RPT, the fluid velocity is obtained by measuring the position-time data of a radioactive particle which can follow the fluid faithfully. In the experiments, Scandium (SC-46), a gamma ray emitter, is used as radioactive tracer which has a half-life of 84 days. In order for the particle to follow the fluid faithfully, it should be neutrally buoyant. This is done by placing the radioactive particle in a hollow polyethylene bead and filling the gap is carefully with Araldite epoxy glue such that the particle density matches that of the water. The sealing of particle also prevents the dilution, dispersion,

and leakage of the radioisotope, which could lead to radioactive contamination both inside and outside the column.

RPT involves two main steps namely calibration and reconstruction (Roy et al., 2022). A radiation detection system, equipped with gamma-ray detectors or suitable measurement devices, is strategically positioned to accurately capture the emitted particle signals. The region between the third and fourth plates from the bottom is chosen as the zone of study. NaI(TI) detectors are utilized to capture the radiation emitted from the particle. Eight detectors are strategically placed around the investigation zone in two planes. In each plane, four detectors are set at an angle of 90° to each other and the detectors at the bottom and top planes are not vertically aligned but at 45° to the nearest detector in the other plane. This configuration is referred to as staggered alignment. The planar spacing and the distance of face of detector from the wall of the column are chosen based on resolution sensitivity studies for a given source strength. Specialized particle tracking software is employed to analyze the detected radiation signals and reconstruct particle trajectories. The calibration curve is generated by comparing the known particle positions and velocities with the measured signals, obtained through controlled experiments. Additional experiments are conducted to validate the system, comparing particle trajectories against the calibrated measurements, ensuring the accuracy and reliability of the RPT system. Following this calibration process, the reconstruction and postprocessing steps are performed to precisely track and analyze the behavior of radioactive particles in the intricate fluid dynamics of a water.

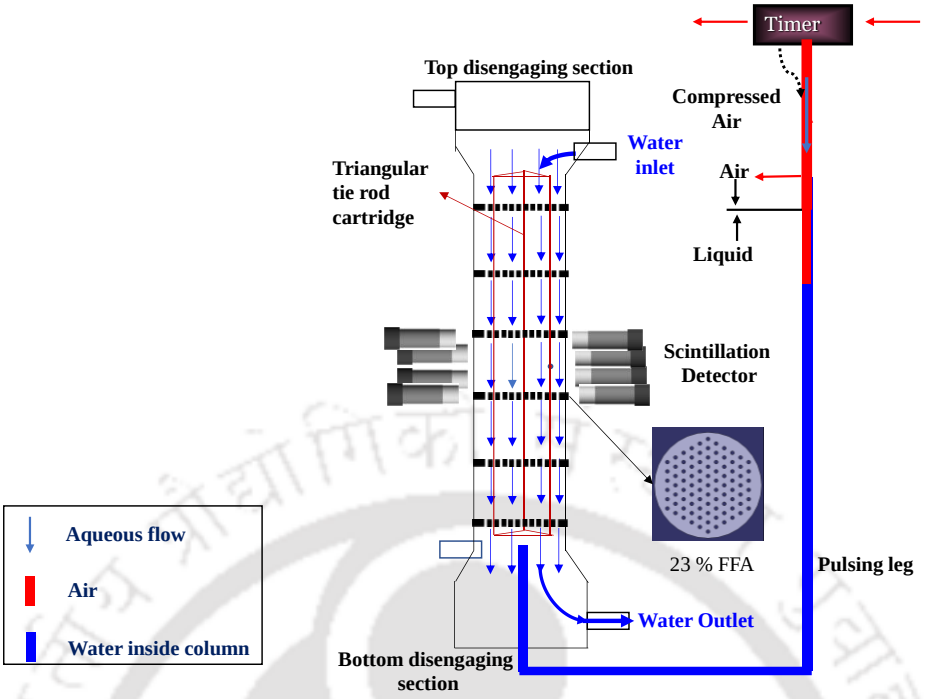

Figure 4.1: The schematic of the experimental setup

Despite some experimental investigations being conducted at a laboratory scale, local field investigations in a pulsed column have not been attempted due to the complex operation of the column and pulsation hardware at a larger scale, as well as issues with control management. However, a recent attempt has been made to undertake this study, and in-house design developments have been envisaged. The experiments were performed using a 23 percent sieve plate as an internal component. Electronic settings of data acquisition are kept same as of our previous work. The key to pulse column operation is maximizing the contact area between a heavy aqueous phase and an organic phase that contains a ligand to remove the desired components from the aqueous solvent. This is achieved through a pulsation mechanism that creates dispersion and maximizes contact area. Additionally, the pulsation frequency and amplitude are two essential operating variables that are used to control the extraction process during operation.

4.3 Results and discussion

The experiments are conducted to obtain velocity field for no net flow condition and upward flow of water in the pilot scale (9 inch) column. The effect of pulsation velocity and flow rate on the velocity field is also investigated (Chaison et al., 2022; Tang et al., 2009; Angelov et al., 2009). The results are compared with those obtained in the lab scale (3 inch) column for the corresponding conditions.

4.3.1 No net flow condition

First the experiments have been performed in the batch mode and there is no net flow through the column. In such a case, the net velocity in the axial direction is close to zero and primarily fluctuations in the velocity are observed in the column. As the fluctuations by the air column is caused in the axial direction, the dominant fluctuations are expected in the axial direction and are shown in Figure 4.2(a) for the four pulsation velocities by solid symbols. Results for the lab scale (3 inch) column are also shown by open symbols for comparison.

However, as the pulsation velocities are different in the two columns, the velocity fluctuations are also different. Therefore, a comparison of non-dimensional axial rms velocity is shown in Figure 4.2(b). The axial rms velocity is scaled by the corresponding pulsation velocity. In the pilot scale column, the velocity fluctuations are zero at the center of the column due to the presence of the rod at the center. The axial rms velocity increases on moving away from the center and becomes maximum in the annular region and then decreases near the wall. As expected, the fluctuations in the axial velocity increase with an increase in the pulsation speed. However, there are only minor differences in the non-dimensional fluctuations in the four cases. A direct comparison of dimensional values can be made in Figure. 4.2(a) for Af = 1.7

cm/s for which the experiments are performed in both the scales. The magnitude of axial rms velocity is observed to be same for both the cases except that there is zero velocity near the center in the pilot scale which causes the velocity in the other regions to be slightly higher than the corresponding values in the lab scale column.

On comparing the profile of the axial rms velocity with that of the lab scale column, the non-dimensional velocity profile is observed to be similar for the both the cases except near the column center. In case of laboratory scale (3 inch) column three tie rods exist, these did not disturb the fluctuations much. Therefore, there is significant fluid velocity at the center in the lab scale column. The rms velocity is observed to be high in the annular zone in the pilot scale column when compared with that in laboratory scale column. This is because of the mass balance.

Another interesting observation can be made from the profiles of non-dimensional axial velocity for lab scale column. The velocity profile is sharp at the lowest Re_o of 1432 and becomes flatter with an increase in Re.

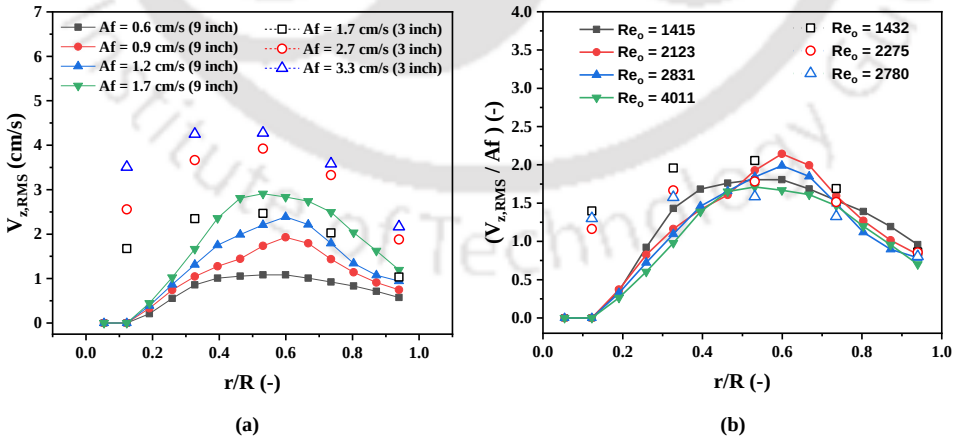

Figure 4.2: (a) Radial variation of axial rms values in single phase flow for oscillatory Reynolds numbers for no flow condition in pilot scale PSPC (9 inch) and its comparison with

the laboratory scale PSPC (3 inch) (b) Dimensionless velocity with its pulse velocity at similar condition

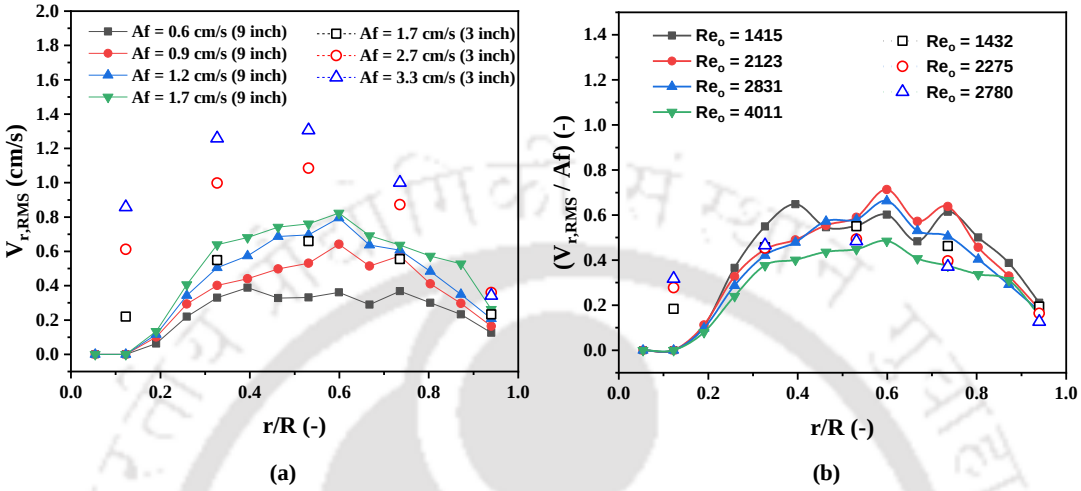

Figure 4.3: (a) Radial variation of rms values of radial component of velocity in single phase flow for oscillatory Reynolds numbers for no flow condition in pilot scale PSPC (9 inch) and its comparison with the values for laboratory scale PSPC (3 inch) (b) Dimensionless velocity with its pulse velocity at similar condition

Figure 4.3 (a) shows the variation of rms radial velocity with the radial location for four different pulsation velocities for no flow condition in pilot scale PSPC (9 inch) and its comparison with the values for laboratory scale PSPC (3 inch). The magnitude of the fluctuations in the radial velocity is clearly less than the corresponding axial rms velocities. As an example, for pulsation velocity of 1.7 cm/s, at r/R = 0.6, the axial and radial rms velocities are 2.54 and 0.78 cm/s, respectively. The variation of the radial rms velocity follows the same trend as the axial rms velocity, negligible at the center, maximum in the annular region and lower in the near wall region. As is the case with the axial rms velocity, the radial rms velocity also increases with an increase in the pulsation velocity. The value of the axial rms velocity for

the lab scale column is higher than that for pilot scale column because of the high values of *Af* in the lab scale column. A comparison of the non-dimensional radial rms velocities shows the values to have the same order of magnitude for the two scales. The main difference between the two cases stems from the difference in the location of rod at the center in the pilot scale column. For the case of Af = 1.7 cm/s, the radial velocities are comparable in the two cases.

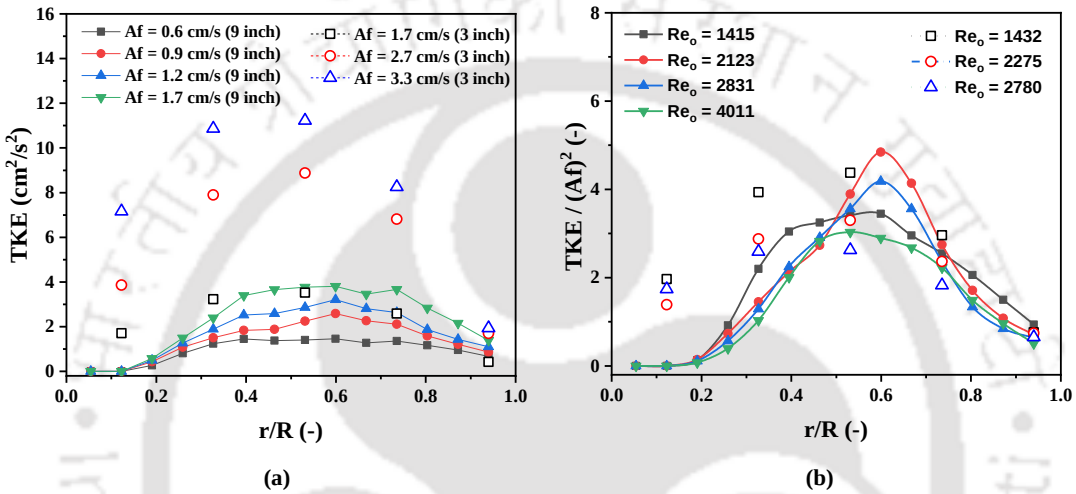

Figure 4.4: (a) Radial variation of turbulent kinetic energy with four different oscillatory Reynolds numbers for no flow condition in pilot scale PSPC (9 inch) and its comparison with the values for laboratory scale PSPC (3 inch) (b) Dimensionless TKE with its squared pulse velocity at similar condition

The turbulent kinetic energy (TKE) and dimensionless turbulent kinetic energy are shown in Figure. 4.4(a) and 4.4(b), respectively. It may be noted that the turbulent kinetic energy is half of the sum of the squares of axial, radial and azimuthal or tangential rms velocities. Therefore, they are expected to show the same trend as axial and radial rms velocities until the azimuthal velocities are significant or show a different trend. Though the azimuthal rms velocities are not reported separately, their values are observed to be same order as the radial rms velocity. As

with the rms velocities, the value of TKE is of the same order for Af = 1.7 cm/s for the two scales. The differences in the two are caused by the presence of the 38 mm rod (r/R ~0.1) at the center.

For non-depersonalization, TKE is scaled by the square of pulsation velocity. The profile of non-dimensional TKE for the lab scale column is sharp for the lowest oscillating Reynolds number and becomes flatter with an increase in the value of Re_O. However, the trend is slightly different for pilot scale column. The profile is flat for the lowest value of Re_O = 1415 and very sharp for Re_O = 2123. A further increase in Re_O results in the profile to become flatter. The same trend can also be observed in Figure 4.2(b) for axial rms velocity though it is observed prominently for TKE as it is square of rms velocities.

In summary, for the no flow case, that the velocity fluctuations on a radial line are typically parabolic with the maximum value in the annular region i.e. r/R ~0.6. The maximum value of axial rms velocity is between 1.5-2 times of the pulsation velocity whereas radial rms velocity is about 0.5-0.6 times of the pulsation velocity.

4.3.2 Effect of pulsation velocity at a constant aqueous phase flow rate

Next, experiments are performed in the continuous mode and water is pumped at a constant flow rate of from top to bottom as shown in Figure. 4.5. First the effect of pulsation velocities is studied at a constant flow rate of 360 LPH (average velocity of 0.29 cm/s) in the pilot scale column. The results in the lab scale column at a flow rate of 120 LPH (average velocity of 0.76 cm/s) are also plotted for comparison. In Figure 4.5 (a), axial rms velocity is plotted along the column radius for four different pulsation velocities in both the columns.

The mean downward velocity of the flowing liquid is 0.29 cm/s in the pilot scale column which is less than half of the smallest value of pulsation velocity of 0.6 cm/s. A net downward flow of water causes a reduction in the axial rms velocities in comparison with the no net flow case in both lab scale as well as pilot scale column. For the pulsation velocity of 1.7 cm/s, the axial rms velocity in the lab scale column is smaller than that in the pilot scale column. This difference is more than that observed in the net flow case. This is because of the difference in downward velocity in the two cases, the higher downward velocity of 0.76 cm/s in the lab scale column causes more reduction in the axial rms velocity as compared to 0.29 cm/s in the pilot scale column.

The axial rms velocity scaled by pulsation velocity is shown in Figure. 4.5(b). Unlike the no net flow case, the magnitude of scaled axial rms velocity is less in the lab scale column than in the pilot scale column. Again, this is because of the relatively higher downward flow in the lab scale column.

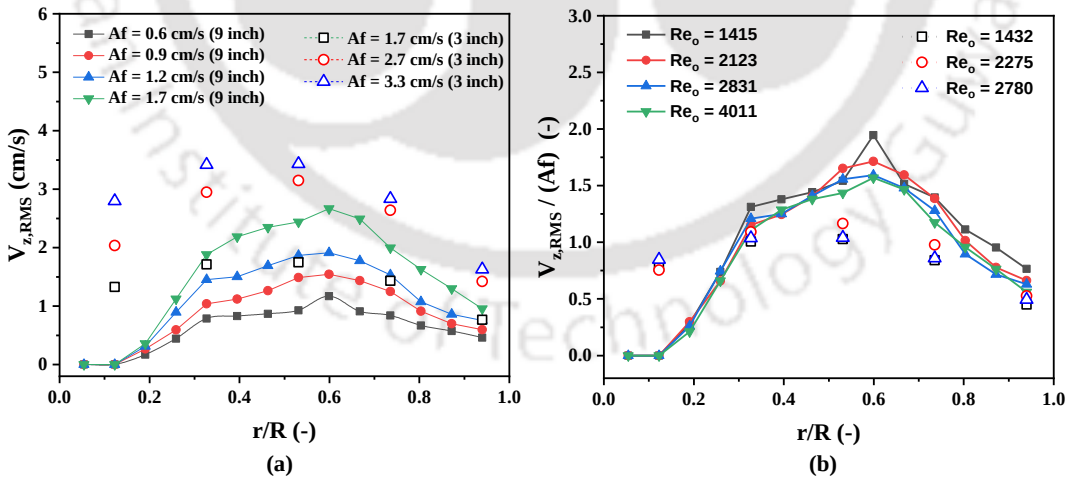

Figure 4.5: (a) Radial variation of axial component of velocity in aqueous phase with four different pulsation velocities for constant 120 LPH flow of aqueous phase in pilot scale PSPC (9 inch) and its comparison with laboratory scale pulsed sieve plate column (3 inch) (b)

Dimensionless velocity with its associated pulse velocity at similar condition (filled symbols for bigger scale and non-filled symbols for smaller scale column)

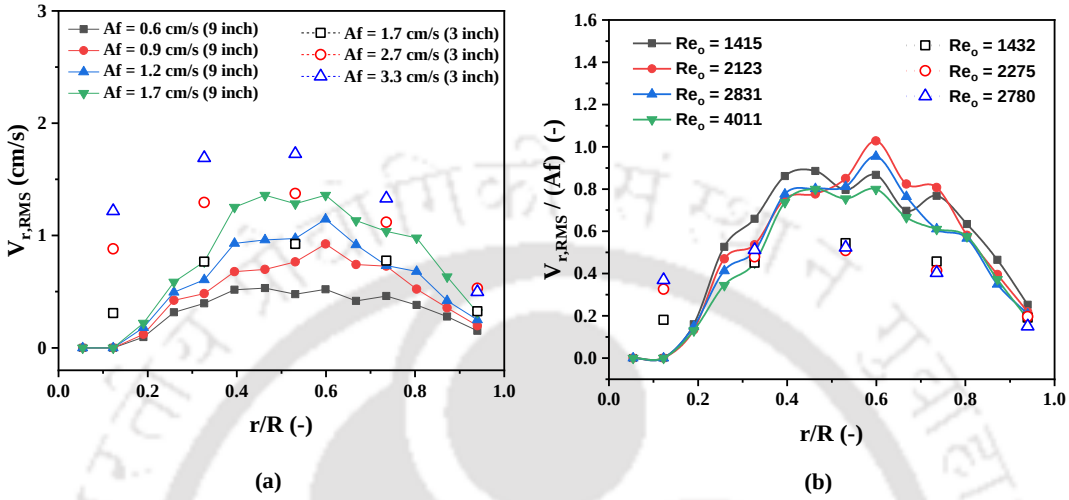

Figure 4.6: (a) Radial variation of radial component of velocity in aqueous phase with four different pulsation velocities for constant 120 LPH flow of aqueous phase and its comparison with laboratory scale pulsed sieve plate column (b) Dimensionless velocity with its associated pulse velocity at similar condition (filled symbols for bigger scale and non-filled symbols for smaller scale column)

Figure 4.6 (a) shows the radial variation of the radial rms velocity for four different pulsation velocities in the pilot scale as well as lab scale column for the conditions shown in Figure 4.5. As observed for the no net flow case, the value of radial rms velocity is significantly less than the axial rms velocity in case of flow also. The value of radial rms velocity for net flow case is more than that in case of no net flow in both the columns for all the pulsation velocities. This suggests that the downward flow causes an increase in the radial rms velocities whereas a decrease in the axial rms velocity. Figure 4.6 (b) shows scaled radial rms velocities.

Interestingly, the scaled rms velocities in the lab scale column overlap for all three pulsation velocities. However, the profiles differ in the pilot scale column.

Figure 4.7(a) shows the variation of turbulent kinetic energy (TKE) along the radius in both the columns at a constant flow rate. In both the columns, turbulent kinetic energy is higher at higher pulsation velocity. As can be guessed from the relative magnitude of axial and radial rms velocities and effect of flow on them, TKE is lower in the flow case than the no net flow case [22]. The scaled TKE is lower in the lab scale column than that in the pilot scale column. Profile of scaled TKE is relatively flat in lab scale column when compared with that in the pilot scale column.

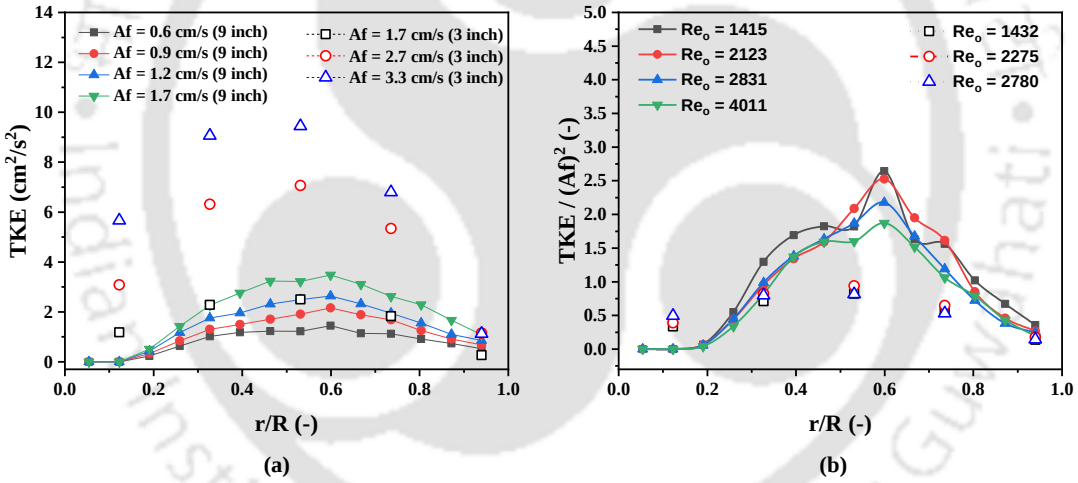

Figure 4.7: (a) Radial variation of turbulent kinetic energy of aqueous phase with four different pulsation velocities for constant 120 LPH flow of aqueous phase and its comparison with laboratory scale pulsed sieve plate column (b) Dimensionless velocity with its pulse velocity at similar condition (filled symbols for bigger scale and non-filled symbols for smaller scale column)

4.3.3 Effect of flow rate at constant pulsation velocity

Further, the effect of flow rate at a constant pulsating velocity on the velocity profile is studied. As the flow rate increases, net downward motion of water increases. Therefore, an increase in the flow rate is expected to cause a decrease in the axial rms velocity. Thus, the oscillatory Reynolds number is different in the two cases. In the pilot scale column, experiments are performed at four different flow rates of 210, 300, 360 and 480 LPH. The corresponding mean fluid velocities in the column are 1.7, 2.4, 2.9 and 3.9 cm/s.

Figure 4.8 (a) shows the radial variation of axial rms velocity for four different flow rates in pilot scale as well as lab scale PSPC. As the flow rate is increased axial fluctuations are attenuated in the lab scale as well as pilot scale column. The pulsation velocity for pilot scale column is 1.2 cm/s whereas for the lab scale column, pulsating velocity is 2.7 cm/s and the flow rates in the lab scale column are lower compared to that in pilot scale column. As a result, the axial rms velocity is high in the lab scale column. Figure 4.8(b) shows the non-dimensional axial rms velocities. The values of flow Reynolds number are similar in both the column for the four cases. However, the oscillatory Reynolds number is higher in the lab scale column (2275) when compared with that in the pilot scale column (2831). Consequently, the non-dimensional axial rms velocity is higher in the pilot scale column for all the flow rates.

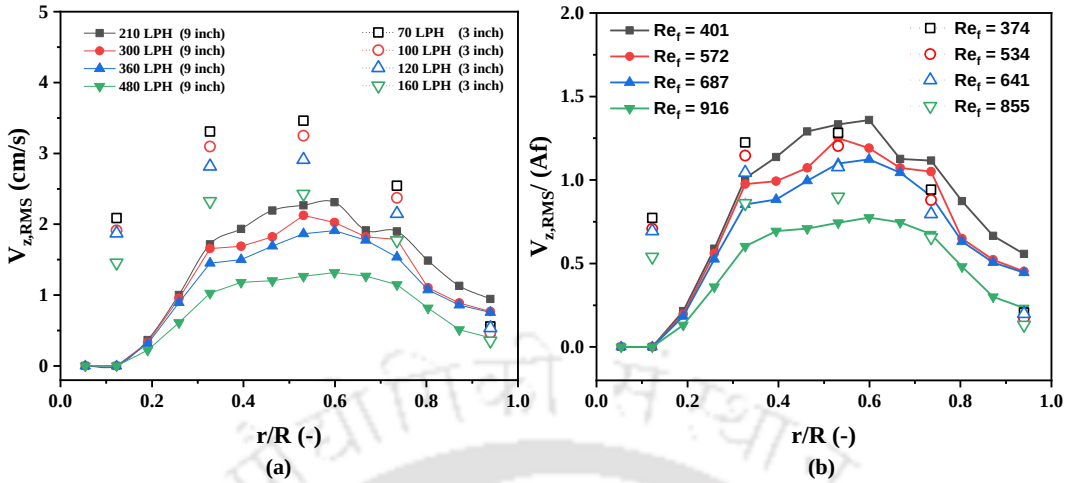

Figure 4.8: (a) Radial variation of axial component of velocity in aqueous phase with four different flowrates of aqueous phase in pilot scale PSPC (9 inch) and its comparison with laboratory scale pulsed sieve plate column (3 inch) (b) Non dimensional velocity with its pulsation velocity for same condition (filled symbols for bigger scale and non-filled symbols for smaller scale column)

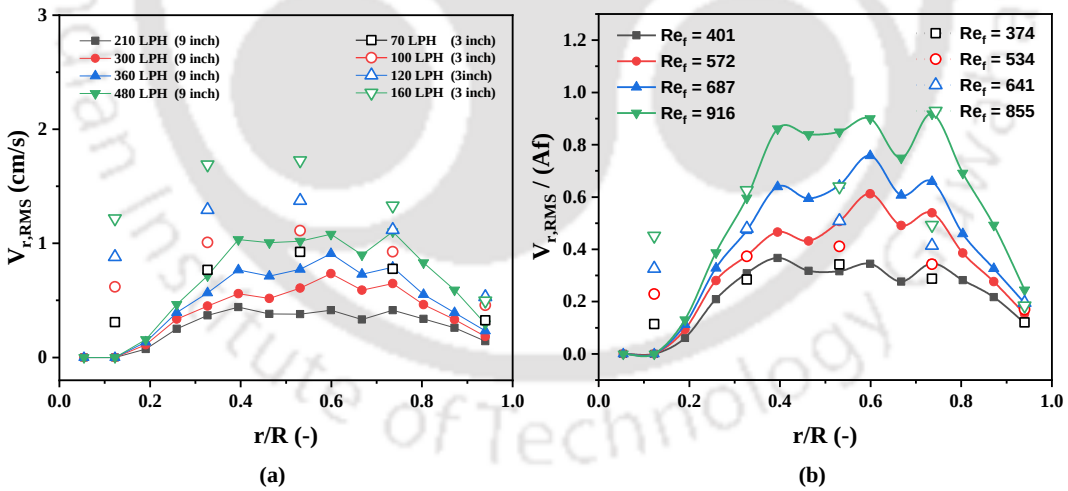

Figure 4.9: (a) Radial variation of radial component of velocity in aqueous phase with four different flowrates of aqueous phase in pilot scale PSPC (9 inch) and its comparison with laboratory scale pulsed sieve plate column (3 inch) (b) Non dimensional velocity with its

pulsation velocity at similar condition (filled symbols for bigger scale and non-filled symbols for smaller scale column)

Figure 4.9 (a) and 4.9(b) show the radial variation of the actual and dimensionless radial rms velocity, respectively, at a constant pulsation velocity of 1.2 cm/s for four different flow rates in pilot scale PSPC and its comparison with the lab scale PSPC at a pulsation velocity of 2.7 cm/s. With an increase in the flow rate, the value of radial rms velocity increases in both the pilot and lab scale columns. This trend is opposite to that for the axial fluctuations.

The non-dimenional radial velocities are very close to each other in the lab scale column. In the pilot scale column, there is small variation in the dimensionless radial fluctuations with change in flow rate but there is no clear trend. This is possibly because of the high oscillatory Reynolds number in the pilot scale column.

Figure 4.10 (a) shows the radial variation of turbulent kinetic energy in aqueous phase with at constant pulsation velocity of 2.7 cm/s for four different flow rates of aqueous phase in pilot scale PSPC (9 inch) and its comparison with laboratory scale pulsed sieve plate column (3 inch).

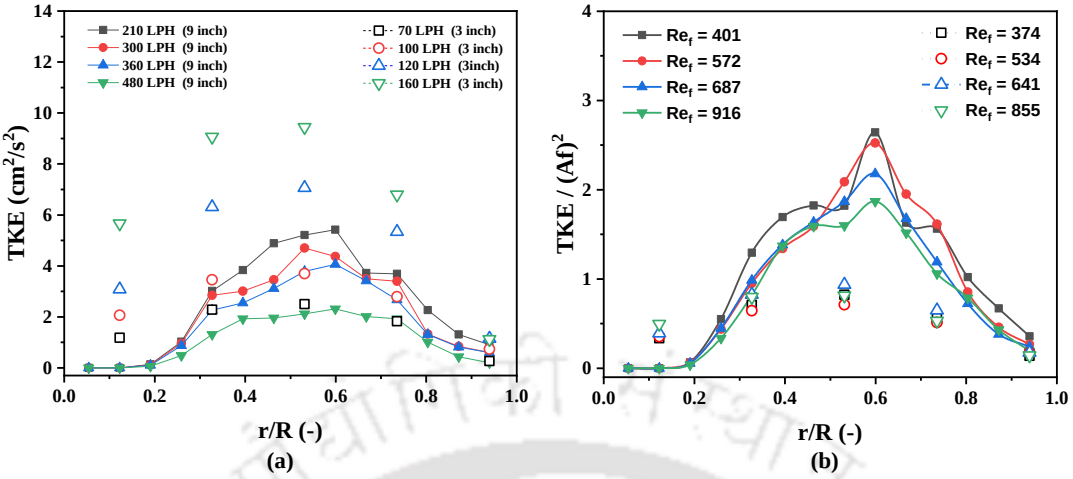

Figure 4.10: (a) Radial variation of turbulent kinetic energy of aqueous phase with four different flowrates of aqueous phase in pilot scale PSPC (9 inch) and its comparison with laboratory scale pulsed sieve plate column (3 inch) (b) Dimensionless TKE with its squared pulsation velocity for similar condition (filled symbols for bigger scale and non-filled symbols for smaller scale column)

Figure 4.10 (b) shows the dimensionless radial variation of turbulent kinetic energy divided by squared pulsation velocity in aqueous phase with four different pulsation velocities for constant pulsation velocity of 2.7 cm/s at different flow of aqueous phase in pilot scale PSPC (9 inch) and its comparison with laboratory scale pulsed sieve plate column (3 inch). In pilot scale at Re= 374 and Re= 534, the values are enhanced because the denominator of these two conditions are less than one and they are squared. The turbulent kinetic energy values are matched for the higher Reynolds numbers Re= 916 (Small column) and Re =854 (Big column).

4.4 Conclusions

The fluctuations in the velocity are measured in a pilot scale pulsed sieve plate column using radioactive particle tracking for three cases: no net flow, constant flow rate and constant pulsation velocity. The effect of pulsation velocity and flow rate on the velocity profile is measured. The results are compared with those for lab scale column for the corresponding flow conditions. For no flow case, the pulsation velocity is observed to an appropriate scaling factor and the dimensionless velocity profiles in the lab scale and pilot scale columns are observed to be same except in the central region of the column where the geometry of the two columns differ. For the no net flow case, the maximum axial fluctuations are typically between 1.5-2 times of the pulsation velocity whereas the maximum radial fluctuations are 0.5-0.6 times of the pulsation velocity. The downward flow of water suppresses the axial fluctuations but enhances the fluctuations in the radial velocity and the effect increases with an increase in the flow rate.

Reference

Angelov, G.; Gourdon, C., 2009, "Turbulent flow in pulsed extraction columns with internals of discs and rings: Turbulent kinetic energy and its dissipation rate during the pulsation". *Chem. Eng. Process. Intensif.* 48, 592–599. https://doi.org/10.1016/j.cep.2008.07.002.

Ahmed, S.M.R., Phan, A.N., Harvey, A.P., 2019, "Scale-Up of Gas-Liquid Mass Transfer in Oscillatory Multiorifice Baffled Reactors (OMBR's)". *Ind. Eng. Chem. Res.* 58, 5929−5935. https://doi.org/10.1021/acs.iecr.8b04883.

Ardestani, F., Ghaemi, A.; Safdari, J., Hemmati, A. 2021, "Progress in Nuclear Energy Modeling of mass transfer coefficient using response surface methodology in a horizontal-vertical pulsed sieve-plate extraction column". *Prog. Nucl. Energy*. 139, 103885. https://doi.org/10.1016/j.pnucene.2021.103885.

Avila, M., Kawas, B., Frederick, D., Poux, M., Xuereb, C., Aubin, J. 2022, "Performance characterization and applications of continuous oscillatory baffled reactors". *Chem. Eng. Process. Intensif.* 180, 108718. https://doi.org/10.1016/j.cep.2021.108718.

Calero, M.; Ronda, A.; Pérez, A.; Yáñez, A.; Carmen, M.; Ronda, A. The scale-up of Cr 3 + biosorption onto olive stone in a fixed bed column. Desalin. Water Treat. 2016, 57, 25140-25152. https://doi.org/10.1080/19443994.2016.1150209.

Caishan. J.; Shuai. M.; Qiong. S. Mass transfer characteristics in a standard pulsed sieve-plate extraction column, *Energy Procedia.* 2013, 39, 348–357. https://doi.org/10.1016/j.egypro.2013.07.222.

Dudukovic, M. P.,2000, "Opaque Multiphase Reactors: Experimentation, Modeling and Troubleshooting", *Oil Gas Sci. Technol.* 55, 135–158. https://doi.org/10.2516/ogst:2000008.

Jain, V., Kalo, L., Kumar, D., Pant, H. J., Upadhyay, R. K., 2017, "Experimental and numerical investigation of liquid–solid binary fluidized beds: Radioactive particle tracking technique and dense discrete phase model simulations", *Particuology.* 33, 112–122. https://doi.org/10.1016/j.partic.2016.07.011.

Juela, D., Vera, M.; Cruzat, C., Astudillo, A., Vanegas, E., 2022. "A case of antibiotic removal on natural adsorbent". *Process. Saf. Environ. Prot.* 2022, 159, 953–963. https://doi.org/10.1016/j.psep.2022.01.046.

Kalaga, D. V., Pant, H. J., Dalvi, S. V., Joshi, J. B., & Roy, S., 2017, "Investigation of hydrodynamics in bubble column with internals using radioactive particle tracking (RPT)". AIChE Journal. 63(11), 4881–4894. https://doi:10.1002/aic.15829.

Kolhe, N. S., Mirage, Y. H., Patwardhan, A.W., V.K. Rathod, V. K., Pandey, N. K., Mudali, U.K., Natarajan, R., 2011, "CFD and experimental studies of single phase axial dispersion coefficient in pulsed sieve plate column". *Chem. Eng. Res. Des.* 89, 1909–1918. https://doi.org/10.1016/j.cherd.2011.01.020.

Larachi, F., G. Kennedy, G., Chaouki, J., 1994, "A γ-ray detection system for 3-D particle tracking in multiphase reactors", *Nucl. Inst. Methods Phys. Res. A.* 338, 568–576. https://doi.org/10.1016/0168-9002(94)91343-9.

Law, R., Ahmed, S.M.R., Tang, N.; Phan, A.N., Harvey, A.P., 2018, "Process Intensification Development of a more robust correlation for predicting heat transfer performance in oscillatory baffled reactors". *Chem. Eng. Process. Process Intensif.* 125, 133–138. https://doi.org/10.1016/j.cep.2018.01.016.

Mcdonough, J.R., Phan, A.N., Harvey, A.P., 2015, "Rapid process development using oscillatory baffled microreactors". Chem. Eng. J. 265, 110–121. https://doi.org/10.1016/j.cej.2014.10.113.

Sen, N., Singh, K. K, Patwardhan, A. W., Mukhopadhyay, S., Shenoy, K. T., 2020, "Computational Fluid Dynamics Modelling to Predict Axial Dispersion in Pulsatile Liquid-liquid Two phase Flow in Pulsed Sieve Plate Columns". *Solvent Extr. Ion Exch.* 1–25. https://doi.org/10.1080/07366299.2020.1840030.

Sarkar, S., Singh, K.K., Shenoy, K.T., 2017, CFD simulations of single-phase flow in pulsed disc and doughnut columns: Axial dispersion and pressure drop. Sep. Sci. Technol. 52, 2861–2875. https://doi.org/10.1080/01496395.2017.1375952.

Saremi, M., Torkaman, R., Safdari, J., Gharib, A., Asadollahzadeh, M., 2021, "A novel model for mass transfer evaluation in horizontal pulsed column by coupling the effects of dispersed phase non-uniformity and continuous phase back mixing". *Int. Commun. Heat Mass Transf.* 122, 105145. https://doi.org/10.1016/j.icheatmasstransfer.2021.105145.

Smith, K.B., Mackley, M.R., 2006, "An experimental investigation into the scale-up of oscillatory flow mixing in baffled tubes". *Chem. Eng. Res. Des.* 84, 1001–1011. https://doi.org/10.1205/cherd.05054.

Somkuwar, N., Kolhe, N., Rathod, V., 2014, "Hydrodynamics of a Pulsed Sieve Plate Extraction". Column, *Indian Chem. Eng.* 56,235–257. https://doi.org/10.1080/00194506.2014.910707.

Roy, S., Larachi, F., Al-Dahhan, M. H., Dudukovic, M. P., 2002, "Optimal design of radioactive particle tracking experiments for flow mapping in opaque multiphase reactors", *Appl. Radiat. Isot.* 56, 485–503. https://doi.org/10.1016/S0969-8043(01)00142-7.

Tang, X., Chen, F., Luo, G., Wang, J., 2009, "Estimation of axial dispersion in pulsed-plate extraction columns". *Chem. Eng. Res. Des.* 87, 1562–1566. https://doi.org/10.1016/j.cherd.2009.04.001.

Tribedi, T., Pillajetti, P., Kumari, R.; Pant, H.J., Tiwari, P., Upadhyay, R.K., 2022, "Measurements of Solid Velocity in a Pilot-Scale Geldart's Group B Circulating Fluidized Bed Using a Radioactive Particle Tracking Technique". *Ind. Eng. Chem. Res.* 61, 9110–9121. https://doi.org/10.1021/acs.iecr.2c01119.

Upadhyay, R. K., Pant, H. J., Roy, S.,2013. "Liquid flow patterns in rectangular air-water bubble column investigated with Radioactive Particle Tracking", *Chem. Eng. Sci.* 96, 152–164. https://doi.org/10.1016/j.ces.2013.03.045.

Yadav, R. L., Patwardhan, A. W., 2008, "Design aspects of pulsed sieve plate columns. *Chem. Eng. J.* 138,389–415. https://doi.org/10.1016/j.cej.2007.06.015.

CHAPTER-5

Two Phase Investigation in Laboratory Scale Pulsed Sieve and Slotted Columns

Chapter 5 : Two Phase Investigation in Laboratory Scale Pulsed Sieve and Slotted Columns

Graphical abstract

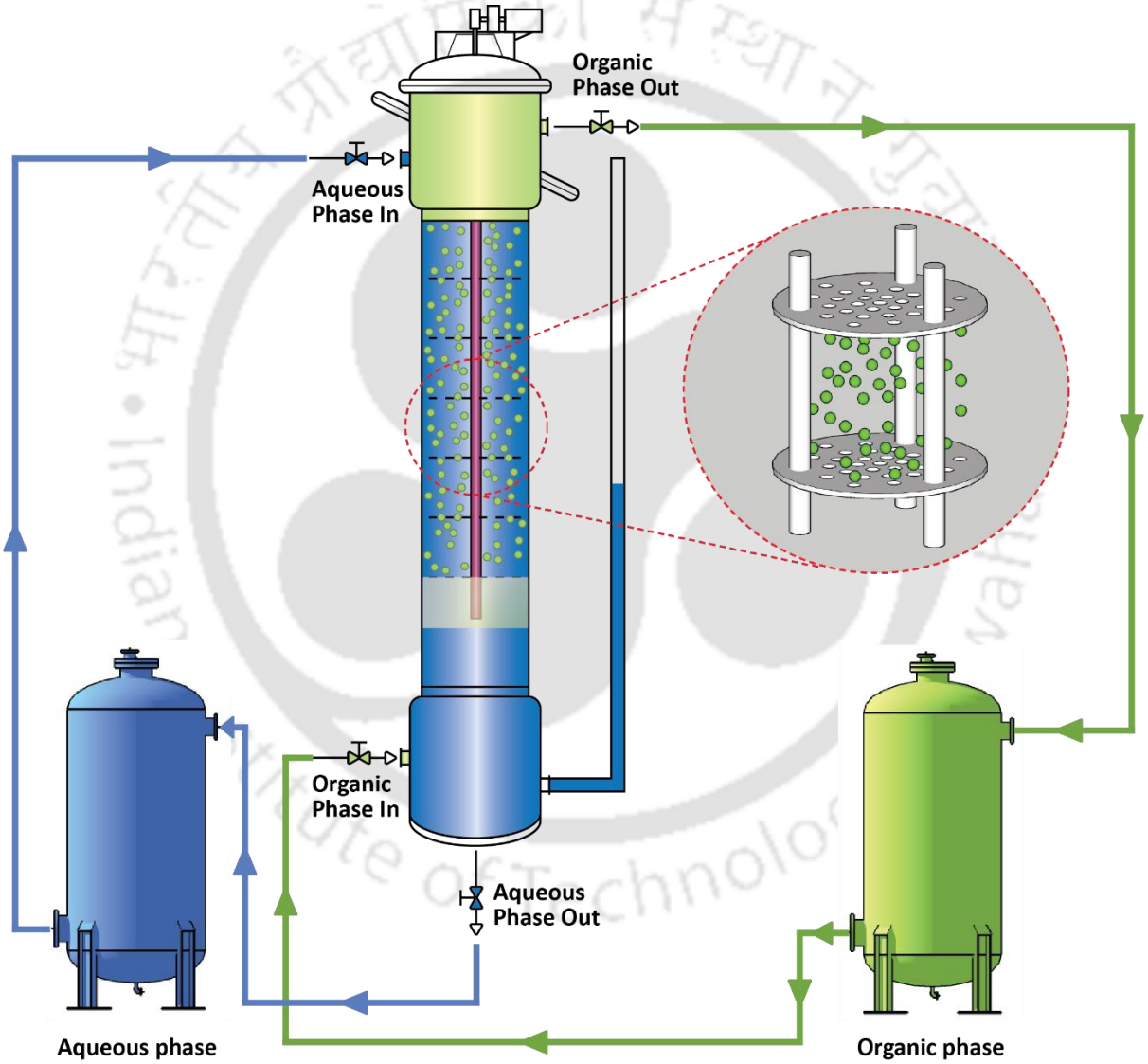

Abstract

Organic flow rate at constant pulsation velocity in absence of flow is studied. Secondly the effect of organic flow at constant pulsation velocity in presence of constant water phase flow is examined. Finally, the effect of pulsation velocity at constant organic and aqueous flow conditions is experimented and the results are discussed. These modes are studied for two different plates namely sieve plate and slotted plate of 17% FFA as discussed in previous chapter 3. Corresponding turbulence parameters are postprocessed using the RPT methodology explained in chapter 2.

5.1 Experimental procedure

The procedure for controlling and stabilizing chemical engineering equipment that utilizes multiphase flow involves progressive steps. First, the column is filled with an aqueous phase in batch mode with specific geometric parameters, such as a 3mm sieve plate hole diameter, 17% FFA, 10 cm plate spacing, and uniform triangular pitch opening distribution. Pulsation velocities are gradually increased and the column is stabilized at a constant velocity. The aqueous pump is then switched on and the column is brought to a steady state. Finally, the secondary dodecane phase is added with a constant flow rate, which has the potential to cause flooding. Proper tuning and stabilization of the separation requires a lot of effort, and the right pulsation velocity is crucial for optimal separation. The knowledge of water velocity fluctuations is crucial during this process, and our previous report focused on the no flow condition to help the operator, assess the ease of control during the steady state establishment with varying pulsation velocities.

This section describes the experimental setup used in the study, which includes an active column section, top and bottom disengagement sections, pulse leg, three-way valve, timer, air compressor, pumps, rotameter, and storage tank. The aqueous phase is fed from the top of the column through a centrifugal pump, and the flow rate is controlled using a rotameter. The active PSPC has an inner diameter of 0.075 m and a height of 0.7 m, with a cartridge consisting of 8 sieve plates (0.0032m sieve holes and 17% open area) used as an internal. A 3-way valve is used to induce pulsation in the column, and the pulsation amplitude and velocity can be controlled and the schematic is shown in Figure 5.1.

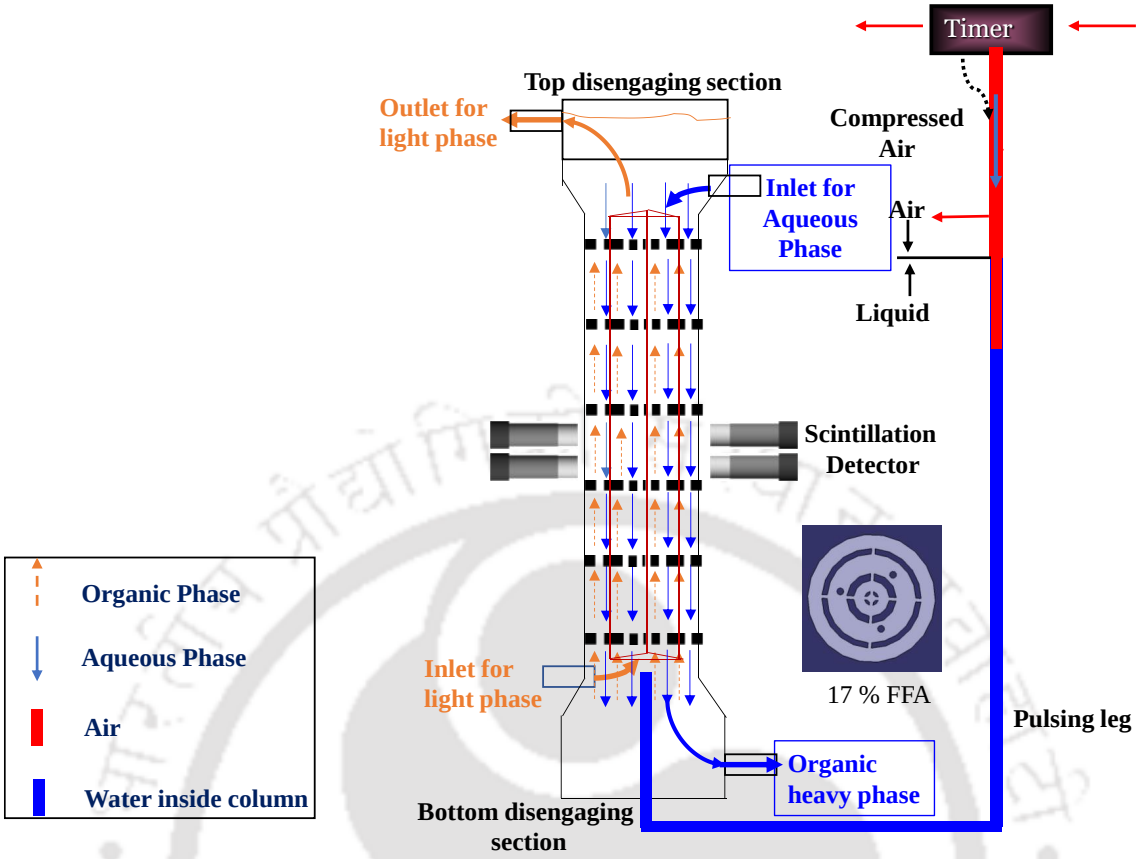

Figure 5.1 Schematic of Experimental setup

Two different plate structures are used for the current manuscript and the schematic is shown in Figure 5.2. Three regions are marked and the investigations are reported in these flow areas.

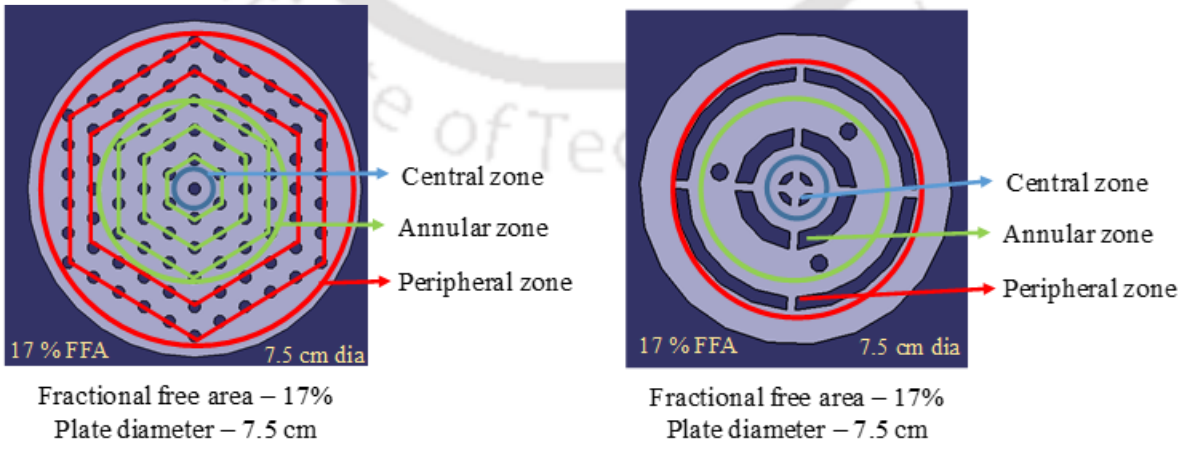

Figure 5.2 Schematic of a) sieve plate and b) slotted plate

Radioactive particle tracking follows a three-step process. The first step is called calibration, where the radioactive source is calibrated with reference to the positioning of detectors. Resolution and sensitivity studies are performed to optimize the detectors' plane, distance from the wall, and orientation. Since different detectors can have different effective distances for the same count, the next plane of detectors will address this issue. Since it is not possible to manually keep the particle at all positions inside the column, the count is generated using optimized parameters such as source strength, wall attenuation, and the dead time of individual detectors. This step is referred to as count generation and optimization, which serves as a look-up table of position versus count data with a ensured reference system. Next, the particle is made neutrally buoyant, which is challenging in the liquid system implementation. The column is operated using this neutrally buoyant tracer. The stokes number of the solid tracer is 0.14 and it followed the flow faithfully. The experiments are performed and the particle position is reconstructed. Finally, Lagrange track velocity is assessed from the postprocessing step of radioactive particle tracking (RPT). As mentioned above the stages of the pulse operation in context of multiphase are detailed in the **Error! Reference source not found.**.

5.2 Results and discussions

5.2.1 With sieve plate as internal

Experiments are carried out for different pulsation velocities as mentioned in Table 5.1.

Table 5.1: Operating conditions

Plate Type	Pulse velocity (Af) (cm/s)	Aqueous flow (LPH)	Organic Flow (LPH)
17% Sieve	2.7	60	70
	3.3	0	50,70,90,110
		70	20,40,50,90
		60	70
	3.8	60	70
	4.4	60	70
17% Slotted	2.7	60	70
	3.3	0	50,70,90,110
		70	20,40,50,90
		60	70
	3.8	60	70
	4.4	60	70

Experiments are performed under three flow conditions: no flow of each phase, flow of one phase only and other phase stationary, both phases flowing. In each case both phases are present in the column. The velocity measurements are done for the continuous (aqueous) phase. The results are compared with those for single phase only case. The experiments have been performed for two different internals: sieve plate and slotted plate.

5.2.1.1 Effect of organic flow rate at constant pulsation velocity in absence of aqueous flow

Initially aqueous flow is turned off and 17 percent sieve plate is used as a internal. The effect of organic phase flow rate is examined at a constant pulsation velocity of 3.3 cm/s and the results are compared with no flow condition. Figure 5.3 (a) shows the variation of axial RMS velocity in aqueous phase along the radius for no flow condition and four different flow rates 50,70,90 and 110 LPH of organic phase. Figure 5.3 (b) shows the radial RMS velocity for the same conditions. Figure 5.3 (c) shows the turbulent kinetic energy for all the cases.

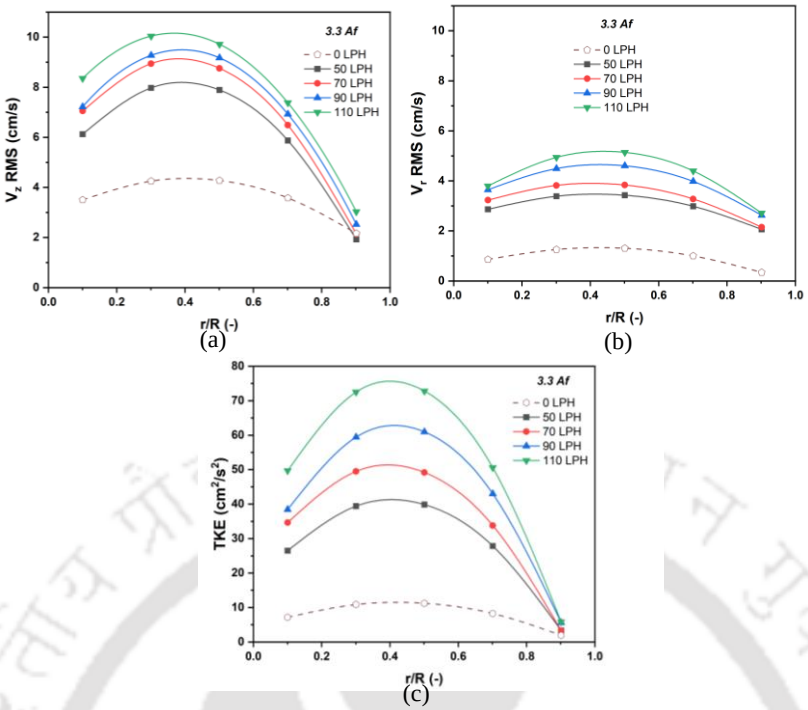

Figure 5.3 Radial variation of a) axial component of velocity b) radial component of velocity c) turbulent kinetic energy in aqueous phase at a constant pulsation velocity of 3.3 cm/s for no flow of aqueous phase

It has been observed that the axial root-mean-square velocity is almost twice as high as the radial fluctuation field. Additionally, the presence of two-phase flow has increased the fluctuations by a factor of three compared to the no-flow condition. Furthermore, there is a greater velocity gradient in the axial direction than in the radial direction for the fluctuation field. The annular zone exhibits the highest level of turbulent kinetic energy for the 17 percent sieve plate, and its enhancement rate is observed to be approximately 1.4 times higher in the annular zone with an increase in organic flow rate.

5.2.1.2 Effect of organic flow at constant pulsation velocity in presence of constant aqueous flow rate

The column is subjected to a constant aqueous flow rate, and the variation of the organic phase flow rate is analysed. Examined results at this condition are shown in Figure 5.4.

.

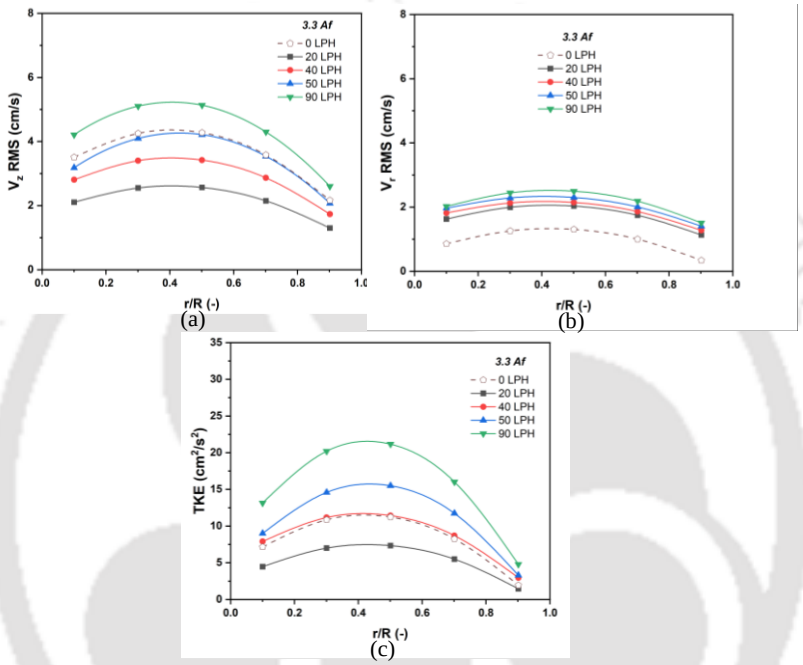

Figure 5.4 Radial variation of a) axial component of velocity b) radial component of velocity c) turbulent kinetic energy at constant pulsation velocity of 3.3 cm/s and at a constant aqueous flow rate of 70 LPH for five different flowrates of organic flow

Figure 5.4 (a) shows the variation of axial RMS velocity in aqueous phase along the radius for 120 LPH flow condition of aqueous phase and four different flow rates 20,40,50 and 90 LPH of organic phase at a constant pulsation velocity of 3.3 cm/s.

Figure 5.4 (b) shows the radial RMS velocity for the same conditions.

Throughout the pulsation cycle between two sieve plates, the absence of downward aqueous flow results in heightened turbulence for the liquid streams, where the stream velocity is amplified by pulsation, and the organic flow mitigates the pulsation in an upward direction. Upon the introduction of the aqueous phase, local turbulence near the sieves intensifies, indicating maldistribution. However, in the central zones, the liquid streams experience a nullifying effect from multiple forces, preventing excessive flow from one cell zone to another. As a result, the overall turbulence decreases when considering the central zone between the two plates.

Figure 5.4 (c) shows the turbulent kinetic energy for all the cases. The axial fluctuations are suppressed by the continuous pumping of the aqueous phase velocity, whereas the radial fluctuations are increased as the flow rate of the organic phase increases. The qualitative pattern of the fluctuations remains consistent, with the highest fluctuations occurring in the annular zone. At a constant aqueous flow rate of 70 LPH, the 90 LPH organic flow condition exhibits the most significant fluctuations, which are significantly higher than the no-flow condition. Finally, the column is examined with the variation of pulsation velocities at constant flow rates of aqueous and organic flow rates.

5.2.1.3 Effect of pulsation velocity at constant organic and aqueous flow conditions:

Subsequently, the variation of pulsation velocity is observed at constant pumping rates of organic and aqueous flow rates. The observations are shown in Figure 5.5. Figure 5.5 (a) shows the variation of axial RMS velocity in aqueous phase along the radius for 70 LPH flow

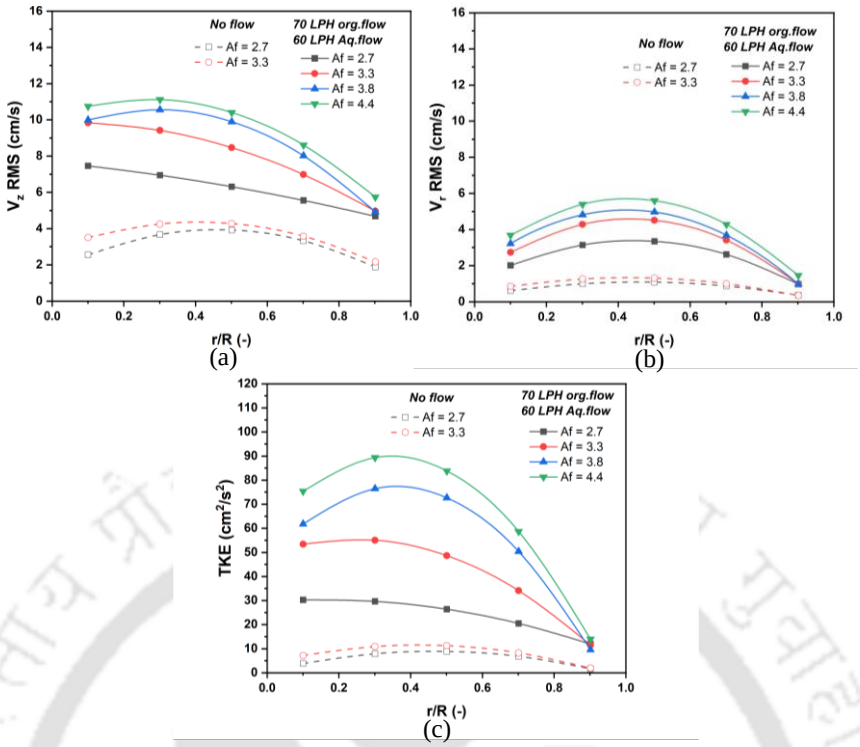

Figure 5.5 Radial variation of a) axial component of velocity b) radial component of velocity c) turbulent kinetic energy at constant aqueous flow rate of 60 LPH and a constant organic flow rate of 70 LPH for four different pulsation velocities

condition of organic phase and 60 LPH of aqueous phase with four different pulsation velocities of 2.7,3.3,3.8,4.4 cm/s. Figure 5.5 (b) shows the radial RMS velocity for the same conditions. Figure 5.5 (c) shows the turbulent kinetic energy for all the cases.

The organic flow rate was set slightly higher than the aqueous flow rate to prevent drop coalescence by ensuring a minimum pulsation velocity above 3.3 cm/s. The results showed that the fluid streams experienced the highest fluctuations at this condition, and as pulsation velocity increased, the fluctuations were enhanced both axially and radially. The column experienced significant fluctuations, resulting in an increase in TKE. After investigating the column with all the operating conditions, the investigations are focussed towards the geometric effect by

changing the internal, keeping same percent of opening area. This structure is called slotted plate and is shown is Figure 5.2. The experiments are repeated by changing the internals and investigation details are mentioned below.

5.2.2 With slotted plate as internal

5.2.2.1 Effect of organic flow rate at constant pulsation velocity in absence of aqueous flow

The effect of organic phase is investigated in absence of pumping of aqueous phase and the results are compared in reference to sieve plate. Figure 5.6 (a) shows the variation of axial RMS velocity in aqueous phase along the radius for 70 LPH flow condition of organic phase and 60 LPH of aqueous phase with four different pulsation velocities of 2.7,3.3,3.8,4.4 cm/s. Figure 5.6 (b) shows the radial RMS velocity for the same conditions. Figure 5.6 (c) shows the turbulent kinetic energy for all the cases. The axial RMS values are found to be 1.5 times less for slotted plate whereas radial RMS values of the slotted plate are found to be slightly high than the flow field fluctuations of the sieve plate. Turbulent Kinetic energy increased with increase in pumping rate of organic flow. The organic flow is lighter and during the upstroke the relative velocity is additive and the time averaged fluctuations are increased significantly.

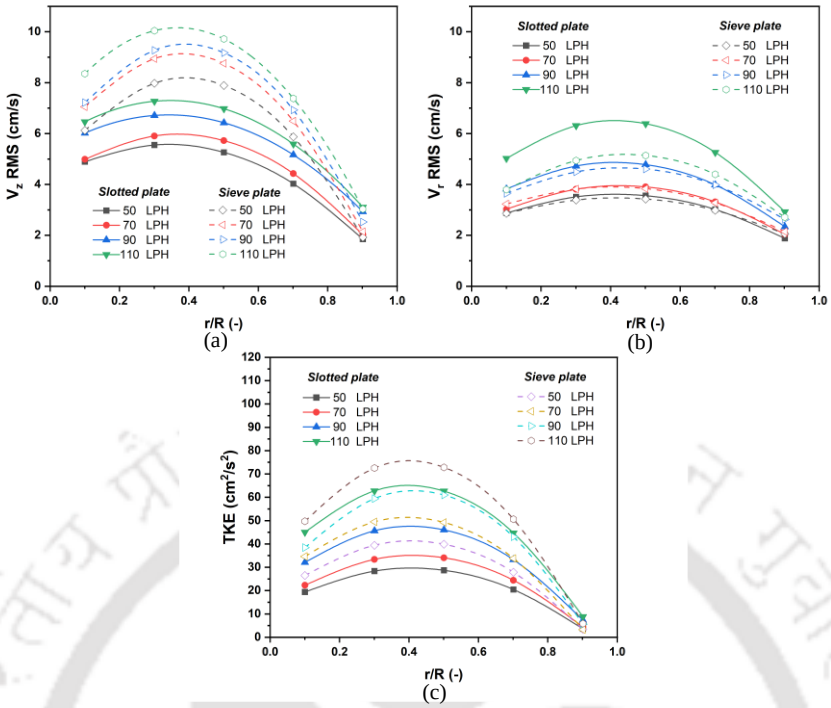

Figure 5.6 Radial variation of a) axial component of velocity b) radial component of velocity c) turbulent kinetic energy in aqueous phase at constant pulsation velocity of 3.3 cm/s for no flow of aqueous phase

The subsequent phase involves the introduction of a constant pumping rate for aqueous flow.

5.2.2.2 Effect of organic flow at constant pulsation velocity in presence of constant aqueous flow rate

Figure 5.7 (a) shows the variation of axial RMS velocity in aqueous phase along the radius for 120 LPH flow condition of aqueous phase and four different flow rates 20,40,50 and 90 LPH of organic phase at a constant pulsation velocity of 3.3 cm/s. Figure 5.7 (b) shows the radial RMS velocity for the same conditions. Figure 5.7 (c) shows the turbulent kinetic energy for all the cases. The qualitative analysis reveals that the annular region experiences the most significant fluctuations. As the organic flow increases, these fluctuations become more

pronounced but are still lower than the values observed when the aqueous flow pumping rate is not activated.

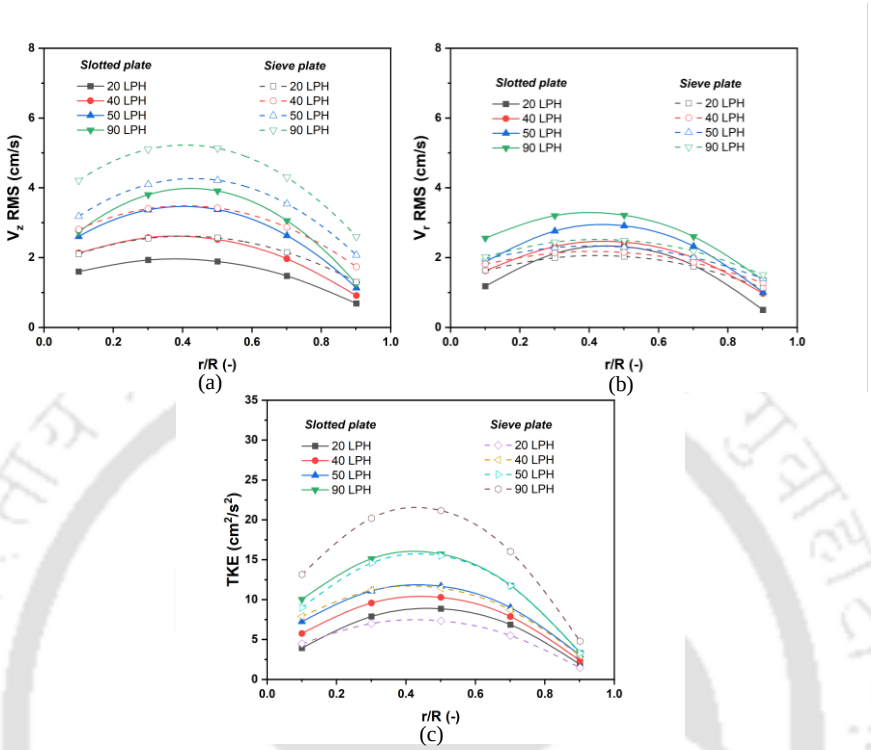

Figure 5.7 Radial variation of a) axial component of velocity b) radial component of velocity c) turbulent kinetic energy at constant pulsation velocity of 3.3 cm/s and a constant aqueous flow rate of 70 LPH for four different flowrates of organic flow

The effects of pulsation velocity at constant organic and aqueous flow rates are examined and are depicted in Figure 5.8. Figure 5.8 (a) shows the variation of axial RMS velocity in aqueous phase along the radius for 70 LPH flow condition of organic phase and 60 LPH of aqueous phase with four different pulsation velocities of 2.7,3.3,3.8,4.4 cm/s. Figure 5.8 (b) shows the radial RMS velocity for the same conditions. Figure 5.8 (c) shows the turbulent kinetic energy for all the cases. At all the conditions of operation, the axial fluctuations of the slotted plate are low compared to sieve plates in all the zones namely central, annular and peripheral zones.

Organic phase flows upward and this helps the upstroke and aqueous phase flow downwards and it aids the downward fluctuations

5.2.2.3 Effect of pulsation velocity at constant organic and aqueous flow conditions

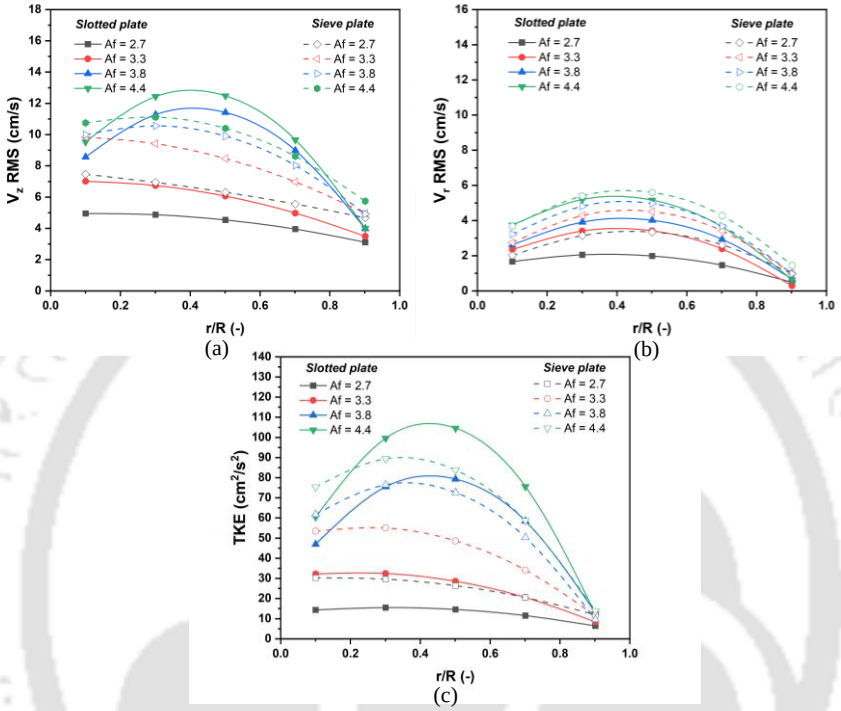

Figure 5.8 Radial variation of a) axial component of velocity b) radial component of velocity c) turbulent kinetic energy at a constant aqueous flow rate of 60 LPH and a constant organic flow rate of 70 LPH for four different pulsation velocities

5.3 Conclusions

Slotted plate showed better performance in radial direction, while the sieve plate showed better performance in axial direction at all the conditions of PSPC operation. With the introduction of aqueous flow, the fluctuations are dampened in axial direction but are amplified in radial direction. With the introduction of organic phase pumping rate, the fluctuations are enhanced

both in axial and radial directions. Fluctuations are highest in annular regions for all the conditions because of the presence of higher opening area in annular zone for sieve plate as well as slotted plate. At a constant aqueous flow rate of 60 LPH and a constant organic flow rate of 70 LPH as the pulsation velocities are increased the fluctuations inside the column are found to be highest and as pulsation velocity increased from 3.3 cm/s to 3.8 cm/s there is a significant rise in fluctuations. This may lead to regime transition from visual observations.

Reference

Amani, P., Safdari, J., Gharib, A., Badakhshan, H., Mallah, M.H. "Mass transfer studies in a horizontal pulsed sieve-plate column for uranium extraction by tri-n-octylamine using axial dispersion model". *Prog. Nucl. Energy.* 2017, 98, 71–84. https://doi.org/10.1016/j.pnucene.2017.02.010

Atallah, R.H.; Ruzicka, J.; Christian, G.D., 1987, "Continuous Solvent Extraction in a Closed-Loop System 2909–2914.

Berger, R.; Walter, K.; 1985. "Flooding in pulsed sieve plate extractors". *Chem. Eng. Sci*. 40, 2175–2184. https://doi.org/10.1016/0009-2509(85)85119-8

Brockkotter, J., Cielanga, M., Weber, B., Jupke, A., 2020, "Prediction and Characterization of Flooding in Pulsed Sieve Plate Extraction Columns Using Data-Driven Models". *Ind. Eng. Chem. Res.* 59, 19726–19735. https://doi.org/10.1021/acs.iecr.0c03282

Bujalski, J. M., Yang, W., Nikolov, J., Solnordal, C. B., Schwarz, M. P., 2006, "Measurement and CFD simulation of single-phase flow in solvent extraction pulsed column, *Chem. Eng. Sci.* 61, 2930–2938. https://doi.org/10.1016/j.ces.2005.10.057.

Caishan. J., Shuai. M., Qiong. S., 2013, "Mass transfer characteristics in a standard pulsed sieve-plate extraction column", *Energy Procedia.* 39, 348–357. https://doi.org/10.1016/j.egypro.2013.07.222.

Chen, J., Kemoun, A., Al-Dahhan, M. H., Dudukovic, M. P., Lee, D. j., Fan, L. S. 1999, "Comparative hydrodynamics study in a bubble column using computer-automated radioactive particle tracking (CARPT)/computed tomography (CT) and particle image velocimetry (PIV)", *Chem. Eng. Sci.* 54, 2199–2207. https://doi.org/10.1016/S0009-2509(98)00349-2.

Dudukovic, M. P. 2003, "Use of gamma Ray computed tomography (CT) and computer aided radioactive particle tracking (CARPT) in multiphase reactors". *Hem. Ind.* 57, 249-261. https://doi.org/10.2298/hemind0306249d.

Gu, J., Xu, Q., Zhou, H., Li, W., Zhang, J., 2016, "Liquid-liquid mass transfer property of two inline high shear mixers". *Chem. Eng. Process. Process Intensif*. 101, 16–24. https://doi.org/10.1016/j.cep.2015.12.005

Kalo, L., Kamalanathan, P., Pant, H. J., Cassanello, M. C., Upadhyay, R. K., 2019, "Mixing and regime transition analysis of liquid-solid conical fluidized bed through RPT technique". *Chem. Eng. Sci.* 207, 702–712. https://doi.org/10.1016/j.ces.2019.07.005.

Kalo, L., Kamalanathan, P., Pant, H. J., Cassanello, M. C., Upadhyay, R. K., 2019, "Time series analysis of a binary gas-solid conical fluidized bed using radioactive particle tracking (RPT) technique data:, *Chem. Eng. J.* 377, 119807. https://doi.org/10.1016/j.cej.2018.08.193

Kolhe, N. S., Mirage, Y. H., Patwardhan, A.W., V.K. Rathod, V. K., Pandey, N. K., Mudali, U.K., Natarajan, R., 2011, "CFD and experimental studies of single phase axial dispersion

coefficient". *Chem. Eng. Res. Des.* 89, 1909–1918. https://doi.org/10.1016/j.cherd.2011.01.020.

Kulkarni, A.L., Patwardhan, A.W., 2011, "Short communication Effect of scale on entrainment in stirred tanks". *Chem. Eng. Res. Des.* 90, 1031–1037. https://doi.org/10.1016/j.cherd.2011.11.012

Lade, V.G., Rathod, V. K., Bhattacharyya, S., Manohar, S., Wattal, P.K., 2013. "Comparison of normal phase operation and phase reversal studies in a pulsed sieve plate extraction column". *Chem. Eng. Res. Des*. 91, 1133–1144. https://doi.org/10.1016/j.cherd.2012.11.005

Mccutcheon, E.B., 1975. Simulation and control synthesis for a pulse column separation system for plutonium-uranium recovery.

Sahu, A., Vir, A.B., Molleti, L.N.S., Ramji, S., Pushpavanam, S., 2016, "Chemical Engineering and Processing: Process Intensification Comparison of liquid-liquid extraction in batch systems". *Chem. Eng. Process. Process Intensif*. 104, 190–200. https://doi.org/10.1016/j.cep.2016.03.010

Sen, N., Singh, K. K, Patwardhan, A. W., Mukhopadhyay, S., Shenoy, K. T., 2016, "CFD simulation of two-phase flow in the pulsed sieve-plate column – Identification of a suitable drag model to predict dispersed phase hold up", *Sep. Sci. Technol*. 51,2790-2803. https://doi.org/10.1080/01496395.2016.1218895

Sen, N., Singh, K. K, Patwardhan, A. W., Mukhopadhyay, S., Shenoy, K. T, 2020, "Computational Fluid Dynamics Modelling to Predict Axial Dispersion in Pulsatile

Liquid-liquid Two phase Flow" *Solvent Extr. Ion Exch.* 1–25. https://doi.org/10.1080/07366299.2020.1840030.

Somkuwar, N., Kolhe, N., Rathod, V., 2014, "Hydrodynamics of a Pulsed Sieve Plate Extraction Column, Indian Chem. Eng. 56, 235–257. https://doi.org/10.1080/00194506.2014.910707.

Upadhyay, R. K., Pant, H. J., Roy, S., 2013, "Liquid flow patterns in rectangular air-water bubble column investigated with Radioactive Particle Tracking", *Chem. Eng. Sci.* 2013,96, 152–164. https://doi.org/10.1016/j.ces.2013.03.045.

Vural, I., Kutup, S., Aalders, J., Wang, Q., Noël, T., Nigam, K.D.P., Kockmann, N., Hessel, V., 2016, "Utilization of milli-scale coiled flow inverter in combination with phase separator for continuous flow liquid-liquid extraction processes". 283, 855–868. https://doi.org/10.1016/j.cej.2015.08.028

Xiaojin, T., Guangsheng, L., 2011, "CFD simulations of flow characteristics in pulsed-sieve-plate extraction columns", *Ind. Eng. Chem. Res.* 50 1110–1114. https://doi.org/10.1021/ie101788b.

Yadav, R.L., Patwardhan, A.W., 2009. "CFD modeling of sieve and pulsed-sieve plate extraction columns". *Chem. Eng. Res. Des.* 87, 25–35. https://doi.org/10.1016/j.cherd.2008.06.010

CHAPTER-6

Conclusions and Future work

Chapter 6 : Conclusions and Future Work

Graphical abstract

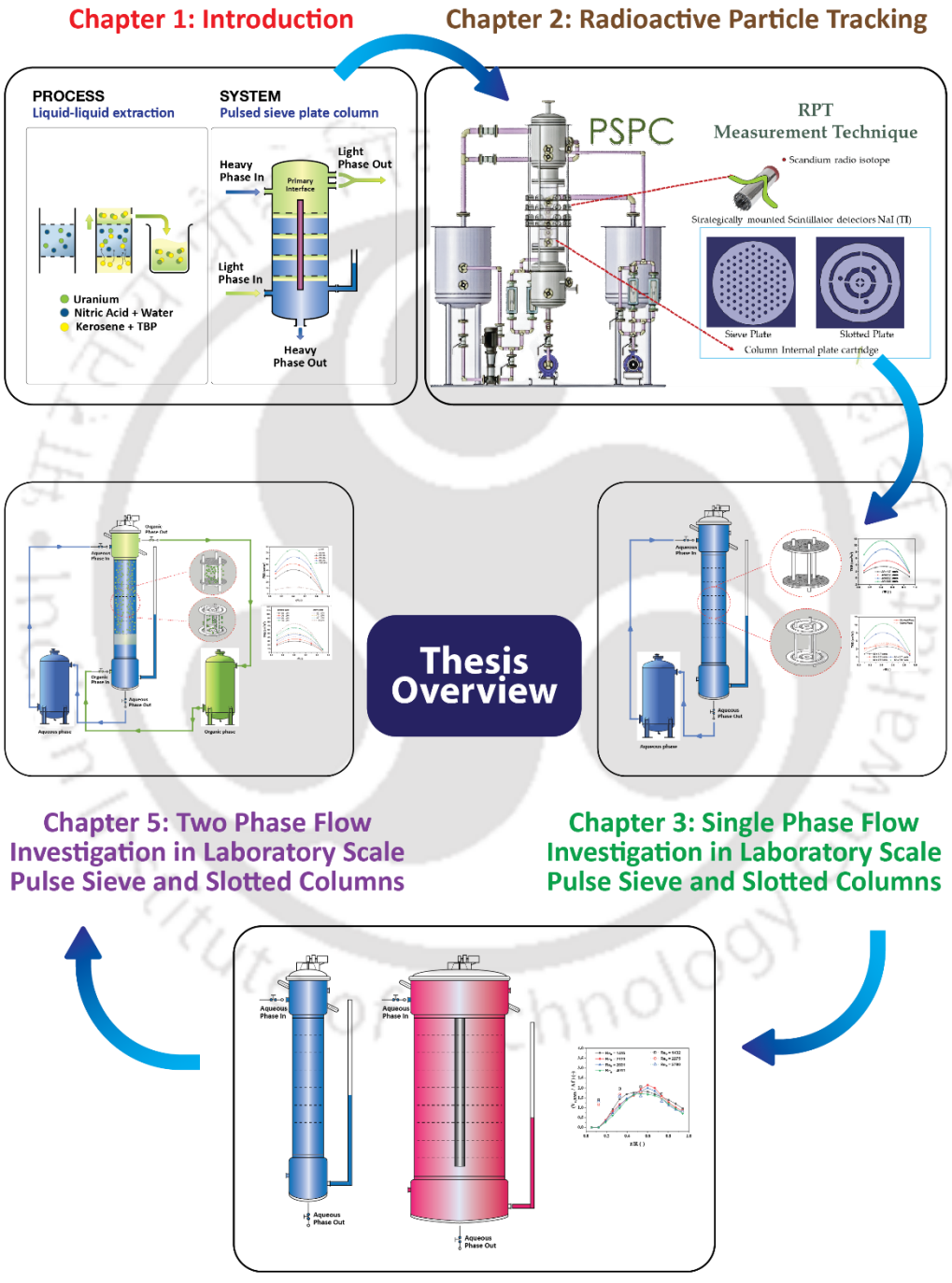

6.1 Summary

In this thesis, velocity field in pulsed plate extraction column is examined experimentally. Experiments are conducted using the radioactive particle tracking to obtain the velocity field between two consecutive plates, which are located away from the inlet and outlet. The experiments are performed in a column of diameter of 3 inch using two different plates, namely, sieve plates and slotted plates for single phase and multiphase flow conditions. In the single phase flow, the velocity fluctuations are obtained under batch or no net flow and downward flow conditions. In the case of multiphase flow, the experiments are performed for the upward flow of dispersed organic phase and downward flow of aqueous phase. The effect of pulsation velocity and flow rate on the velocity field is studied in each case. Further, the investigations are carried out on a pilot scale sieve plate column of diameter 9 inch.

6.2 Major findings of the current dissertation

6.2.1 Single phase Sieve Plate Column (PSPC)

The experiments are performed in a pulsed sieve plate column of diameter 3 inch. The main findings are:

- The mean axial velocity is positive in the region $0.2 < r/R < 0.6$ and negative near walls, suggesting fluid recirculation between adjacent sieve plates.
- In the pulsed sieve plate column, the radial root mean square (rms) velocity remains lower than axial rms velocity for all the cases, indicating the dominance of axial flow.
- The pulsation-induced fluctuations decrease in the axial direction due to the net downward flow of liquid.

- Higher axial (rms) velocity and turbulent kinetic energy result from increased pulsation velocities in no-flow as well as flow condition.
- The axial and rms velocities are observed to be high in the annular region as compared to that in the regions near the centre and wall of the column.

  The experiments are performed in a pilot scale column of diameter 9 inch and the results are compared with the lab scale (3 inch) column. The design of the scale up of column was done such that the geometric parameters are scaled up in the same proportion, in the ratio of one to three. However, a central rod is used in the pilot scale column to hold the plates in place of three rods that were used in the lab scale column.
- Qualitatively, the results in the pilot and lab scale columns are observed to be the same except in the central region because of the geometric differences between the two columns. The velocity at the centre is zero in the pilot scale column.
- A comparison of the velocity fluctuation scaled by the corresponding pulsation velocities shows the fluctutations to have similar magnitude in the two columns for the no net flow case. Therefore, the pulsation velocity is an appropriate scaling factor when there is no net flow.

6.2.2 Single phase Slotted Plate Column (PSLPC)

While the open area for the slotted plate is same as that for the sieve plates, the flow is distributed in the slotted plate in small holes in the sieve plate whereas it is concentrated in few region in the slotted plate. This resulted in:

- The radial rms velocities in the slotted plate column are higher than those in the sieve plate column. In fact, the radial rms velocities are of the same order as the axial rms velocities at high flow rates in the slotted plate column making it a column of choice at high throughput.

- An increase in the pulsation velocity resulted in the fluctuations whereas downward flow of water caused damping of the fluctuations.

6.2.3 Multiphase PSPC and PSLPC

- Upward flow of organic flow causes an increase in the fluctuations in all cases.
- In two-phase flow, increased organic flow rate leads to significantly higher axial rms values and a rise in radial rms values.
- Downward flow of aqueous phase causes the damping of fluctuations in the axial direction but amplifies them in the radial direction.
- As observed for single phase flow, the radial fluctuations are of the same order as the axial rms velocity at high flow rates and low pulsation velocities in the slotted plate configuration.

In summary, this thesis contributes to the existing knowledge of flow behaviour in pulsed sieve plate columns in the form of experimental data on the axial and radial rms velocities and turbulent kinetic energy in two scales of columns for single and two-phase flow under different conditions. Furthermore, the velocity field data for the novel slotted plate design, developed at Bhabha Atomic Research Centre (BARC), India, have been generated and the plate has been shown to provide better mixing at high flow rates.

6.3 Future scope

There are several studies in the literature investigating the residence time distribution, flow regimes, droplet size distribution and mass transfer coefficient between the two phases. This thesis has contributed significantly towards by providing the velocity field data for single and

two-phase flow conditions. However, further research data is needed to correlate the distribution of the dispersed phase and droplet size with the velocity field and vice versa i.e. how the velocity field affects the two-phase flow parameters. Another direction should be correlating mass transfer with the local velocity field data. This should be achieved via a combination of experimental and computational investigations. The experimental data can be used to validate and guide the methodology for the development of the mathematical model whereas the Computational Fluid Dynamics model can provide detailed information about the flow and mass transfer.

Annexure II

Research outcome

List of publications

1. **Pillajetti, P**.; Gupta, R; Upadhyay, R. K.; Pant, H. J.; Goswami, S.; Sen, N.; Singh, K. K.; Shenoy, K. T. "**Investigation of Velocity Field Inside a Single-Phase Pulsed Sieve Plate Column Using Radioactive Particle**", *I & ECR.* 2022, 61(41), 15423-15432.
2. Pillajetti, P.; Gupta, R; Upadhyay, R. K.;Pant, H. J.; Goswami, S.; Sen, N.; Singh, K. K.; Shenoy, K. T. "**Single-phase flow studies in an air pulsed column having a novel plate internal using Radioactive Particle Tracking"** *I&ECR 2023, 2024, 63, 1, 797–805*
3. Pillajetti, P.; Tribedi, T.; Gupta, R; Upadhyay, R. K.;Pant, H. J.; Goswami, S.; Sen, N.; Singh, K. K.; Shenoy, K. T. "**Investigations of Velocity Field in a Pilot-Scale Pulsed Sieve Plate Column using Radioactive Particle Tracking" CEJ to be submitted**

Other publications

1. Tribedi, T.; **Pillajetti, P**.; Kumari, R.; Pant, H. J.; Tiwari, P.; Upadhyay, R. K. "**Measurements of Solid Velocity in a Pilot-Scale Geldart's Group B Circulating Fluidized Bed Using a Radioactive Particle Tracking Technique**", *I & ECR*. 2022, 61(25), 9110–9121.

List of conferences

1. Pillajetti, P.; Gupta, R; Upadhyay, R. K.; Pant, H. J.; Goswami, S.; Sen, N.; Singh, K. K.; Shenoy, K. T. "**Experimental Investigation of pulsed column using radioactive particle tracking (RPT) technique",** *ISCRE,* 6-9 December 2021. [Poster Presentation- International conference]
2. Pillajetti, P.; Gupta, R; Upadhyay, R. K.; Pant, H. J.; Goswami, S.; Sen, N.; Singh, K. K.; Shenoy, K. T. "**Comparative sieve and slotted plate investigation of pulsed column using radioactive particle tracking (RPT) technique**", *CHEMCON,* Kanpur, 27-30 December 2022. [Oral Presentation - National conference]
3. R Kumari, P Pillajetti, R Gupta, RK Upadhyay, HJ Pant "Application of gamma-ray densitometry technique in gas-liquid reactors" *Proceedings of the DAE-BRNS 2022* [Poster Presentation - National conference]

Appendix: Error bar plots

For the slotted plate the experiments are repeated to represent the reproducibility analysis

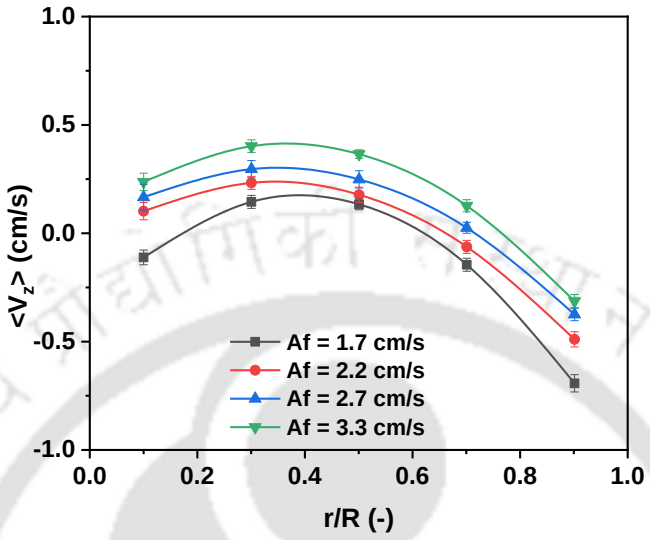

Radial variation of mean axial velocity of aqueous phase at no flow condition

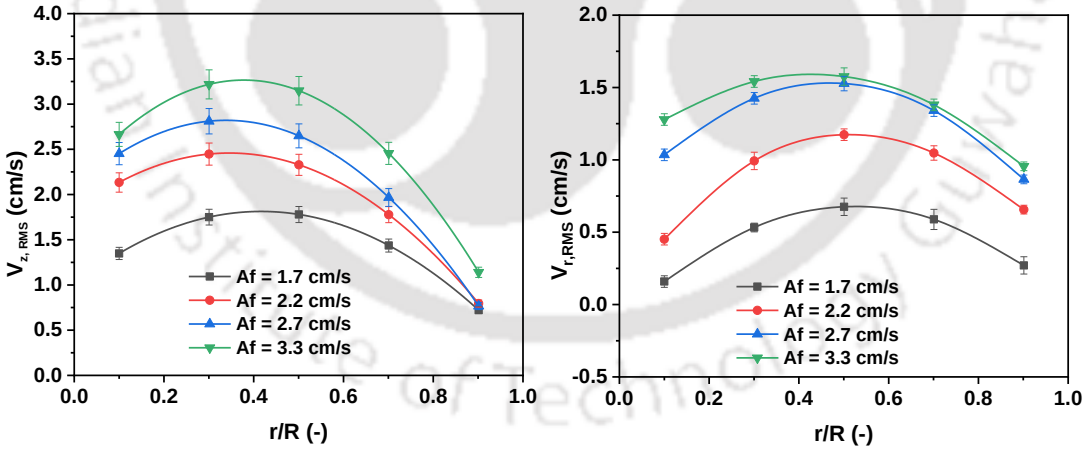

Radial variation of (a) axial rms velocity (b) radial rms velocity for different pulsation velocities at no flow condition with reference to sieve plate

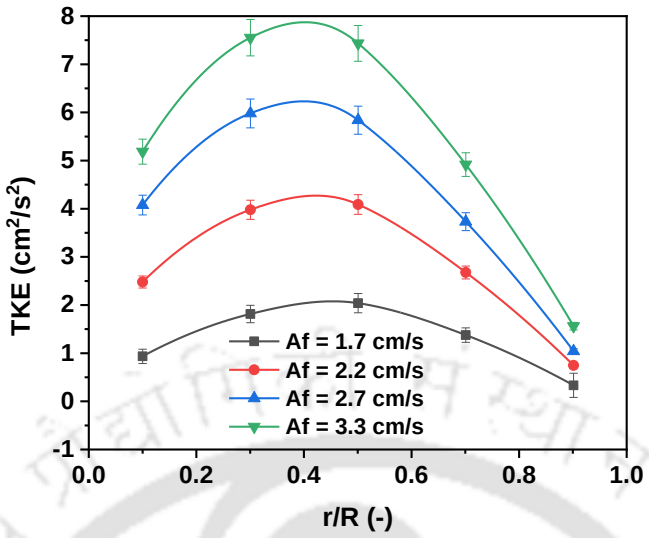

Radial variation of turbulent kinetic energy (TKE) at no flow condition

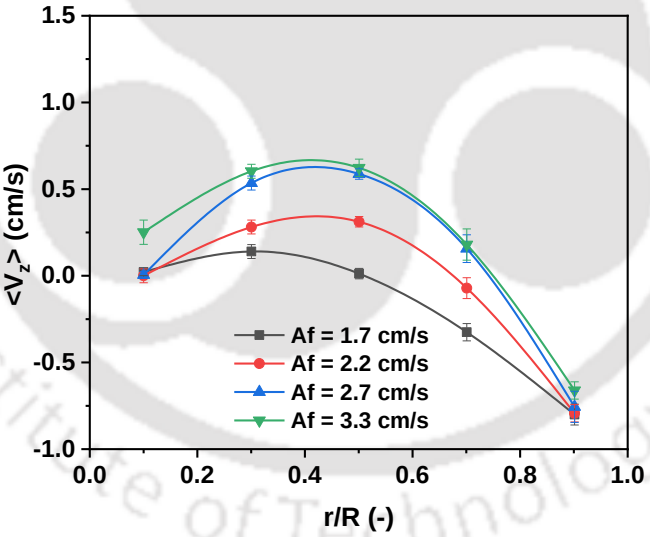

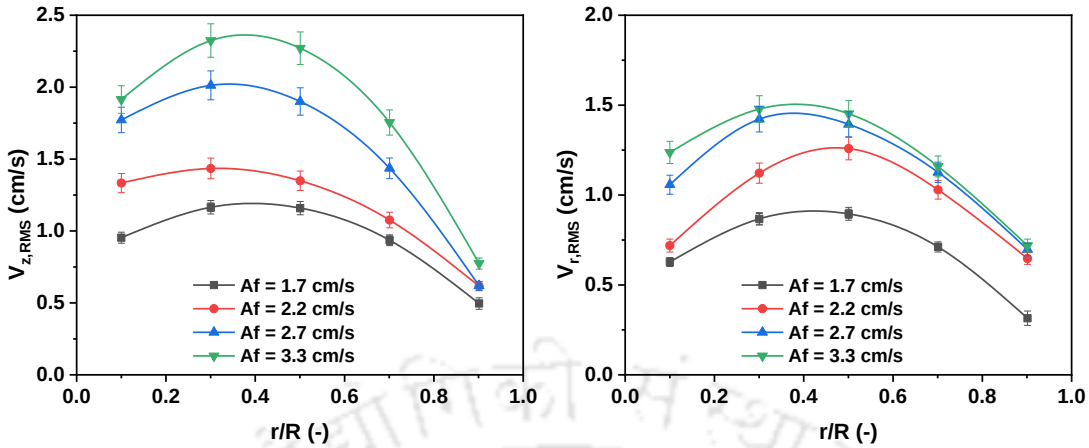

: Radial variation of (a) axial rms velocity (b) radial rms velocity for different pulsation velocities at aqueous phase flow of 120 LPH

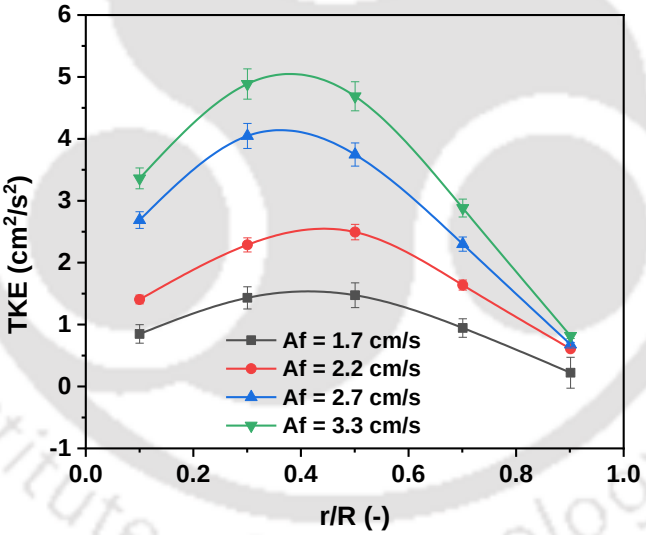

Turbulent kinetic energy (TKE) at aqueous phase flow of 120 LPH for different pulsation velocities

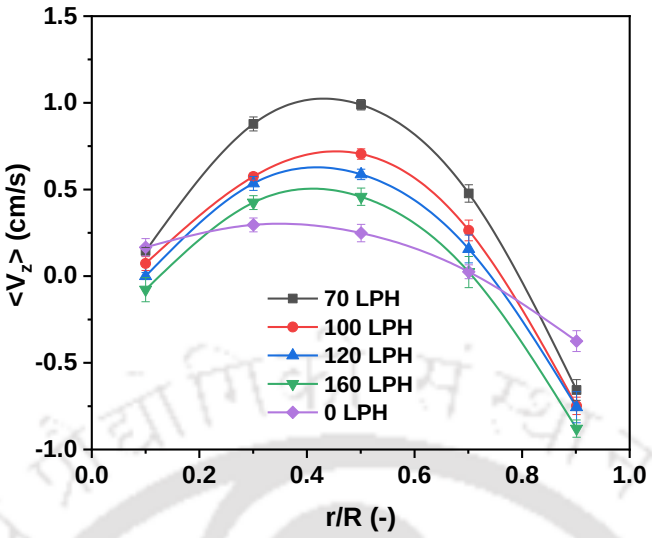

Radial variation of mean axial velocity at Af = 2.7cm/s for different aqueous phase flow rates

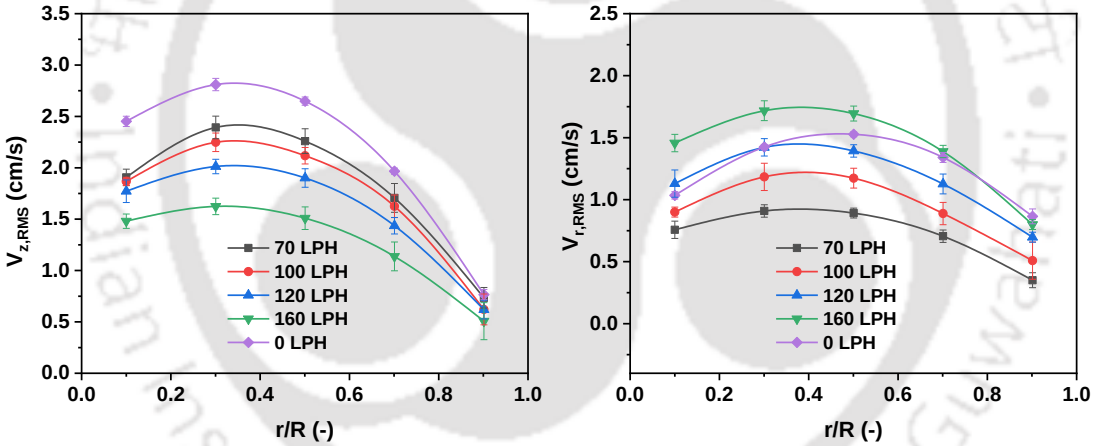

Radial variation of (a) axial rms velocity (b) radial rms velocity for different aqueous phase flow rates at Af = 2.7cm/s

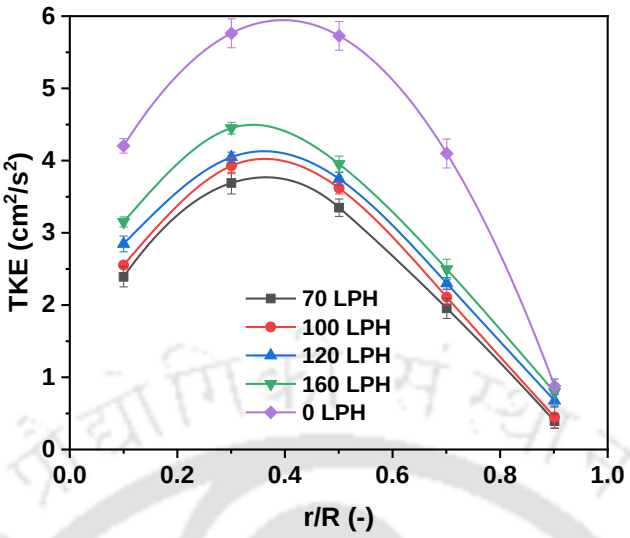

Kinetic energy of turbulence for different aqueous phase flowrates at Af = 2.7 cm/sec